# Integration of Vanadium Redox Flow Batteries in grid-connected Microgrids

**Jessica Papenheim**

Thesis to obtain the Master of Science Degree in

## Energy Engineering and Management

Supervisors: Prof. Maria de Fátima Grilo da Costa Montemor

Dipl. Ing. Alexander Pfnier

### Examination Committee

Chairperson: Prof. Francisco Manuel Da Silva Lemos

Supervisor: Prof. Maria de Fátima Grilo da Costa Montemor

Member of the Committee: Prof. Sónia Maria Nunes dos Santos Paulo Ferreira Pinto

**November 2019**

# Abstract

Microgrids facilitate the integration of intermittent renewables. They rely on energy management systems to schedule optimally their distributed resources. The incorporation of battery energy storage assures a reliable and stable electricity supply and enlarges the business opportunities. Vanadium redox flow batteries are among the suitable technologies and are very versatile in its applications. This thesis establishes an operation optimization model for a grid-connected microgrid that integrates the battery specific characteristics of vanadium redox flow technology as depth of discharge, state of charge dependent power limitations and dynamic efficiencies. To test a hybrid operation, it also defines the model for the more established lithium-ion technology and includes typical features such as capacity degradation. The microgrid energy management is formulated as a non-linear optimization problem. In addition, it applies model predictive control to determine the optimal charging cycles and grid power exchange that will achieve the maximum net profit for the Microgrid. A case study with real techno-economic input data from the German Microgrid Pellworm has been simulated. The scheduling results for different market applications revealed that the highest revenues from battery operation can be obtained by primary frequency regulation. The second-best option is stacked application, which combine arbitrage with secondary frequency regulation or grid supportive peak-shaving. A hybridization of vanadium flow with lithium-ion batteries is proposed, since it allows to fulfill market entry barriers in a cost-effective way and a combined operation can reduce total power losses and degradation.

# Keywords

Microgrid operation, Vanadium Redox Flow Battery, Energy Management System, Model Predictive Control, Scheduling approach

# Resumo

Micro-redes facilitam a integração de fontes de energia renovável instáveis. Estas redes dependem sistemas de gestão de energia para fazer a distribuição ótima dos seus recursos. A incorporação de baterias assegura que o sistema de distribuição de eletricidade é seguro e estável e aumenta o número de oportunidades de negócio. As baterias redox de vanádio estão entre as tecnologias mais adequadas e são aplicáveis a vários sistemas. Nesta tese foi desenvolvido um modelo de otimização da operação para uma micro-rede ligada á rede elétrica cujas baterias têm as propriedades específicas de uma bateria redox de vanádio e de uma bateria de lítio tais como profundidade de descarga, estado de carga, limitações de potencia derivadas do estado de carga, eficiência dinâmica e degradação de capacidade. O sistema de gestão energética da micro-rede, formulado como um problema de otimização não linear, aplica um método de controlo preditivo para determinar os ciclos de carga ótimos bem como o comércio de energia com a rede que maximiza o lucro para a micro-rede. Foi simulado um caso de estudo com dados tecno-económicos reais da micro-rede alemã Pellworm. O estudo das diversas aplicações de mercado revelou que a operação de micro-redes com baterias obtém lucro máximo quando são usadas para regulação primária, seguindo-se a utilização híbrida para arbitragem e regulação secundária ou apoio para peak-shaving. É proposto o uso híbrido de baterias redox de vanádio e de lítio, já que permite a satisfação dos critérios de entrada no mercado de forma económica e que uma operação combinada permite a redução de custos totais e degradação do sistema.

# Palavras-chave

Controlo de micro-redes, Baterias redox de vanádio, Sistema de gestão energética, Controlo preditivo, Método de agendamento

# Table of contents

# List of figures

# List of tables

# List of acronyms

| | |
|---|---|
| AC | Alternating Current |
| aFRR | automatic Frequency Restoration Reserve |
| AMI | Advanced Metering Infrastructure |
| BESS | Battery Energy Storage System |
| BMS | Battery Management System |
| C&I | Commercial & Industrial |
| CAES | Compressed Air Energy Storage |
| CSP | Concentrated Solar Power |
| DC | Direct Current |
| DER | Distributed Energy Resource |
| DoD | Depth of Discharge |
| DSO | Distribution System Operator |
| DWD | Deutscher Wetterdienst |
| EDL | Electric Double Layer |
| EFC | Equivalent Full Cycle |
| EMS | Energy Management System |
| EoL | End-of-Life |
| ESS | Energy Storage System |
| FCR | Frequency Containment Reserve |
| GA | Genetic Algorithm |
| HESS | Hybrid Energy Storage System |
| HMI | Human Maschine Interface |
| HVAC | Heating, Venting and Air Conditioning |
| ICT | Information and Communication Technology |
| LiB | Lithium-ion Battery |
| MAPE | Mean Average Percentage Error |
| mFRR | manual Frequency Restoration Reserve |
| CHP | Combined Heat and Power |
| MG | Microgrid |
| MGCC | Microgrid Central Controller |
| MILP | Mixed Integer Linear Programming |
| MPC | Model Predictive Control |
| OCV | Open Circuit Voltage |
| PbA | Lead-acid |
| PCC | Point of Common Coupling |
| PCS | Power Conditioning System |
| PEM | Proton Exchange Membrane |
| PHES | Pumped Hydro Energy Storage |
| PMS | Power Management System |
| POI | Point Of Interconnection |
| PSO | Particle Swarm Optimization |
| PV | Photovoltaic |
| QP | Quadratic Programming |
| RES | Renewable Energy System |
| RET | Renewable Energy Technology |
| RFB | Redox Flow Battery |
| RH | Receeding Horizon |
| RMSE | Root Mean Square Error |
| SMES | Superconducting Magnetic Energy Storage |
| SoC | State of Charge |
| TES | Thermal Energy Storage |
| TSO | Transmission System Operator |
| UPS | Uninterruptable Power Supply |
| VPP | Virtual Power Plant |
| VRFB | Vandium Redox Flow Battery |
| SCR | Self-Consumption Rate |
| SSR | Self-Sufficiency Rate |
| SH Netz | Schleswig-Holstein Netz AG |

# List of symbols

| | |
|---|---|
| $E_o$ | Standard potential [V] |
| $E$ | Open circuit voltage [V] |
| $N$ | Number of cells per stack |
| $U_{stack}$ | Stack voltage [V] |
| $I_{stack}$ | Stack current [A] |
| $P_{stack}$ | Stack power (DC) [W] |
| $Q_{dis/charge}$ | Capacity dis/charged [Ah] |
| $P_{loss,int}$ | Internal battery losses [W] |
| $R_{int}$ | Internal resistance [Ω] |
| $T_s$ | Sampling interval [h] |
| $T_p$ | Length of prediction horizon [h] |
| $t_p$ | Time where prediction ends |
| $t_0$ | Time where prediction starts |
| $N_p$ | Number of sampling intervals within the prediction horizon |
| $\mathbf{u}$ | Vector of control variables |
| $\mathbf{x}$ | Vector of state variables (e.g. SoC) |
| $\boldsymbol{y}$ | Vector of algebraic variables (e.g. active power consumption, prices) |
| $P_{ess}$ | Power output ESS (AC) [kWh/h] |
| $P_{grid}, u_{grid}$ | Power imported (positive)/ exported (negative) from the utility grid [kWh/h] |
| $P_{res}$ | Power output (AC) of DER (wind, PV, CHP) [kWh/h] |
| $E_{ess}, x_{ess}$ | Energy level of ESS at beginning of step k [kWh] |
| $SoC$ | State of charge at beginning of step k [%] |
| $E_{nom}$ | Nominal energy capacity [kWh] |
| $P_{ess}^{min}$ $P_{ess}^{max}$ | Maximum charge and discharge power [kW] |
| $SoC_{min}, SoC_{max}$ | Minimum and maximum state of charge [%] |
| $SoC^{rc}$ | SoC at which charging power is reduced [%] |
| $SoC^{dc}$ | SoC at which discharging power is reduced [%] |
| $p^{true}$ | Real power data for RES (wind, PV, CHP) and load [kW] |
| $p^{forecast}$ | Created forecast data with error e [kW] |

| | |
|---|---|
| $e$ | Error factor for forecast |
| $\Delta C_{rp}$ | Increment in battery replacement costs between $T_{min}$ and $T_{shelf}$ [EUR] |
| $DoD$ | Battery depth of discharge, $DoD = 1 - SoC$ [%] |
| $T_m$ | Daily mean temperature [°C] |
| $\eta_{energy}$ | Battery (DC) roundtrip efficiency [%] |
| $\eta_{\mathrm{bat}}^{\mathrm{c}}$ | Battery efficiency during charging [%] |
| $\eta_{\mathrm{bat}}^{\mathrm{d}}$ | Battery efficiency during discharging [%] |
| $\eta_{aux}$ | Efficiency of auxiliary components incl. pumps and inverter [%] |
| $\eta_{\mathrm{inv}}^{\mathrm{c}}$, $\eta_{\mathrm{inv}}^{d}$ | Inverter efficiency during AC/DC, DC/AC conversion [%] |
| $\eta_{sys}^{\mathrm{rt}}$ | Roundtrip energy system efficiency [%] |
| $\Phi$ | Degradation as inverse of cycle life [%] |

# 1 Introduction

## 1.1 Motivation

During the past decades the electricity system has been undergoing major changes in response to global climate change and emission reduction targets for the energy sector. The growth of intermittent renewable energy and distributed energy resources has changed the needs of the electricity system, which now requires more flexibility and a smarter coordination. As an answer to the paradigm change from a centralized and “blind” electricity system to a more decentralized and smarter one, concepts like “Microgrids” (MG) or “energy community” have evolved. They can be understood as clusters of Distributed Energy Resources (DERs) and loads coordinated by an intelligent Energy Management System (EMS) and can operate either islanded or in grid-connected mode [1]. They share significant features like the ability to integrate Demand Response (DR), generation of distributed renewable energy and its storage at the distribution level and thus provide a solution to facilitate the expansion of intermittent renewables. However, the fluctuating nature of power output from renewable energy systems (RES) still involves challenges and in all MGs, there is a serious need to develop appropriate flexibility options and optimal scheduling to guarantee a reliable microgrid operation.

Consequently, Energy Storage Systems (ESS) are considered critical components for microgrids, assuring a reliable, stable and secure electricity supply and enlarging the potential business opportunities in the presence of high intermittent RES penetration. If dispatched optimally, ESS may significantly reduce conventional fuel costs and emissions in MGs [2]. [3] notes that although the benefits of ESS have been verified in theory and practice, we still lack ways to optimally configure the ESS in particular for MG-based applications and calls for development of proper models and tools which address key integration issues such as optimal sizing, placement and techno-economic operating schemes.

Today, several technologies of ESS have been commercialized, possessing different characteristics concerning power or energy densities, performance, safety, cost and sustainability. Whereas pumped hydro storage has been the predominant ESS technology for decades, the deployment in microgrids is restricted by requiring certain geographical conditions. Lead acid batteries have been around the longest with regard to off-grid power systems and grid backup systems, but their low life expectancy has been a major drawback. In the past years, lithium-ion batteries (LiB) received the most attention in terms of research and pilot projects, evoked by the ongoing cost decrease of lithium-ion batteries due to the growing demand caused by electric vehicle manufacturers.

The work of [4] compares storage properties versus application specific requirements. Their research suggests that Vanadium Redox Flow Battery (VRFB) technology is a promising electrochemical energy storage system for a wide range of applications including energy as well as power applications, enabling the integration of renewable energies and capable of reducing the carbon footprint of electricity generation. It is primarily used as a large-scale stationary storage technology and assumed to be a

suitable battery type for the integration in microgrids. Vanadium flow batteries have unique characteristics compared to other battery types such as a much longer lifetime, non-toxic materials, a flexible energy to power ratio but also a higher control complexity due to active elements like electrolyte pumps.

In terms of storage system integration, there is increasing research interest covering a wide range of aspects: The papers [5]–[7] discuss optimal unit sizing and the authors in [8] analyze optimal placement for energy storage systems in a microgrid. Another important facet deals with how to precisely describe the operation characteristics and determine the optimal operation strategy of the ESS in the MG. The scheduling or unit commitment is a function of the microgrid energy management system (MG-EMS). The MG-EMS tries to dispatch its flexible resources including energy storage systems under a predefined goal, such as minimizing operation costs or maximizing economic profits. Although research papers propose different energy management systems and strategies [11] [12], few of them study flow batteries or take into account battery specific characteristics of VRFB. Accordingly, there is the need to consider storage technology- and application-specific constraints in the control and management strategies. This will allow microgrid operators (MGO) and investors to estimate the actual economic value of their ESS asset.

## 1.2 Research objectives

This thesis seeks to advance the knowledge on the operation of ESS in particular vanadium flow batteries within microgrids. It analyzes existing control architectures and operation strategies for microgrids with ESS. On the basis of this analysis it proposes a new energy management strategy based on MPC, which takes into account VRFB specific characteristics and thus allows maximizing its performance. Learning from simulation and comparison of a real-life microgrid case with a VRFB, it intends to develop suggestions how to manage VRFB efficiently and provide implications on the technical and economic viability of a VRFB integration in microgrids. These considerations lead to the following general research question:

How can a Vanadium Redox Flow Battery system be operated efficiently in a microgrid to maximize benefits?

To answer this question, two specific research questions are formulated:

RQ1: How can the optimal dispatch in a MG with a VRFB battery be determined?
RQ2: What are the economic benefits of a MG with a VRFB, in contrast to or complementary to other batteries?

## 1.3 Methodology

To answer the research questions, this thesis follows three main steps: Firstly, an extensive literature study is conducted to provide the background on microgrids, VRFB and control and operation of microgrids, and to identify relevant information to form the underlying model and algorithm of the MG-EMS. The second step is the design and mathematical formulation of the proposed energy management

system. The system components as well as applications are modeled, and its operation is formulated as an optimization problem in MATLAB. Finally, a series of simulations is conducted based on real battery and case study data from the North-sea Island Pellworm. The case study results are analyzed and compared to obtain insights for the research questions developed above.

## 1.4 Structure

This thesis is divided into seven chapters. After the introduction, which highlights the topic's relevance, Chapter 2 gives an overview of the basic background starting with the microgrid concept and energy storage systems. It highlights the redox flow battery storage system, their components and their characteristics with respect to competing storage technologies. In Chapter 3 the integration of storage systems in MGs is reviewed, it summarizes current applications for storage and existing MG control mechanisms. Chapter 4 describes the theoretical development and mathematical formulation of the proposed MG-EMS. Chapter 5 introduces the case study and case specific data input and presents the results from the simulation. Chapter 6 discusses the findings, compares them with previous research and deduces practical implications. In conclusion, the study's limitations and recommendations for future research are derived in Chapter 7.

# 2 Theoretical background

## 2.1 Overview microgrids

### 2.1.1 Definition and concept

A conventional power grid is based on a centralized structure with a few large generation units providing the necessary power, which must be transmitted to the loads often located far away from the generation centers. This kind of structure usually does not allow enough control at lower grid levels and impedes the integration of intermittent RES or electric loads such as electric vehicles. To tackle these problems microgrids with smaller generation units distributed at lower grid levels closer to the load, have gained popularity.

According to the U.S Department of Energy a Microgrid is a "*group of interconnected loads and distributed energy resources (DERs) with clearly defined electrical boundaries that acts as a single controllable entity with respect to the grid and can connect and disconnect from the grid*" [11].

MGs have been known for decades. Commonly they have been implemented in critical infrastructure such as military bases, hospitals and data centers, but with the ongoing energy transition and more RES, microgrids show advantages over conventional grid structures. As reported by Navigant Research the microgrid market has been growing lately: It passed 4 GW installed capacity and is expected to have tripled the number by 2025. Accordingly, market revenues are estimated to rise from EUR 6.75 billion to EUR 20 billion by 2025 [15] [16].

### 2.1.2 Components

The main components of a microgrid include loads, DERs, a control system, smart switches and protective devices. The MG can be represented as a multi-layer block diagram of field, communication and control layer (cf. Figure 1).

The **field layer** includes all physical components:

*DERs* are various small-scale energy resources, that can be placed anywhere from utility facilities to private properties. Many DERs are renewable generators like photovoltaic or wind turbines, others are Combined Heat and Power (CHP) units providing heat and electricity from either biomass or conventional fuels. The DERs are equipped with local controls which regulate the current and voltage of each module within the DER unit to achieve the requested power. Many DERs are not suitable for being directly connected to MGs therefore power electronic interfaces are required to enable or improve their integration.

*Non-controllable or controllable loads* from consumers create the power demand within a defined geographical area. They include loads from households, industries, agriculture and public services. It is also possible to integrate demand response in the form of controllable loads into a microgrid.

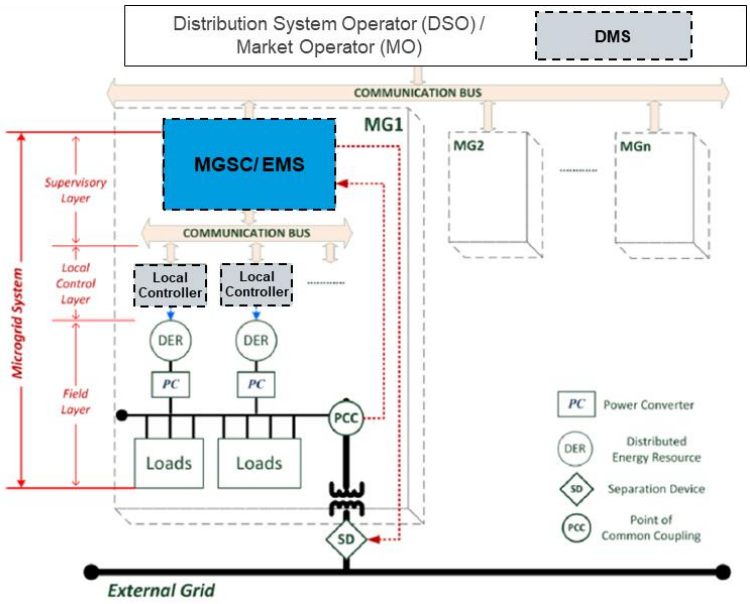


Figure 1. General overview microgrid layers and components. Adapted from [14]

*Energy storage systems* refer to systems able to convert electrical energy into an energy form which can be stored and then converted back to electricity when needed [15]. ESS are often substantial in microgrids, especially to guarantee the possibility of an islanding mode and to integrate fluctuating renewable generation. As they require energy storage technologies, that can be easily integrated for small/medium sized electrical networks, the most frequently used storage systems in microgrids are batteries for stationary applications. In fact lead acid batteries are the most common type [16]. A short overview on ESS feasible for microgrids is given in Chapter 2.2.

*Grid components* include power converters, transformers, distribution lines and the main *switch,* which is at the *Point Of Interconnection* (POI), also referred to as Point of Common Coupling (PCC). It is the physical connection to the main grid and enables the microgrid to become independent from the utility grid when switched to “islanding mode”. This islanding operation mode is a key attribute of a microgrid. If in grid-tied mode, the Distribution System Operator (DSO) views the MG as either a generation unit or a load, depending on the direction of power exchange.

The **control layer** can be distinguished into **local control** and **supervisory control**.

The *local control* is in charge of the device control and follows instructions coming from upper control levels. It is often realized by controlling the DER inverter. The *supervisory level* is in charge of the microgrid’s interaction with the utility grid, makes the decision to switch between interconnected and islanded modes and is responsible for the optimal operation of all resources [17]. This layer is sometimes also called the *Energy Management System (EMS) or Microgrid Central Controller* (MGCC) [14].

The International Electrotechnical Commission (IEC) defines an EMS as “*a computer system comprising a software platform providing basic support services and a set of applications providing the functionality needed for the effective operation of electrical generation and transmission facilities so as to assure adequate security of energy supply at minimum cos*t” [18]. Thus, with the help of knowledge about grid states, resource availability and market prices the EMS software performs the scheduling within the

microgrid. The scheduling can be considered an optimization problem, with various constraints and the objective to minimize the total cost of energy. Although the IEC restricts the objective by focusing on minimal costs, theoretically other objectives are possible as well, for example to maximize the share of renewables with the given assets. The MG supervisory control is fully responsible for the microgrid operation but in grid-tied operation mode it also interacts with the central control system of the DSO, which is called Distribution Management System (DMS).

To allow interactions between field and control layers there is the **communication** layer including different Information and Communication Technology (ICT). In order to provide sufficient data to the EMS so it can run its optimization, the control system uses *Advanced Metering Infrastructure (AMI)* and other *connecting devices* to monitor and enable bidirectional data transmission [19].

Table 1. Overview and classification of microgrid components.

| | Component | Type | Description | Examples |
|---|---|---|---|---|
| **Distributed Energy Resources (DER)** | Distributed Generators (DG) | Non-renewable | Based on diesel, gas, H2 | Diesel genset, gas turbine, fuel cell |
| | | Renewable | Based on wind, sun, ocean waves | PV, wind turbine, tidal/ocean energy turbine |
| | Energy Storage System | Short term application | High power | Supercapacitors, flywheels, Li or redox flow batteries |
| | | Long term application | Energy during long periods | Pumped hydro, CAES, several batteries |
| **Loads** | Non-controllable loads | Critical loads | Require constant power supply | Hospitals, military, data center |
| | | Non-shiftable | Operate at specific times | Residential, some industrial loads, lighting |
| | Controllable loads | Shiftable loads | Can be scheduled | Dryer, washing machine, dishwasher, (heat pumps, electric boilers) |
| **Control** | Supervisory & Local controllers | Actuator | Respond to signals and initiate control actions | PI converter-embedded controllers, intelligent electronic devices, microprocessor-based (CRIO, Arduino) |
| **ICT** | Advanced metering infrastructure (AMI) | | Monitors power system, transmits data to controllers | Sensors, smart meters, remote terminal units, phasor measurement units |
| | Connecting components and devices | | Link components | Wires, antennas, I/O or gateway devices |

Adapted from: [19] [20].

### 2.1.3 Classification and types

MGs can have various designs based on the chosen power topology, control architecture, applications, and whether grid-connected or islanded.

The grid power topology of a microgrid can be founded on AC, DC or hybrid structures, and either one phase or three phases: A DC distribution is finding increasing research interest since a lot of systems naturally provide DC output such as PV panels, electric vehicles, LED lighting etc. [21]. The advantage would be that conversion stages can be removed by charging the battery directly on the DC bus. However, for all grid-tied microgrids an AC/DC inverter is still required to connect it with the main grid. Worldwide the grids are dominated by an AC infrastructure, which is why the technology and AC integration is more mature and optimized than any DC microgrids. AC microgrids use a common AC bus, which connects all kinds of loads (AC/DC) and generation via individual inverters. AC structures allow the best controllability and flexibility. Hybrid structures have only been tested for a few years. Within a hybrid microgrid, photovoltaics and battery are connected to a common DC bus, whereas the load is connected to an AC bus. A central inverters links the two [22].

According to Guerrero et al. [23] a single control and energy management system in complex microgrids would not be sufficient to make all necessary decisions. Therefore, hierarchical control structures are commonly implemented of minimum a strategic level consisting of the energy management layer and an operational layer consisting of the local controller. Yet, depending on the microgrid complexity there will be more than these two layers. The operation decisions can be either made centrally or decentralized at the local control.

Finally, microgrids can be distinguished by market segments based on the main initiator/owner and the connectivity (remote or grid-connected). Microgrids originated from their use for military or public institutions and remote applications. Up to now remote applications still constitute around 45 % of the total microgrid capacity. Nevertheless Commercial & Industrial (C&I), community or utility owned microgrids in grid-connected regions are on the rise [12], [24].

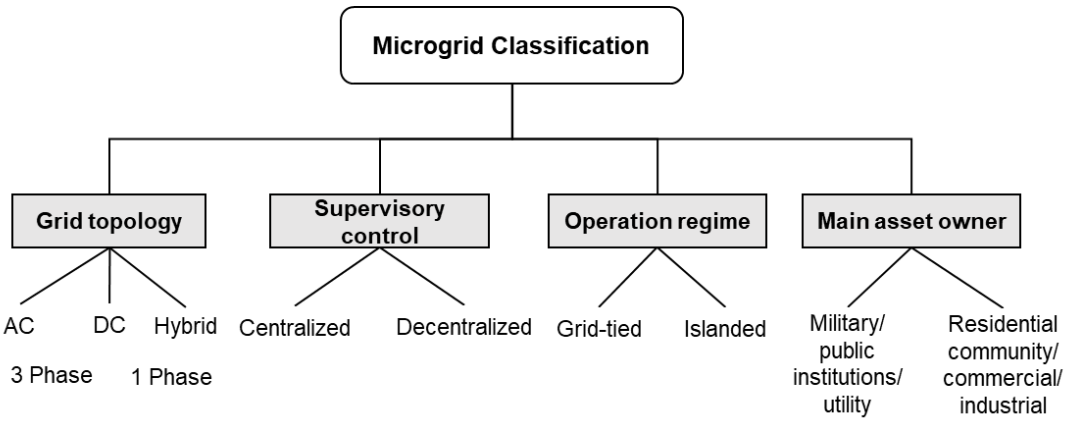


Figure 2. MG classification. Adapted from [24]

### 2.1.4 Opportunities and challenges

The opportunities of microgrids can be described from three viewpoints: technical, economic and environmental. Microgrids accelerate the electrification and allow to power remote communities, increase efficiency and reduce vulnerability to external circumstances. In recent years threats from cyber or terrorist attacks and natural disasters combined with the growing dependency on electricity, has increased concerns regarding the security of the grid. Microgrids offer improved reliability due to their ability to disconnect from the main grid. The authors Basu et al. [25] describe MGs merits from an economic perspective: opportunities are seen in the reduction of transmission and distribution losses since the transmission distances are smaller, minimized fuel costs and smaller capital costs. In contrast to large generation facilities, microgrids based on DERs offer low construction cost and time, which cuts down expenditures related to financing. Environmental benefits result from improved integration of RES and reduction in pollutants and emissions in comparison to central mainly fossil fuel-based generation.

Nevertheless, microgrids also face certain challenges: The lack of rotational inertia from dispatchable generators requires strategies or resources like ESS to ensure the stability of the MG. Based on the definition microgrids have to be able to work independently from the main grid, which means they have to provide the same grid functions as large-scale grids i.e. balancing services to maintain a high reliability. The unpredictability and weather dependence of its renewable generation makes microgrid operation difficult. Another challenge microgrids face is the seamless transition from grid-connected to island operation. Apart from high technical requirements regarding the connection also the costs in terms of connection fees are high [16]. In addition, MGs comprise various DERs, power electronics and local controls and in order to achieve a safe, reliable and autonomous operation the coordination remains a crucial challenge.

## 2.2 Energy storage systems

### 2.2.1 Importance for the energy system and microgrids

A major role in the energy transition towards large shares from renewable energy resources will be played by stationary energy storage systems. According to the IEA annual energy storage deployment for utility scale and behind-the-meter installations has been growing in recent years to more than 3 GW in 2018 (cf. Figure 3) [26]. Supportive regulations led to large volumes of new storage installations especially in Korea and China.

In energy systems with major generation shares from intermittent solar and wind, transmission and distribution system face challenges. Storage can help to avoid costly upgrades which are only necessary due to congestion in limited time periods.

ESS can serve for a wide range of applications depending on their energy and power capacities: For short time periods ESS can provide the solution for power quality and grid stabilization, substituting conventional fossil-fuel-based generators, which are expensive and not environmentally friendly. Over mid and long time periods ESS serve as backup power for critical infrastructure (military, hospitals,

airports), or are used as reserve to match demand and supply at any time. Other applications include energy shifting for arbitrage, which flattens the tariff curve either over a typical day but can also target deviations across weeks or different seasons. Only by providing efficient, cost-effective, safe energy storage systems, the reliability of the electricity supply can be achieved.

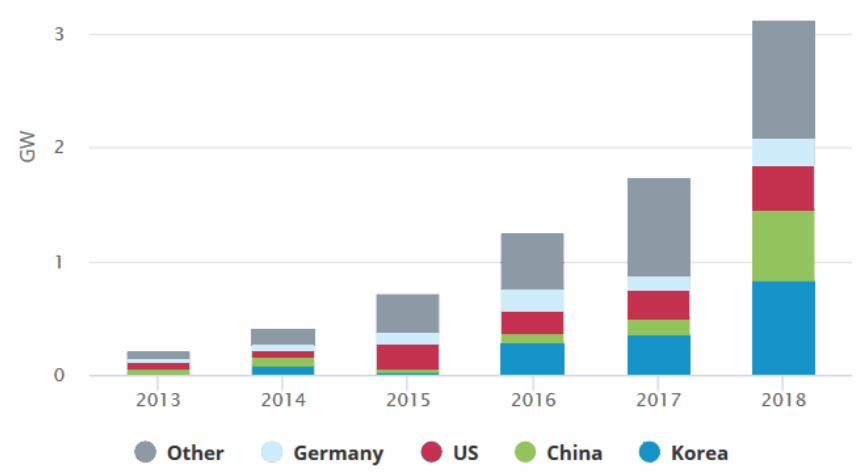


Figure 3. Annual deployment of stationary storage in GW (utility scale & behind the meter). Adapted from [26].

Also, in microgrids energy storage has emerged as an increasingly valuable component. Navigant Research estimates that the ESS storage capacity in MG will grow from 240 MW in 2017 to 3,300 MW by 2026 [27]. Serving a variety of roles, it increases the flexibility of the operation by allowing to optimize the microgrids performance and making it more economical. Major drivers are reduction of fuel consumption and facilitation of renewable integration. Besides, storage enables islanded operation at lower operation cost than fossil back-up generators, also in cases when RES generation is not sufficient. The transition to islanded operation requires very fast control actions, with high power and fast response characteristics, while the islanded operation itself requires long discharge times. Thus, especially the application of Battery Energy Storage Systems (BESS) in MGs has gained popularity and is expected to grow. Additional information on BESS applications in MGs is provided in Chapter 3.1.

### 2.2.2 Overview of energy storage technologies

Storage technologies can be clustered depending on the principle how the energy is stored. The most dominant examples are described in the following section:

Table 2. Classification of energy storage technologies.

| Mechanical | Chemical/Electrochemical | Electrical | Thermal |
|---|---|---|---|
| • Pumped Hydro Storage<br>• Compressed Air Energy Storage (CAES)<br>• Flywheel | • Secondary battery (PbA, LiB)<br>• Flow battery<br>• Hydrogen (electrolysis + fuel cell) | • Capacitor<br>• Supercapacitor (EDL)<br>• Superconducting Magnetic (SMES) | • Sensible<br>• Latent heat storage |

- **Mechanical**

Most large scale storage systems that exist worldwide are pumped hydro storage [28]. The storage capacity is based on the altitude difference. During off-peak hours the water is pumped into the upper reservoir and during peak-hours it is released through the turbines to produce electricity. For MGs the crucial disadvantage is the dependency on certain geographic conditions and the scale of the investment necessary.

Flywheels store energy in the form of kinetic energy. During charge motors are used to convert the electric energy into kinetic energy by accelerating the flywheel to high speed and during discharge they work as generators. On the one hand flywheels offer high power density, quick response time, long lifespan and low maintenance, on the other hand they have a high self-discharge rate, making them unsuitable for mid- and long-term energy storage applications [28].

Compressed Air Energy Storage (CAES) pressurizes air during off-peak hours and stores it in underground reservoirs such as salt caverns or aquifers and releases the stored energy via a turbine and generator during peak time. CAES system can store the energy over long periods but suffer from a low efficiency. Besides they usually rely on specific geographical conditions as storage facilities [29].

- **Electrical**

Capacitors store electrical energy directly, as an electrostatic field between two conducting electrodes. The supercapacitor, also known as ultracapacitor has a higher energy and power density due to an electrical double layer with high surface carbon electrodes. There are two main types: The Electric Double Layer supercapacitor (EDL) and the pseudo capacitor. The EDL works as an electrostatic storage by separation of charge in a Helmholtz double layer, whereas the pseudo capacitor, which as the name implies - actually is an electrochemical energy storage, since it involves redox reactions between the electrolyte and the electrode. They are applied for fast response short term services, which require high power peaks within short periods, commonly from milliseconds to some minutes [30]. They have been widely applied when short time response and high power is required.

Superconducting Magnetic Energy Storage (SMES) stores electrical energy in the form of a magnetic field, created by the current flow through a superconducting coil, which possesses the material property that it loses its resistance at very low temperatures. They provide good performances and extremely long lifetimes but the low temperature requirement for the superconductor materials make its infrastructure more complex and expensive and restrict the applications.

- **Thermal**

There are two types of Thermal Energy Storage (TES), sensible and latent heat storage. The storage of sensible heat is most widespread, for example in the form of domestic hot water tanks. Thermal energy is solely stored through a change of temperature in a storage medium. The second type is latent heat storage, using phase change materials as storage media. The thermal energy is stored in from of the energy exchanged during a phase change (e.g. the melting of ice). Thermal energy storage can be applied in combination with Concentrated Solar Power (CSP), which primarily produce heat which can be stored in the form of molten salt and can be converted into electrical energy via a steam turbine when

needed [31].

- **Electrochemical**

Electrochemical storage systems, which include batteries, redox supercapacitors and hydrogen plus fuel cell storage, convert electrical energy into chemical energy by means of electrochemical reactions.

Among them are Power-to-X technologies. Their main idea is to use cheap or “excess” electricity to produce a gas or liquefied gas (the fuel) from another chemical through electrolysis and further synthetization. The best known is hydrogen electrolysis from water. The energy is stored either in the hydrogen itself or it is further converted to methane (SNG) or ammonia to increase its energy density. When the electricity is needed a fuel cell running with hydrogen and oxygen is used to convert the chemically stored energy into electrical energy. Although hydrogen is a flexible energy carrier applicable in different sectors including mobility and heating, the disadvantage is that the efficiency of the conversion chain is still low (< 40%). Furthermore, the energy density if stored at gaseous state is very low, which is why it is often liquefied using either pressure or very low temperatures [32]. Hence, H2 storage is expensive since it requires dedicated solutions.

Batteries are an electrochemical storage technology with an enormous market growth in the last decade. Despite its prevalence for portable electronics, the share of batteries in large scale grid related applications is only 0.2 % [33]. Examples are lead-acid, lithium-ion, metal-air batteries and redox flow batteries. Batteries can be distinguished into primary and secondary. The latter can be recharged electrochemically several times while the formed are discarded after discharge. The lead-acid battery is one of the oldest, most mature electrochemical storage technologies. A cell is composed of metallic lead and lead dioxide electrodes which are in contact with an aqueous solution of sulphuric acid. The nominal cell voltage is 2.1 V and the specific energy density is 35-60 Wh/kg. It is very robust and is almost 100 % recyclable. There is a growing demand for Lithium-ion Batteries (LiB), mainly because they are superior in terms of energy and power density and thus can be used in portable devices and electric mobility. LiB batteries have a cell voltage of 3.2-3.6 V and, depending on the exact chemistry, energy densities from 100-150 Wh/kg. LiB batteries are also entering the stationary storage market. In many cases as 2$^{nd}$ life batteries. However, they require high safety standards since they can explode or catch fire. Although much longer than for lead-acid, lifetime still needs to be improved.

### 2.2.3 Technology comparison

The ESS technologies available cover a wide range of characteristics and have their individual advantages and disadvantages. A short comparison is presented based on four major characteristics: Specific energy and power density, capital cost, efficiency and lifetime.

- **Specific energy (Wh/kg) and specific power (W/kg):**

These are essential characteristics to identify the necessary weight to meet power and energy requirements of the application. Energy and power densities, measured in Wh/l and W/l, respectively are similar metrics but in regards of the required volume. For this work the weight aspect is considered more relevant, since space is not a major problem for stationary applications, but most costs of e.g. raw

materials are weight dependent.

- **Cycle efficiency (%):**

The cycle efficiency is the roundtrip efficiency and is the quotient of the electrical energy output versus the energy input. Flywheels and supercapacitor have a very high efficiency (>90 %) but are limited in their applications due to their low energy density. Cycle efficiency influences the operational costs, since more energy is lost if the cycle efficiency is low. Technologies with low cycle efficiency are CAES, TES and the entire hydrogen plus fuel cell technology chain.

Table 3. Comparative overview of different energy storage technologies.

| | Specific energy density (Wh/kg) | Specific power density (W/kg) | Cycle efficiency (%) | Cycle life |
|---|---|---|---|---|
| **Pumped Hydro** | 0.5-1.5 | - | 70-85 | >20000 |
| **CAES** | 30-60 | - | 40-60 | >10000 |
| **Flywheels** | 5-80 | 1000 | 90-95 | >20000 |
| **Capacitor** | 0.05-5 | 4000 | 60-80 | >50000 |
| **Supercapacitor** | 0.5-15 | 500-10000 | 93-98 | >50000 |
| **Hydrogen fuel cell** | 800-10000 | >500 | 20-50 | 1000-20000 |
| **TES** | 80-200 | 80-500 | 30-60 | |
| **Lead-acid** | 20-35 | 25 | 70-80 | 200-2000 |
| **Ni-Cd** | 40-60 | 140-180 | 60-70 | 500-2000 |
| **LiB** | 100-200 | 360 | 75-90 | 1000-7000 |
| **VRFB** | 25 | 80-150 | 60-85 | >16000 |

Data from: [32]–[34]

- **Cycle lifetime** (number of cycles)

Electrical storage technologies have the longest lifetime in cycles. They last several tens or hundreds of thousand cycles. Mechanical and TES systems also have a long cycle life. They are based on standardized mechanical components which have been optimized and engineered for long lifespans. Conventional batteries like PbA or Ni-Cd have shorter cycle life than VRFB since their electrodes take part in the redox reaction.

- **Captial cost (CAPEX in EUR)**

The capital cost is the initial investment cost needed to purchase or built the ESS. They can be specified as specific capital cost per power unit and per energy unit. It should be noted that due to learning and scaling effects these numbers change quickly, especially for technologies which have not reached the maturity stage like VRFB, lithium-ion, supercapacitors and hydrogen storage. However, for mechanical energy storage technologies like pumped hydro storage and CAES, which are well established, no significant CAPEX reduction is expected. Figure 4 shows that they have lowest energy specific investments but higher power specific costs than electrochemical storage technologies. Among the electrochemical storage, lithium-ion batteries achieve the lowest power specific CAPEX but VRFB

reveal better energy specific cost and a high cost reduction estimation for the future. Lead-acid have very competitive power and energy specific investment cost, yet due to their low cycle life, they are not necessarily the cheapest option from a life cycle perspective [35].

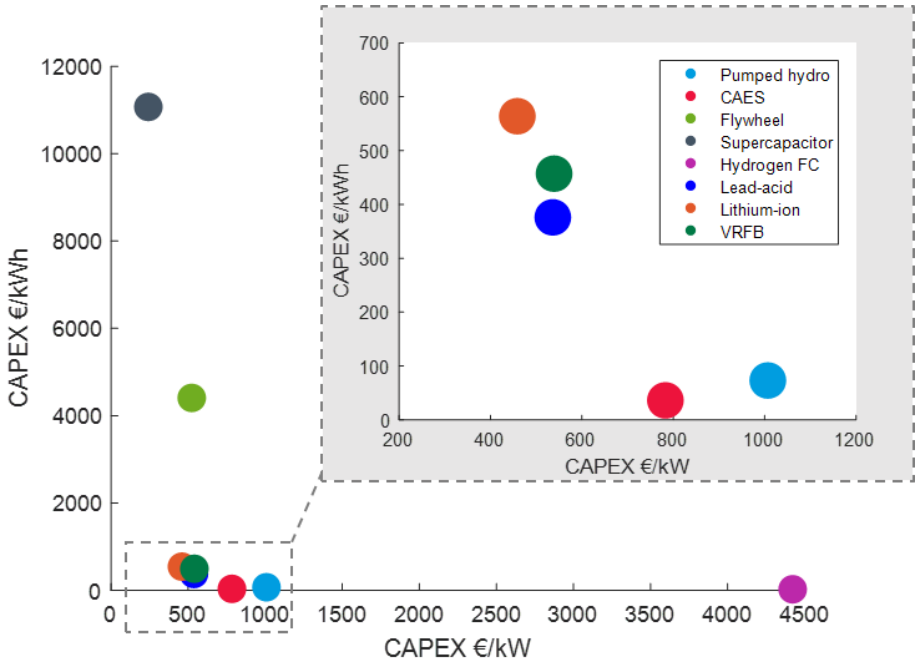


Figure 4. Overview of ESS power and energy specific initial investment cost in 2018. Own elaboration. Data from [35], [36]

- **Levelized Cost of Storage (LCOS):**

The example of lead-acid with its short cycle life shows that initial investment cost are not the only relevant costs when comparing ESS technologies. Therefore, the levelized cost of storage are a more holistic economic parameter to compare ESS. LCOS can be defined as the total lifetime cost of the investment divided by its cumulative delivered electricity [34]. It is an analogous concept to the levelized cost of electricity (LCOE) and reflects the internal average price at which electricity has to be sold for the net present value of the investment to be zero. Recent studies have attempted to calculate the LCOS for various technologies [35], [37], [38]. Nevertheless, they use different data input and different methodologies to calculate the LCOS, which is why the findings differ quite significantly. End-of-life (EoL) costs, capacity degradation and self-discharge are not always taken into consideration. Eq. (1) displays the calculation proposed by Schmidt et al. [35]. $r$ denotes the discount rate, $N$ the total lifetime in years.

$$LCOS = \frac{CAPEX + \sum_n^N \frac{O\&M}{(1+r)^n} + \sum_n^N \frac{charging\ cost}{(1+r)^n} + \sum_n^N \frac{EoL}{(1+r)^n}}{\sum_n^N \frac{Elec_{discharged}}{(1+r)^n}} \quad (1)$$

The final LCOS for each ESS technology depends on its application. Although the results vary in absolute LCOS, the studies agree that for daily energy arbitrage, which makes use of typical price differences during 24 h, pumped hydro was the cheapest technology, followed by VRFB and LiB. Seasonal storage was only feasible with pumped hydro, CAES and hydrogen. For investment deferral of transmission and distribution grid PHS, CAES and VRFB had the lowest LCOS, but their ranking

depends on the paper's calculation method. For very short-term primary frequency response application, the flywheel and lithium-ion were most economical in 2015. For in-front-of-the-meter applications Lazard's study [39] suggests VRFB or LiB, whereas for residential and commercial use cases which belong to behind the meter applications, LiB and advanced lead acid are recommended.

The future outlook on LCOS in 2030 (cf. Figure 5) predicts that there will be changes in the ranking which technology is the most economic for many applications and a sharp decrease of the mean LCOS for this technology.

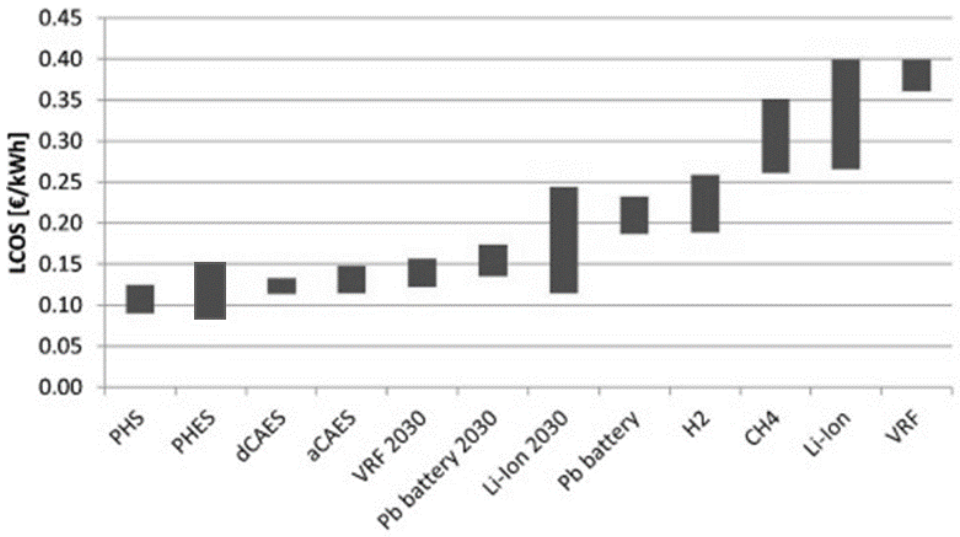


Figure 5. Comparison of average LCOS for a large scale utility application. [40]

## 2.2.4 Redox flow battery energy system

### *2.2.4.1 Work principle*

Redox flow batteries belong to the category of electrochemical storage systems. As the name "redox" indicates the main principle is based on *reduction* and *oxidation* between two active materials. Their development started in the 70s introduced by NASA, which was searching for stationary energy storage solutions and came up with the first RFB based on the electrolyte couple Fe/Cr [41].

Redox flow batteries mainly consist of two key elements: the cell stacks where chemical energy is converted to electricity in a reversible process and the electrolyte which is stored in external tanks outside of the stack and is circulated through the cell stack with pumps (cf. Figure 6). The size of the stack determines the power rating of the system (kW) and the amount of electrolyte defines the energy (kWh) that can be stored.

Although flow batteries comprise similar elements as most batteries, they differ from conventional batteries as the reaction occurs between two electrolytes, the anolyte and the catholyte, rather than between an electrolyte and an electrode.

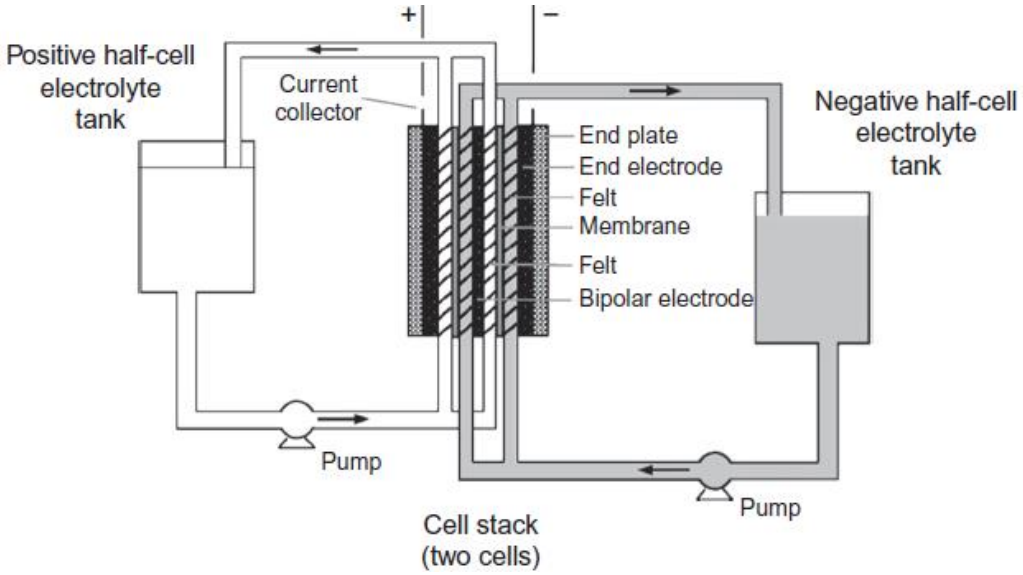


Figure 6. Schematic structure of a redox flow battery. [42]

Similarly, to all other batteries, the basis of the RFB are redox reactions. During discharge electrons are removed from the anolyte (negative half-cell) and via the external circuit they are transferred to the catholyte (positive half-cell). An Ion Exchange Membrane (IEM) separates the two electrolytes from each other but allows the passage of ions, which closes the electric circle. The flow of electrons is reversed during charge. Now the reduction occurs in the anolyte and the oxidation takes place in the catholyte.

Discharge:

$$Oxidation: A \rightarrow A^+ + e^- \qquad (2)$$

$$Reduction: C^+ + e^- \rightarrow C$$

Charge:

$$Oxidation: C \rightarrow C^+ + e^- \qquad (3)$$

$$Reduction: A^+ + e^- \rightarrow A$$

### *2.2.4.2 Different RFB technologies*

Flow batteries are characterized by the type of the chemical electrolyte couples which have been used. There are three groups, which are distinguished by the phase of the electroactive species which are either 1) all liquid phase, 2) all solid phase or 3) hybrid where there are two phases involved e.g. liquid and gaseous. Examples are 1) all vanadium, 2) lead-lead dioxide and 3) hybrid zinc-cerium [43].

Various active redox electrolyte couples have been tested for the use as RFB. They differ in the achieved cell voltage and provided energy densities, which are summarized in Table 4.

The iron-chromium RFB has been studied extensively at NASA. The battery reaction involves $Fe^{3+}/Fe^{2+}$ at the negative electrode and $Cr^{3+}/Cr^{2+}$at the positive electrode. Due to the kinetic rate of reduction of $Cr^{3+,}$ a catalyst is required on the chromium electrode. Catalysts which have been applied are gold, lead, thallium and bismuth [43].Yet, those are expensive and the energy density of the system is very low.

Early commercialization was hindered by the lack of affordable ion exchange membranes which had enough chemical stability in the highly oxidizing electrolyte. The exchange membranes are not completely impermeable to the species of ions which are supposed to be separated so that over time some amount of *cross contamination* of the electrolytes in the two half cells occurs, which results in performance degradation [44].

The vanadium redox flow battery avoids this cross-contamination problem by using different charge states of vanadium ions in the two half cells. In this case cross contamination degrades the energy efficiency but this degradation is easily recoverable. The vanadium redox flow battery has the highest market maturity. It employs the same metal in both half-cells. The negative contains $V^{2+}/V^{3+}$ and the positive $V^{4+}/V^{5+}$. Vanadium can be dissolved in different supporting electrolytes which are sulfuric acid and hydrochloric acid. The use of HCl allows a greater operation temperature range, however during charging the generation of HCl vapors has to be monitored, which is why usually the maximum SOC range is limited to less than 85 % [42].

Another option is a Vanadium-Bromine RFB, which has the advantage of higher energy density. Till now, the main challenge for the V/Br RFB is the need to prevent the oxidation of bromide ions and thus the formation of bromine vapors when the battery is charged.

Hybrid redox flow batteries involve either solid species or gaseous species in one half-cell. Zinc-bromine or zinc-chlorine are the best-known examples of two phase RFB.

Table 4. Comparison of different RFB technologies.

| | **All-Vanadium in $H_2SO_4$ (G1)** | **V/Br in HCl (G2)** | **All-Vanadium in HCl (G3)** | **Fe/V In mixed $SO_4^{2-}/Cl^-$** | **Fe/Cr in HCl** | **Zn/Br** |
|---|---|---|---|---|---|---|
| **Negative** | $V^{2+}/V^{3+}$ | $V^{2+}/V^{3+}$ | $V^{2+}/V^{3+}$ | $V^{2+}/V^{3}$ | $Cr^{2+}/C^{3+}$ | $Zn/Zn^{2+}$ |
| **Positive** | $V^{4+}/V^{5+}$. | $Br^+Cl^-$ $/ClBr_2^-$ | $V^{4+}/V^{5+}$. | $Fe^{3+}/Fe^{2+}$ | $Fe^{3+}/Fe^{2+}$ | $Br^-/Br_2$ |
| **OCV [V] @50% SOC** | 1.3-1.4 | 1.2 | 1.4 | 0.85-1.0 | 1.18 | 1.8 |
| **Electrolyte energy density (80% SOC) [Wh/L]** | 38-50 | 42-63 | 35-40 | 20-25 | <25 | 60 |
| **Specific energy density (80% SOC) [Wh/kg]** | 27-36 | 30-45 | 35-40 | 15-20 | <10 | 65-75 |
| **Temperature range/ optimal Temp. [°C]** | 10-40 /35 | 0-50 | 0-50 | 5-50 | -/25 | 20-50 |

Data from [42], [43], [45]

### 2.2.5 CellCube vanadium redox flow battery system

CellCubes are based on vanadium redox flow technology. The battery is offered for large scale storage applications in different variations: due to the modular structure the nominal power and energy storage capacity can be chosen separately from each other.

### 2.2.5.1 *Working principle*

The working principle is based on redox reactions as described before. Negative and positive vanadium containing electrolytes are stored in individual tanks and are circulated through the power stacks where they are oxidized/reduced when dis/charged. The negative half-cell employs the $V^{2+}$ /$V^{3+}$ redox couple whereas the positive half-cell is filled with the $V^{4+}$/$V^{5+}$ redox couple. During the discharge cycle, $V^{2+}$ is oxidized to $V^{3+}$ in the negative half-cell and an electron is released to the external circuit. The positive half-cell accepts an electron and $V^{5+}$ in the form of $VO_2^+$ is reduced to $V^{4+}$ in the form of $VO^{2+}$. The corresponding charge and discharge reactions are formulated in equations (4)-(7). The ion-exchange is enabled with the Proton-Exchange Membrane (PEM), which selectively allows $H^+$ to pass through. The VRFB is a preferred type of RFB due to its simplicity related to the usage of the same electrolyte in both half cells. In an all-vanadium flow battery four oxidation states of vanadium occur, which can be distinguished by their color (cf. Figure 7) and when the battery is charged or discharged only the valence of the vanadium ions in the electrolyte changes.

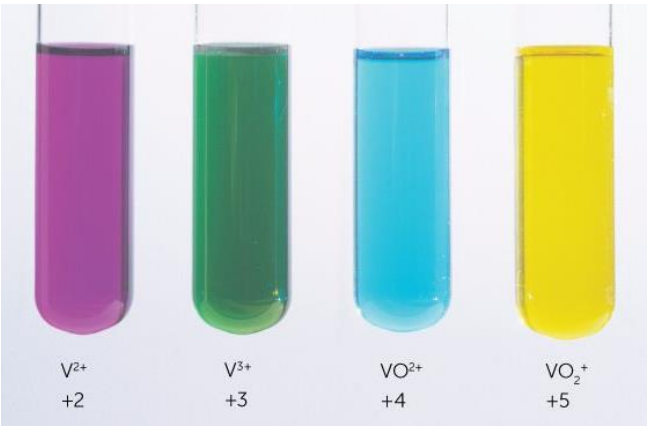


Figure 7. Oxidation states of vanadium. [46]

During charging the following reaction take place at the negative and positive electrode:

(negative) $$V_{(aq)}^{3+} + e^- \rightarrow V_{(aq)}^{2+} \quad (4)$$

(positive) $$VO_{(aq)}^{2+} + H_2O \rightarrow VO_2{}^{+}_{(aq)} + 2H_{(aq)}^{+} + e^- \quad (5)$$

During discharge:

(negative) $$V_{(aq)}^{2+} \rightarrow V_{(aq)}^{3+} + e^- \quad (6)$$

(positive) $$VO_{2(aq)}^{+} + 2H_{(aq)}^{+} + e^- \rightarrow \mathrm{VO}_{(aq)}^{2+} + H_2O \quad (7)$$

### 2.2.5.2 *Components*

In general, any BESS, in this case the all-Vanadium Flow Battery Energy System (FBES) contains several component groups (cf. Figure 8). First, the Flow Battery System (FBS) which consist of the flow cells, the storage tanks for electrolyte and the Balance of Plant (BOP). The BOP comprises all other

necessary components for operation such as electric pumps, filters, sensors, heat exchangers and the Battery Management System (BMS). To integrate the FBS into the grid additionally a Power Conditioning System (PCS) is needed, which is controlled by the Power Management System (PMS) and converts the DC output from the FBS into usable AC power. In the next section the sub-components of each of these groups are described in more detail.

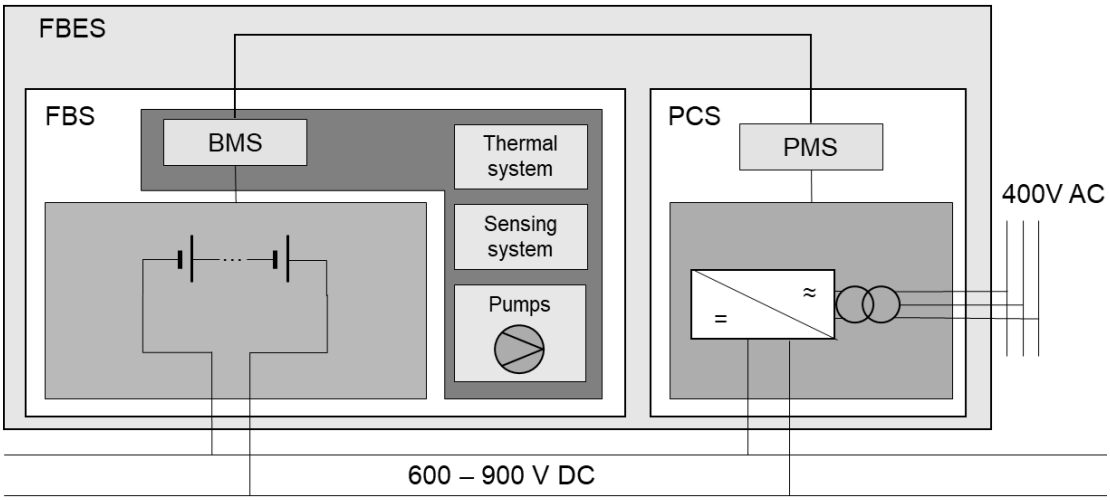


Figure 8. Schematic structure of a FBES. Adapted from Enerox.

**VRFB Stack (power unit)**

To create a cell stack multiple cells are connected electrically in series and hydraulically in parallel. The number of cells defines the stack voltage, whereas the electrode surface area determines the current. CellCubes are consist of stacks of 20 cells (earlier versions) or 27 cells.

Each cell is constructed from two half-cells, each containing a bipolar plate, current collectors, insulating frame and the electrode. To increase the current, the *electrodes* are usually composed of high surface materials like carbon or porous graphite. The electrode felt is treated to increase the surface area and heated to enhance conductivity and stability. In contrast to other batteries the electrodes do not store energy, but they offer the surface for the redox reaction to take place and the electric conductivity, so that the electrons are collected. A PVC *frame* holds the electrodes. PVC is a suitable material as it is resistant to acidic corrosion. The *current collectors* are made of copper and the *bipolar plates* of composite graphite materials. They connect the cells within a stack electrically while separating them physically, hence the material must be highly conductive but chemically stable in the acidic cell environment. The two cell-halves are separated by a *Proton Exchange Membrane* (PEM), which only allows ionic exchange to close the circuit but physically separates the two electrolytes by sealing the half cells. As PEM a sulfonated-tetrafluoroethylene-based polymer (commercially known as Nafion) proton exchange membrane is most commonly chosen, with a low internal resistance. On top of the first and last bipolar plate in a stack, current collectors made of copper and massive aluminum endplates are placed. They have threaded bolts and nuts to clamp the cell stack together, to assure a high unique pressure in the whole stack.

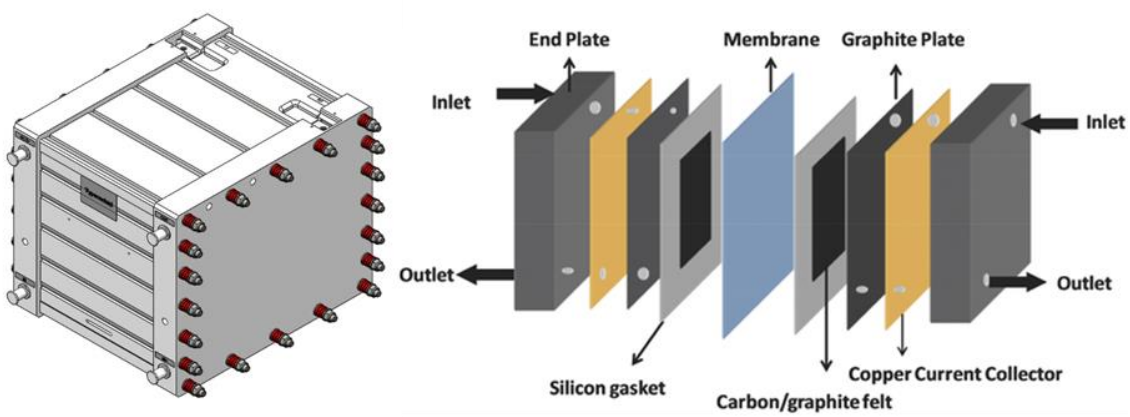


Figure 9. CellCube stack (left). Enerox.
Overview cell components (right). [41]

**Electrolyte and storage tanks (energy unit)**

Redox couple of $V^{2+}/V^{3+}$ (negative half-cell) and $V^{4+}/V^{5+}$ redox couple (positive cell) are used as soluted electrolytes. When charged the energy is stored as reduced and oxidized electroactive species in the electrolyte. This is a major difference to conventional batteries, where the energy is usually stored within the electrode structure.

To gain the active vanadium-based electrolyte when the system is installed there are different procedures. One approach uses Vanadyl-Sulfate ($VOSO_4$) dissolved in an $H_2SO_4$ solution containing $V^{4+}$ as a starting point. To obtain an SoC of zero, half the nominal energy capacity is needed for initial charge. After an initial charge and applying a reducing agent to the catholyte $V^{3+}$ (anolyte) and $V^{4+}$ Ions (catholyte) occur with the same concentration [47]. Sulphuric acid ($H_2SO_{4aq.}$) is the most common supporting electrolyte for VRFB. The acidity of the electrolyte serves the purpose of increasing the ionic conductivity of the electrolyte and of providing hydrogen ions. The total concentration of vanadium species defines the energy density but is limited by the solubility, which has a high temperature dependency. Hence, the operating range is limited to 10°C to 40°C.

The electrolytes are stored in large tanks outside the cell stacks, which are made of polymer materials to be resistant to corrosion at low pH, and when charged or discharged are circulated through the cell stack. The electrolyte in each cell can be divided into the negative electrolyte (anolyte) which releases electrodes during discharge and the positive electrolyte (catholyte) which absorbs the electrons in the discharge process. Hence, at least two tanks exist, one for the anolyte and one for the catholyte. Yet, to increase modularity some CellCubes have more tanks and pump circulation systems.

The electrolyte enters the cells in a parallel setting (hydraulic). In this case each cell is at the same SOC and has approximately the same voltage. Also, the pumping energy is lower than for a series flow. However, for parallel flow shut currents occur due to the interconnection of the common manifold, which can be an issue as shunt currents reduce the overall efficiency [42]. As visible in Figure 10, each stack is connected hydraulically via four manifolds to the electrolyte tanks and circulation (one inlet and one outlet for each electrolyte).

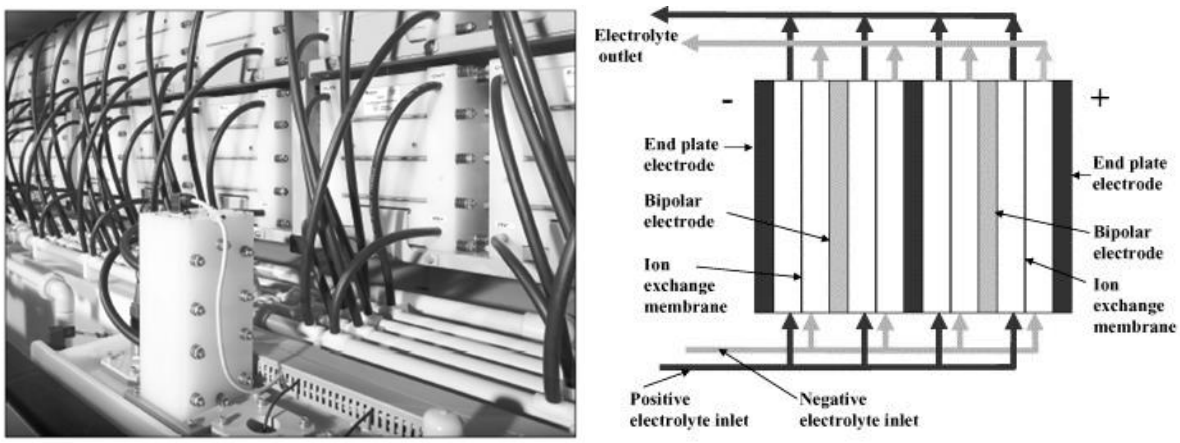


Figure 10. CellCube stacks and hydraulic connections (left)
Parallel distribution of electrolyte among cells (right). [48]

**Balance of Plant (BOP)**

The BOP contains at least two circulation loops including *pumps,* piping and manifolds, *thermal management* components such as heat exchanger to regulate the electrolyte temperature and *sensing systems* that measure OCV, electrolyte temperature, pressure, leakages etc. Pumps and hydraulic systems guarantee the electrolyte circulation. The pumps are AC-grid-connected and thus require external power supply. It would also be possible to supply them directly with power from the battery, however this is difficult when the battery has not been operated for a longer time, which means that the charge in the stack is lost and cannot supply sufficient power to start the pumps. Pumps, valves and piping should be resistant in low pH environments. In large-scale containerized systems a Heating, Venting and Air Conditioning (HVAC) system is utilized to keep the temperature within its ideal operation set points.

Every FBS also contains a computer-controlled *Battery Management System (BMS)* which organizes the operating procedure to ensure efficient operation and long cycle life. The BMS is specific for the operational characteristics of the flow battery and ensures that the battery operates within its recommended design parameters. Hence, the BMS is linked to active components such as pumps and heat exchangers and sensors.

**Power Conditioning System (PCS)**

The PCS and Power Management System (PMS) covert DC to common AC and vice versa, which is then injected or taken from the distribution grid. A common architecture is to use an AC/DC and a DC/DC converter which first upgrades low and varying voltage to a higher and constant voltage. Due to the low cell and stack voltage and large SoC dependent voltage variations, the PCS for a flow battery is usually more complex than for other types of batteries [49]. PCS with low DC input voltage are required.

### *2.2.5.3 VRFB performance and special characteristics*

**Cell and stack voltage**

The standard potential $E_0$ expresses the difference between the two electrode potentials (positive and negative) at standard conditions $(25°C)$ and balanced molar concentration $c_x$ (SoC=0.5). For VRFB it is 1.26 V [42]. It is an important part of the Nernst equation, which is used to determine the equilibrium voltage $E$ or Open Circuit Voltage $U_{OCV}$ of a single cell under any conditions. As seen in (8) $E$ is also affected by the ion and proton concentration on each side of the membrane. Relating the vanadium concentration to the SOC with Eq. (15) and (16) the influence of the SoC (SoC=0 discharged, SoC=1 charged) becomes evident in Eq. (9). Herein, $c_{H^+}^0$ denotes the initial concentration of hydrogen protons and $c_V$ the total vanadium concentrations, $R$ is the universal gas constant and $F$ is the Faraday's constant [50].

In many papers a simplified Nernst equation (10) is applied, which neglects the hydrogen protons and results in lower OCV (cf. Figure 11). This can be corrected by adding the proton concentration to the standard cell potential, which is then called the formal cell potential $E_0'$, which can be obtained experimentally form measurements at an SoC of 50 %.

Nernst equation:
$$E = E_0 + \frac{RT}{F}\ln\left(\frac{c_{VO_2^+} * (c_{H+})^2 * c_{V^{2+}}}{c_{VO^{2+}} * c_{V^{3+}}}\right) \quad (8)$$

$$E(SoC) = E_0 + \frac{2RT}{F}\ln\frac{SoC * (c_{H+}^0 + c_V * SoC)}{1 - \mathrm{SoC}} \quad (9)$$

Simplified:
$$\approx E(SoC) = E_0 + \frac{2RT}{F}\ln\frac{SoC}{1 - \mathrm{SoC}} \quad (10)$$

Corrected:
$$E(SoC) = \boldsymbol{E_0}' + \frac{2RT}{F}\ln\frac{SoC}{1 - \mathrm{SoC}} \quad (11)$$

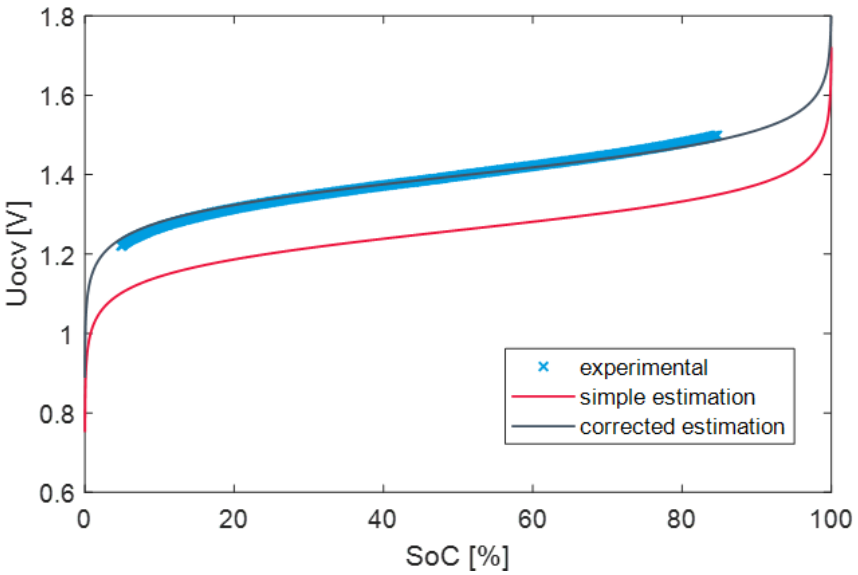


Figure 11. Comparison of OVC modeling approaches and experimental measurements with CellCube. Own elaboration.

Since the singe cell voltage is low, cells in a stack are connected in series, which means that the internal stack voltage or stack open circuit voltage $U_{ocv\ stack}$ is determined by multiplying the cell potential $E$ with the number of cells $N$.

$$U_{OCV,stack}(SoC) = N * E \tag{12}$$

Yet, when a current $I_{stack}$ is flowing through the stack, the equilibrium conditions no longer apply. Hence the stack voltage $U_{stack}$ is then defined by the difference between equilibrium potential and the internal losses $U_{loss}$.

$$U_{stack}(SoC) = \mathrm{N} * \mathrm{E} - \mathrm{R}_{int} * \mathrm{I}_{\mathrm{stack}} \tag{13}$$

**SoC calculation**

In all batteries the SoC is an important parameter, it is equivalent to the fuel gauge of a car and indicates how much energy has currently been stored in the battery. Different methods exist like coulomb counting using either expensive instrumentation or computational heavy models, OCV measurements or Kalman filters. In VRFB the SoC is exactly determined by the concentration of the vanadium species in the electrolytes. When the total vanadium concentration $c_{Vtotal}$ is the same in both electrolytes the SoC can be simplified to:

$$SoC = \left(\frac{c_{V^{2+}}}{c_{V^{2+}} + c_{V^{3+}}}\right)_{anolyte} = \left(\frac{c_{VO_2{}^+}}{c_{VO_2{}^+} + c_{VO^{2+}}}\right)_{catholyte} \tag{14}$$

$$SoC = \left(\frac{c_{V^{2+}}}{c_{V_{total}}}\right)_{anolyte} = \left(\frac{c_{VO_2{}^+}}{c_{V_{total}}}\right)_{catholyte} \tag{15}$$

$$1 - SoC = \left(\frac{c_{V^{3+}}}{c_{V_{total}}}\right)_{anolyte} = \left(\frac{c_{VO^{2+}}}{c_{V_{total}}}\right)_{catholyte} \tag{16}$$

Applying the Nernst equation (12), the SOC can be obtained from the measured open circuit voltage $E$. To measure the OCV an open circuit bypass cell is integrated.

$$\mathrm{SoC} = \frac{e^{\frac{F}{2RT}(E-E_0{}')}}{1 + e^{\frac{F}{2RT}(E-E_0{}')}} \tag{17}$$

However, as the OCV gives a value of the two half-cells assuming they are balanced, the value is not 100 % accurate, since the half cells can get out of balance due to side reactions or transfer of vanadium ions across the membrane [42].

**Losses and efficiencies**

The energy losses of VRFB systems consist of internal and parasitic losses. Internal battery losses include coulombic and overvoltage losses. Parasitic losses are related to auxiliary components and consider the energy losses for pumps, controllers and the inverter losses.

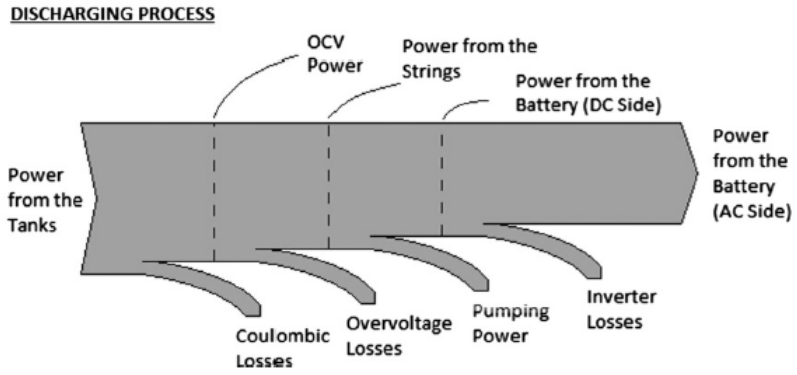


Figure 12. Losses during discharging of a VRFB system. [51]

Overpotential losses reduce the voltage efficiency and can be split into ohmic, activation and concentration losses. Ohmic or internal resistance losses are caused by the internal ohmic resistance from membrane, electrolyte and conducting bus bars between the stack during charging and discharging. Ohmic resistive losses increase when charge/discharge current/power is increased. Since those losses go as the square of current as seen in Eq. (14), faster charge or discharge results in higher losses. The activation and the concentration losses are electrode phenomena and are associated with the energy required to initiate a charge transfer. Coulombic losses are related to crossover, side reactions like gassing and shunt current losses [52].

$$P_{loss,int} = I_{stack}^2 * \mathrm{R_{int}} \tag{18}$$

Efficiencies are an important metric to assess and compare performances of storage systems. Efficiency defines the ratio of energy output $E_{out}$ to energy input $E_{in}$. Different types of efficiencies are important when looking at battery systems.

*Coulomb efficiency*

The coulomb efficiency $\eta_{coulomb}$ describes the ampere hour efficiency for one complete cycle, with $I_{charge}$ the current level during charge and $I_{discharge}$ during discharge respectively. The amount of charge that flows into a battery is not equal to the amount that leaves during discharge. Coulomb losses are caused by self-discharge resulting from ion crossover and hydrogen evolution and shunt current losses.

$$\eta_{coulomb} = \frac{Q_{discharge}}{Q_{charge}} = \frac{\int I_{discharge}(t)dt}{\int \left|I_{charge}(t)\right| dt} \tag{19}$$

*Voltage efficiency*

The voltage efficiency $\eta_{voltage}$ is a measurement for ohmic and polarization losses during cycling. It measures the ratio of integral battery voltage for discharging $U_{discharge}$ and charging $U_{charge}$ at a **constant** current.

$$\eta_{voltage} = \frac{\int U_{discharge}(t)dt}{\int \left|U_{charge}(t)\right| dt} = \frac{\eta_{energy}}{\eta_{coulombic}} \tag{20}$$

*Energy efficiency*

The energy efficiency $\eta_{energy}$ or roundtrip efficiency defines the ratio between the energy provided by the battery during discharge to the energy required during charge. Unless otherwise stated, the energy efficiency refers to the ratio of DC stack power.

$$\eta_{energy} = \frac{\int P_{discharge}(t)dt}{\int \left|P_{charge}(t)\right| dt} \tag{21}$$

DC-DC roundtrip efficiency $\eta_{energy}$ ranges around 70-87 % for VRFB and include only DC-DC conversion losses [41], [53], [54]. DC conversion steps commonly present lower losses than AC/DC conversion steps. The AC-AC roundtrip efficiency $\eta_{energy\ AC}$ considers also transformer losses from the PCS since during charging and discharging losses occur due to voltage drops across switching devices, decreasing the roundtrip efficiency.

*System efficiency*

Energy, coulomb and voltage efficiency usually refer only to the battery stack. Yet, to have an operating flow battery as seen in Figure 8 auxiliary components such as pumps, thermal management, BMS and PCS are required, which cause additional losses, called parasitic losses. Since it also includes the inverter losses, some authors refer to the system efficiency as AC-AC roundtrip energy efficiency. Recorded system efficiencies range between 50-78 % [55], [57].

$$\eta_{system} = \eta_{energy}\eta_{aux} \tag{22}$$

**Response time:** The time required for the system to deliver full power depends whether it is in hot-standby mode or not. If so, the response can be achieved within microseconds. Hot stand-by means that the electrolyte in the cells are charged and hence the electrolyte is pumped through the system [58]. However, if the pumps have been turned off and the cells are empty, it will require a few minutes to deliver full power.

**Lifetime:** Aging of a battery refers to a permanent loss of capacity as a result of battery use and/or the passage of time [59]. Subsequently, capacity fade can be divided into calendric capacity fade and exercised capacity fade. For VRFB the cycle life is theoretically unlimited because any capacity loss can be recovered by either remixing the two half-cell solutions or chemically/electrochemically rebalancing the solutions. One approach is automatic rebalancing by connecting the anolyte and catholyte tank(s) with a narrow hydraulic shunt, allowing to constantly balance the tank volumes and reverses losses via vanadium ion diffusion. Yet, other side reactions like hydrogen evolution and air oxidation require more complex rebalancing techniques. Cycle life is primarily limited by the cell components, mainly the membrane which degrades over time [42]. According to Eckroad [53] at 1000 cycles per year the stack is assumed to have a lifetime of 10-15 years. Other components like tanks, piping, power electronics are expected to have a longer lifetime of at minimum 20 years [53].

### *2.2.5.4 Advantages and remaining challenges*

Vanadium is an appealing choice since cross contamination is not a critical problem, it does not release toxic vapors or gases, has low risk of explosion and can be cycled from any state of charge and discharge without permanent damage.

**Power energy independency*:*** A major advantage of all redox flow batteries is the scaling flexibility. As mentioned, the energy storage capacity is independent from battery power rating, which allows a modular structure and increases the adaptability to different applications and retrofit ability.

**Operation:**

*Thermal management* is easier and more feasible for flow batteries. Since, conventional batteries reject the heat mainly passively by thermal conduction through the case, the cell temperature remains higher and is difficult to control, which impacts the lifetime. For VRFB the electrolyte is cooled and when circulated through the stacks it works as an active coolant. Thus, the heat dissipates with the electrolyte flow during charging and discharging and the stack is cooled faster and equally.

Flow batteries show lower *self-discharge rates* than other battery types like Nickel-Cadmium or Alkaline batteries. The positive and negative electrolyte are stored in two separate tanks, so that no self-discharge occurs, except in the cell section, when the VRFB is not in use [60].

In contrast to other RFB the all-vanadium flow battery does not require a catalyst for each half cell reaction since the reaction rates are relatively fast. In addition, as mentioned previously, *cross-contamination* in vanadium flow batteries does not cause significant problems, as with earlier flow battery types (i.e. Fe/Cr). Due to the usage of vanadium in both half cells the process can be reversed.

**Safety:** VRFB does not share the same fire or explosion risk as LiB since the electrolyte is not flammable and if any deviation from safe operating parameters is noticed, the system pumps will trigger a shutdown and reduce the risk of large amounts of $H_2$ generation. Also, in comparison to PbA batteries the VRFB is categorized as safer. VRFB does not include toxic lead and although the vanadium is toxic in powder form, the electrolyte only contains small concentration levels. In addition, shock hazard only exists when there is electrolyte in the cell stack whereas if the system is turned off or in cold stand-by there is no measurable voltage. Most other battery types always keep a charge and have a constant shock hazard risk.

**Cycle and service life:** As mentioned the long cyclability is a major advantage. More than 20,000 charge and discharge cycles have been demonstrated [61].

**Environmentally friendly**: Since the transition towards renewable energies is driven by environmental concerns, also the installation and use of BESS should investigate associated environmental impacts. The Life Cycle Assessment (LCA) by Weber et al. [62] revealed that the environmental impact of VRFB is low in particular in comparison to LiB but also to PbA when used in combination with renewables. Long lifetime and the recyclability of the electrolyte reduce the impact. The main contributors to the total GWP are the production of Vanadium Pentoxide ($V_2O_5$) in countries like South-Africa with a coal-dominated electricity mix and the emissions associated with the energy losses during the usage phase.

Despite major technological advances, VRFB still face a number of challenges:

**Energy density:** An existing challenge which limits practical applications to stationary energy storage is the low specific energy density of 25-30 Wh/kg. The energy density in VRFB depends on the concentration of vanadium species in the electrolyte. Unfortunately, the solubility is limited due to the precipitation of solid vanadium compounds, which restricts the maximal concentration of active ions and thus the energy density, which is smaller than most other ESS. Due to precipitation in the $V^{5+}$electrolyte at temperatures above 40°C and solidification of vanadium oxides in the $V^{2+}$and $V^{3+}$electrolyte at temperatures below 10°C the vanadium concentration in sulphuric acid is limited to approximately 2 M [43].

Flow batteries suffer from **parasitic energy losses** related to energy requirements from pumps and leakage currents [63]. RFB rely on liquid electrolytes rather than gaseous like in a fuel cell. The viscosity is higher and pipe cross sections have to be larger, which means higher pressure drops and **pumping losses** [64]. Besides that, stacks containing in series-connected cells fed hydraulically in parallel with circulating electrolyte will experience Shunt Currents (SCs).

**Initial cost:** Although cost is expected to decrease significantly in the future, the initial battery investment costs per battery power (~540 €/kW) are still higher than for other battery technologies like lead-acid or lithium-ion based batteries. The initial costs per energy of VRFB (~460 €/kWh) can compete with lithium but are higher than lead-acid [35]. System cost which include inverter and installation cost are 10-20 % higher. The electrodes and Nafion PEM membranes are the most costly component of the power stack and researchers are still searching for cheaper materials [65].

# 3 Integration of ESS into microgrids

The integration of a VRFB into a MG brings up certain issues and challenges, which need to be solved to guarantee proper operation. The first integration concern is to identify suitable applications and ways how a ESS like VRFB can bring economic benefit. Beyond that, information is necessary on what the control and operation architecture of microgrids looks like and which strategies prevail to identify the optimal schedule. The chapter focuses on the operation of ESS in MGs. Although proper storage system sizing and the determination of the right location are important decision processes as well, they are excluded in this thesis due to time and scope limitations.

## 3.1 Applications of ESS in microgrids

Literature suggests various use cases for VRFB in microgrids. It should be noted that studies are inconsistent in terms of definition and nomenclature of different stationary energy storage applications [66]. For this thesis the classification scheme proposed by Battke and Schmidt [67] is adopted, which distinguishes the applications according to the main source of value creation and its location in the power system value chain (cf. Figure 13). The original aim during the development of the VRFB was load following, allowing to operate fossil generation at their maximum efficiency points. Current relevant microgrid applications are focusing on renewable energy integration and ancillary services in the form of frequency control.

| | Generation | | Transmission & Distribution | End-consumer |
|---|---|---|---|---|
| | Fossil | RET | | |
| *Power Quality* | | RET Smoothing | Frequency & Voltage Regulation | Endconsumer PQ |
| *Power Reliability* | Black Start | | Reserve Capacity | Emergency Power |
| *Increased Utilization of Existing Assets* | Load Following | RET Firming | T&D Investment Deferral | Increase of Self-Consumption |
| *Arbitrage* | | RET Arbitrage | Wholesale Arbitrage | Arbitrage with flexible grid tariffs, load shifting |

RET Integration: Directly Indicrectly

Figure 13: Most relevant applications for energy storage systems in Microgrids. Adapted from [67]

### 3.1.1 Power quality

Power quality applications compensate electrical disturbances and anomalies in order to maintain the performance of the power system at an optimal level. They include all operations that are necessary to guarantee reliable and stable power supply without deviations from optimal *frequency* and *voltage*

levels.

On the generation side, BESS allow to smooth RES-infeed without creating voltage sucks or harmonic distortions. On the distribution and transmission level, BESS services can be used to control the grid frequency and voltage level. *Frequency regulation* is achieved by active power balancing between load and power input from generation units. It is particularly important for microgrids which have a lot of intermittent renewables but no inertia. BESS with low response time, sufficient power and high ramp rates can be used to control the frequency and act as virtual inertia.

In grid-connected microgrids there is access to the frequency capacity control markets which has three types of reserve products for frequency control: primary control known as Frequency Containment Reserve (FCR), secondary or automatic Frequency Restoration Reserve (aFRR) and tertiary or manual Frequency Restoration Reserve (mFRR). Finally, some European TSOs also contract Replacement Reserve capacity (RR), yet in Germany this is not the case. The existing markets for frequency regulation differ depending on the required response time (few seconds to minutes), whether they are activated automatically or manually and the delivery duration (cf. Figure 14).

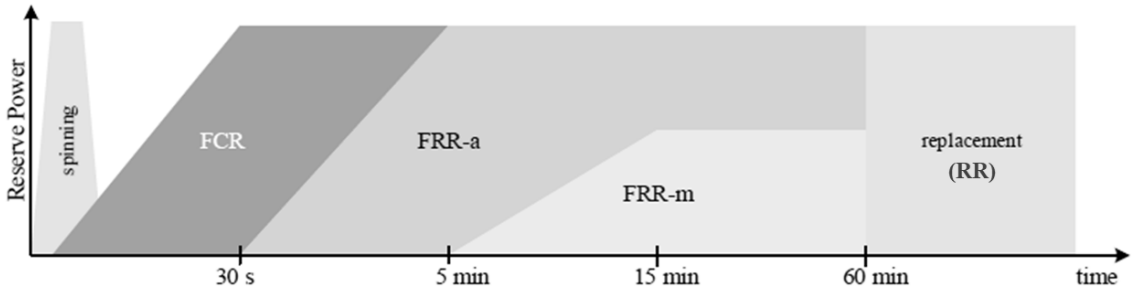


Figure 14. Overview of European balancing market products. [68]

Apart from frequency regulation *voltage support* is an additional power quality service to maintain a stable voltage level in the distribution and transmission grid. It requires a quick response to fluctuations in reactive power by adjusting the system voltage.

### 3.1.2 Power reliability

Power reliability applications create economic value by assuring an uninterrupted power supply and support during emergencies. In case of power outages battery storage can provide emergency power to organize the black start of other generation devices, for important grid assets such as protection and control devices. Also end consumers with critical needs such as hospitals, data centres, security equipment or sensitive industries for example producing semiconductors, where even small outages would harm the quality of the product, rely on back-up power applications. Although the frequency of activation is very low (< 10 cycles a year), in order to be able to respond immediately if an outage occurs, the BESS will have to be in standby mode and assure a high SoC to provide sufficient energy till the electricity system is restored.

### 3.1.3 Improved utilization of existing assets

Increased utilization of existing assets summarizes those applications which create value by improving the use of existing generation or transmission capacity. ESS are able to help the integration of renewables since they provide dispatchable load and allow RES to follow the load curve, reducing the need and costs for additional fossil generation or large RES overcapacities. The main value is created by avoiding RE curtailment and reduction of expenses for expensive peaker technologies (e.g. diesel or gas), with high operation and fuel costs and emissions respectively.

In power networks congestion occurs, which conventionally will require transmission or distribution line reinforcement (e.g. cables, transformers). However, such investments require long planning and lead to high costs or even public resistance when new lines must be built. In those cases, large-scale batteries can be used for load leveling, which involves storing power during light loading and delivering it locally during periods of high demand. Congestion management via load leveling or peak shaving reduce the load factor and thus thermal overload and this way allows *investment deferral* and helps MGO/TSOs/DSOs to postpone or avoid network reinforcement. Load-leveling is similar to peak-shaving and the terms are often applied interchangeably although peak shaving focuses more on a short term reduction of the maximum peak (cf. Appendix A-1)

By using ESS for load-shifting, prosumers (e.g. with solar PV) can increase their self-consumption and thus make optimal use of their renewable asset. In cases where the cost of generation from customer site-generation is lower than the retail price, it is more economic to maximize self-consumption rather than feeding back to the grid.

### 3.1.4 Arbitrage

For grid-connected microgrids, there is a possibility to trade electricity. The function of arbitrage with energy storage is similar to time-shifting. Arbitrage applications use price differentials to create economic value. The daily load fluctuations between peak and off-peak times, which is also known as the duck curve in combination with intermittent RES generation in-feed, create fluctuating electricity prices. Price volatility exists on the day-ahead market, where hourly products are traded till 24 hours before delivery as well as on the intraday spot market, which is the exchange for quarter hour products traded till 30 min before delivery. The generated electricity i.e. from renewables (RET arbitrage) is stored to sell it at times with higher demand and higher electricity prices. This became important since inflexible feed-in tariffs are being replaced by direct marketing of RES.

Whole-sale arbitrage buys energy at power markets during low prices, stores it and sells it when the prices peak.

End consumer arbitrage makes sense for all consumers with contracts that have time flexible energy prices, ESS can shift the load to times with low purchasing prices and thus provide them economic benefit. Arbitrage by load-leveling can also be beneficial for consumers who are paying a peak-power based demand charge. Examples with demand charge components in the electricity apply usually for commercial and industrial customers.

Table 5. Applications for stationary energy storage with flow batteries.

| Category | Service | | Stakeholder | Power Size (MW) | Response time | Time of discharge | Annual cycles |
|---|---|---|---|---|---|---|---|
| **Power quality / ancillary services** | RET smoothing | | Generation | | sec | | |
| | FCR (pos & neg) | Primary Frequency Control | | 1-100 | ms-sec | 1-30 sec | 1000-5000 |
| | FRR-a (pos & neg) | Secondary Frequency Control | | 1-100 | sec-min | sec – 15 min | 1000 |
| | FRR-m (pos & neg) | Tertiary Frequency control | TSO /DSO<br>Microgrid operator | 1-100 | 10-15 min | 30 min – 2h | 10-100 |
| | RR | Reserve Replacement. Voltage control | | 1-10 | ms | sec-1 min | 1000-5000 |
| | Voltage support | Reactive power provision | | 130 kW-3 MW | ms | 5 sec-1 min | 1000-5000 |
| **Power reliability** | Black start | | Generation asset owner | 0.1-400 | <1h | 1-4 h | <1 |
| | Reserve capacity | | DSO, TSO, MGO | 10-2000 | <15 min | 15 min-2 h | <10 |
| | Back-up security | | Industry, Public Sector (hospitals, military), MGO | 1 kW-10 MW | sec | 1 min – 10 h | <10 |
| **Improved utilization of existing assets** | Integration of RES<br>Load following | | Generation<br>Microgrid-Operator | 10-500 | min | 2-10h | 300 - 500 |
| | Investment deferral<br>Congestion management | | DSO, TSO, MGO | 10-200 | Sec-h | 1-10h | 300-500 |
| | Increase self-consumption | | Prosumer | 1 kW-10 MW | <15 min | min-h | 300-3000 |
| **Arbitrage** | RET & Wholesale Arbitrage | Day-ahead<br>Intraday market | Generation asset owner, MGO | 100-2000 | >1h | 8-24h | 200-1000 |
| | Time variable contracts | | Industry, households | | | | |

Data from [33], [35].

## 3.2 Operation and control of microgrids with ESS

To exploit the benefits of microgrids and their energy storage devices, advanced tools and techniques assuring optimal operation and management are necessary. To implement these, different control architectures exist.

### 3.2.1 Microgrid control architectures

Control architectures can be **communication-based** or **autonomous.** In the latter, no information is exchanged but the control actions are implemented based on local measurements.

In an autonomous MG control scheme, each DG or battery has a local control but there is no communication link between the controllers. The droop control method is the most popular method to for communication-less EMS. It uses the drop characteristics of voltage amplitude and frequency to signal the DERs or storage to insert more or less power into the microgrid [69]. The obvious advantage is that no communication technology is required which increases reliability. However, there are essential drawbacks. Neither nonlinear loads nor nonlinear load sharing between DERs can be considered. The resulting mismatch in output can cause stability problems [70].

Depending how the information is exchanged, the communication-based control scheme is further divided into different categories. Each of those can be realized using different communication technologies such as microwave, power line carrier, fiber optics, infrared, or wireless radio networks.

In the **centralized control** strategy, the MGCC has a major role. It monitors, collects and processes all information, and accordingly sends all the set points for all the controllable units in the microgrid to the Local Controllers (LC) [69]. It is called centralized, because the MGCC “knows everything” in the MG. The advantage of this set-up is the simplicity of implementation and the observability of the whole system in real time. Yet, finding a global optimal solution will require more processing speed the more units are connected to the system and a failure in the communication system can lead to an overall system shutdown. It is very suitable for small scale MGs, MGs where all entities share a common goal and MGs which are already fixed and will not require expandability [16].

In a **decentralized control** architecture, the MGCC does not exist or has limited functionality. Instead all the local controllers are connected and communicate with each other and make their own decisions. Algorithms decide based on the information from local measurements and neighboring devices. The architecture is also called a multi-agent system. The approach tries to simplify large complex problems to small and autonomous subsystems and uses e.g. neural networks or fuzzy systems to identify each DG operation point [16]. The advantage is that is easier to scale up, as new devices can be added or removed via plug and play. Besides, the computation burden is smaller and divided between the local controllers and MGCC/EMS only needs to perform information sharing/coordination [71]. Yet, the decentralized operation is more complex, requires good synchronization among the LC units and information security is more critical [14].

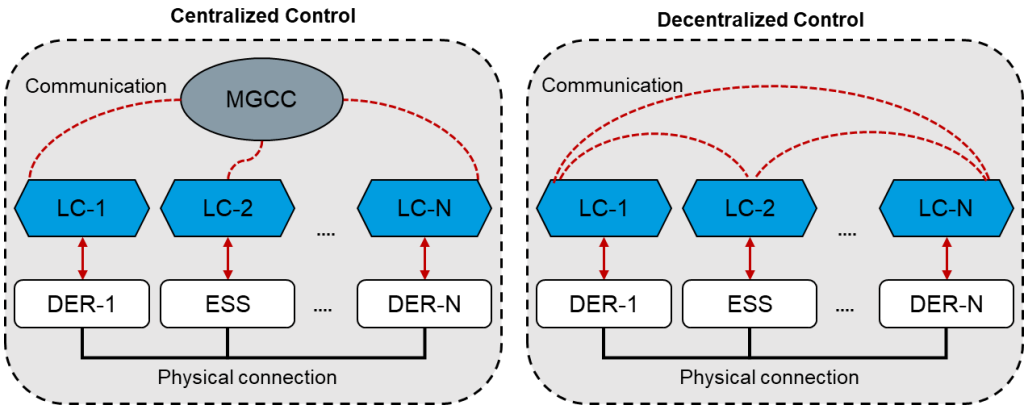


Figure 15. Centralized versus decentralized MG control. Own elaboration.

As an overall microgrid control architecture **hierarchical control** is widely accepted and standardized. Depending on the intelligence of the local controllers, it can be designed as more decentralized or centralized. Literature suggests hierarchies with three to four levels from local power generation control with RESs (first level) to synchronizing activities of the MG with other MGs and the main grid (fourth level). It should be noted, that the terminology is not coherent among papers. Palizban and Kauhaniemi [72] places the energy management functions into secondary control. This thesis takes the terminology from the authors in [14], [18], [73] who propose a hierarchical control structure with four levels/blocks.

*Level one* is the inner device control regulating each DER voltage, current output based on the incoming reference signal, assuring device fault protection etc. It performs simple actions such as droop control or system shutdown when communication is lost, to support microgrid stability [74].

The reference value for the inner control is generated by the *secondary level* control, in charge of the system stability and power quality control such as voltage and frequency restoration. It is usually implemented on local controllers. In conventional grids the secondary control utilizes rotating inertia, however in MG which apply DC/AC converters and other electronic interfaces, this is not possible. Converters can be distinguished into grid-forming and grid following. Grid-forming converters work on voltage control. In island mode at least one of the MG converters needs to operate in this mode to provide the voltage reference for other converters. Grid-following converters apply current control via PI or PR controllers.

*Tertiary level* attempts to optimize the MG operation based on the defined interests, mostly economic. The tertiary control collects information from the MG itself and the main grid, forecasts and schedules the system with included look-up tables or optimization algorithms. It measures frequency and voltage amplitude, compares the measurements with the incoming references from the main grid and sends out signals to the secondary control based on the measurement error.

Finally, *level four* includes grid interactive control functions such as managing the power connection and information exchange between the MG and the main network and the distribution management system. It sees the microgrid as one entity. By measuring the P/Q ratio at the PCC the grid's active and reactive power can be compared with the desired reference.

### 3.2.2 Energy management system

Whenever there are various energy sources involved in a microgrid or flexible loads, that need to be “scheduled” an EMS is required [75]. The EMS serves as the main controller in the microgrid control system. It can control the DERs and BESS by communicating them an optimal operation point (power output, frequency).

The **EMS core level functions** include *Dispatch* and *Transition*. The dispatch function dispatches individual devices in a specific operation mode and with specific setpoints according to operational requirements. The dispatch has to serve the loads in terms of power while maintaining power quality requirements specified by the connection agreement. The exchange levels (P, Q) at the POI are also determined as part of the dispatch function. The transition function supervises the transitions between “connected” and “islanded” state. There are four main transition modes based on the desired state and whether an error has occurred: unplanned islanding, planned islanding, reconnect and black start. Permanently islanded off-grid MG only implement the dispatch function. The dispatch function operates on a time-range of hours to minutes, while the transition function has a time frame of milliseconds.

In turn, the EMS dispatch ensures the availability of the assets and matches total production and demand in an optimal way. To determine the optimal set points, data monitoring, data analysis and forecast predictions of various parameters including generation, load, grid states etc. are required. Based on these different sub-functions the MG-EMS can be structured into a modular architecture.

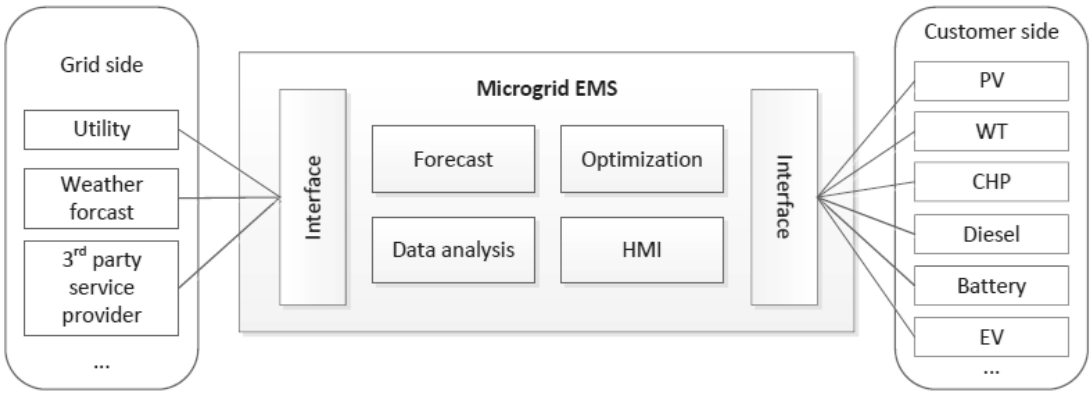


Figure 16. Modular architecture of a microgrid energy management. [76]

Each module has different functional requirements:

I. Forecasting activities

One way of dealing with uncertainty, is to make forecasts and to make decision based on these. Forecasting activities include load, price and generation forecasting and are critical to avoid any mismatches in the microgrid. The more accurate the forecasting system the better the performance of the EMS. Nonetheless, forecasting is challenging in microgrids due to the intermittency of DERs and uncertainty regarding consumption behavior. Forecasting is ideally executed in various time scales (hour-ahead, day-ahead etc.) and then fed into the optimization module of the EMS. The nature of the predictions is that they are quite good for the upcoming minutes or hours, but the further they look into

the future, the larger the errors will get. The forecasting time horizon is classified into very short-term (from second to half an hour), short-term (half an hour to 6 h), medium-term (6 h–24h), long-term (>24 h). Very short term is used for achieving dynamic control, whereas short term is used to schedule the energy flow among power generators and medium and long-term for price settlements or maintenance scheduling [77]. Existing studies use historical data, weather data, mathematical models, machine learning and societal data to generate accurate predictions.

The existing forecasts can be classified into three typical approaches: *physical* methods, *statistical* methods and *computational intelligent* methods [78]. Latest state-of-the art research focuses on computational algorithms, which neglect the inner physical model and apply neural networks which can learn from historical data. The simplest way is to perform a persistence method, which assumes that the future is highly correlated to the past and thus shows good performance for short term predictions.

II. Data analysis

To monitor and optimize the microgrid operation, the EMS must acquire, processes and store different signals: including unit and MG powers, voltages and currents, grid frequency, power factor at PCC, battery SoC, rotation speed and unit temperatures. In addition, it needs to be able to detect the availability status of ESS, generation assets, the PCC switch. The data is analyzed to improve the performance of the forecast and the optimization model.

III. Human machine Interfaces

The HMI module has the functionality to allow different users / stakeholders to monitor the system and modify the input parameters. It aims at providing understandable information rather than raw data. Hence, the data from different devices, the PCC and the aggregated microgrid is visualized. Relevant stakeholders are the MGO, the DSO and flexible asset owners.

IV. Optimization

Every EMS needs a suitable decision support model, which is responsible for the decision making, sending optimal control set points to each generation, storage and dispatchable load unit. The MG scheduling is typically formulated as a mathematical optimization problem, seeking to minimize or maximize a real function. The main objective needs to be defined, it can vary and depends on the MGO's needs but usually includes minimizing the operation costs of the microgrid, while maintaining grid stability. While optimization as part of MG sizing tools regards initial capital costs as influenceable, for the MG-EMS dispatch and scheduling function pre-defined BESS and DER size are considered.

The objective formulation should allow multiple applications to different stakeholders (grid operator, consumer, asset owner). Secondary goals can be maximizing RES shares, minimizing environmental impacts or minimizing power exchange with the grid during certain periods. When it comes to managing ESS in a microgrid, the most commonly desired objectives are the improvement of energy efficiency, extension of storage lifetime and the adherence to internal ESS constraints for e.g. no over-dis/charge [79]. In multi-objective EMS designs, it will happen that constraints are conflicting and thus it will be difficult to identify an optimal decision.

### 3.2.3 Scheduling methods for optimal MG operation

The MGCC is the physical entity responsible for ensuring optimal MG operation, to do so the EMS comprises algorithms, energy management strategies, optimizing the power flows and determining the economic dispatch. Apart from traditional rule-based strategies, various optimization-based techniques have been applied by research to solve the problem of energy management in microgrids. The choice is essential for the operation and determines the microgrid performance [17]. They can be distinguished based on several categories:

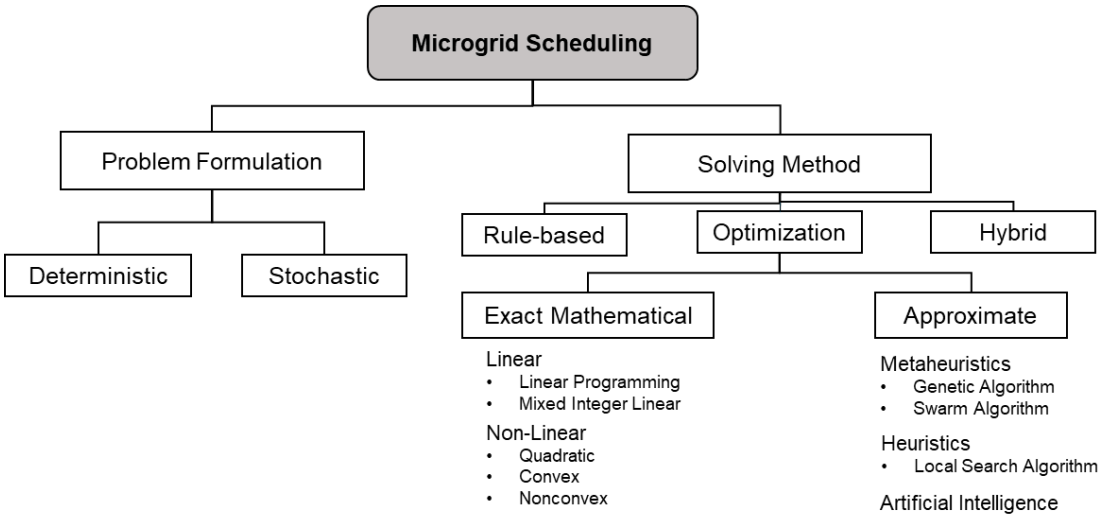


Figure 17. Techniques used for scheduling of dispatchable resources in microgrids. Own elaboration.

**Rule-based strategies** determine the reference points on the basis of certain input parameters of the present situation and predefined scenarios making use of decision trees. Since no input of future periods or forecasts is used, they are called reactive techniques. Their advantage is the simplicity and runtime performance, which allows real-time control, but they do not generate optimal output results [20].

**Optimization-based strategies** can identify local and global optima, based on maximization or minimization of an objective function under satisfaction of set constraints. In the context of the microgrid scheduling problem different optimization approaches have been discussed. Depending on the mathematical formulation of the objective function and constraints (deterministic or stochastic) and solving methods (mathematical exact or approximate) different cases can be identified [80].

*Deterministic* optimization models apply analytical properties and relations. They have known inputs, generate a unique set of outputs and do not contain any random variables. For an identical input one specific optimal output will be obtained. Yet, since the accuracy of the output solutions depends on the accuracy of the input variables, the presence of uncertainty will often result in a deviation from the real-world optimum for the underlying problem [81].

*Stochastic* optimization models are applied to handle the prevailing uncertainties, which are caused by the intermittent nature of RES, fluctuating loads and market prices. In contrast to deterministic models the random variables appear in the objective function or the constraints. The uncertain inputs have a probabilistic distribution function, which can be estimated. Since the objective function contains random

influence an identical input will return different or a distribution of output values.

The methods to solve the formulated problem, can be placed in two broad categories: exact and approximate methods. As solving methods mathematically *exact algorithms* are able to find the global optimum but require the design of a model and mathematical problem formulation. They can be further distinguished based on the problem type, whether the problem is linear or non-linear, convex or non-convex, continuous or discrete. A mathematical problem is called linear when the objective function and constraints are linear. A common linear approach applied for EMS is Mixed Integer Linear Programming (MILP) i.e. [20] [79]. MILP solves linear optimization problems where some decision variables have integer values while others are continuous.

If any term is non-linear the whole problem is categorized as non-linear optimization [20]. A non-linear example is Quadratic Programming (QP), which is similar to linear programming but with the addition of a quadratic term in the objective function.

*Approximate algorithms such as heuristic or meta-heuristic solving* approaches implement random or knowledge-based search processes to identify the approximate optimum. Usually they are applied when solving speed is relevant or exact methods cannot find an optimum. They can handle non-linear and non-convex objective functions and constraints. Nevertheless, due to the random nature the quality of the solution and its optimality and completeness cannot be guaranteed. Moreover, if the problem size becomes more complex, the likelihood of finding the global solution decreases [83].

Examples in literature of meta-heuristic methods apply bio-inspired Genetic Algorithm (GA) and Swarm algorithms. The paper by Chen et al. [9] developed a Smart Energy Management system which optimized the MG operation with a matrix based Genetic Algorithm. GA is an adaptive search technique derived from natural evolution and its principles of natural selection and “survival of the fittest” [9]. Given a set of current solutions, the population, random changes are applied to generate better solutions. Another approach suggested by Li et al. [84] proposes an EMS strategy using Particle Swarm Optimization (PSO), which is a method that iteratively updates the best candidate solution by making use of swarm intelligence. It was inspired by a swarm of birds looking for food.

All optimization-based EMS can be operated in either open or closed-loop fashion. Whereas early versions adopted open loop approaches such as day-ahead optimization, which implements the set points from a single optimization for a whole day based on a day-ahead prediction, recent systems are using Receding Horizon (RH) optimization techniques. RH has the advantage enabling the integration of feedback loops updating system states from the MG and perform a reoptimization based on the updated input.

# 4 Proposed energy management scheduling approach

This chapter describes the mathematical formulation of the scheduling optimization problem for a grid-connected microgrid, which will determine the operation regime of the flow battery. The main objective is to provide a tool that optimizes the battery operation in such a way that maximum economic value can be obtained within the MG. The mathematical models for all controllable resources including the vanadium redox flow battery system and a lithium-ion battery system as well as relevant constraints are defined, and the chosen solution approach is explained. As discussed in the previous chapter the EMS is typically implemented as one level of a hierarchical control structure. Here, the dispatch problem is solved by a single entity, which schedules all units in the MG.

Different possible applications, of VRFB in a microgrid are integrated in the algorithm. The primary use case addresses the cost reduction for the MG operator by energy arbitrage in a grid-connected microgrid. Also, grid supportive operation is modeled, improving the use of existing assets and minimizing congestion and reduction of RES curtailment. Finally, model adjustments are made to perform a simplified techno-economic evaluation of a participation in frequency markets.

In order to allow the application of the energy management scheduling approach to different microgrid settings or country markets, the problem formulation in this chapter is kept general and then specified with case specific data in Chapter 5.

## 4.1 Simulation methodology

Motivated by the above analysis on existing energy management strategies in 3.2.3 and in order to deal with the uncertainties related to fluctuating renewable power output, demand and price signals, an energy management based on a model predictive control strategy is proposed. The dispatch schedule is repeatedly optimized based on the current system state and the latest forecast.

MPC is an advanced control method for multivariable control problems which accounts for current and future constraints in the optimization to determine the control action. MPC uses an internal system model to compute the behavior of the system for a finite time period, called the prediction horizon $T_p$.. It minimizes the cost function $C_k$ over the next $N_p$ steps. Only the first element $u_k(t)$ of the output control sequence $u_k \triangleq u_k(t), u_k(t+1) \dots u_k(t+T_p-1)$ is implemented for sampling duration $T_s$.

$$\approx min \sum_{\mathrm{t=k}}^{k+Tp-1} \mathrm{C_k}(t) \tag{23}$$

By repeating this calculation with a receding or rolling horizon as seen in Figure 18, the infinite minimization problem as formulated in Eq. (24), can be approximated to Eq. (23). In the RH framework the predicted values are updated every time the prediction window rolls the next time step $k+1$ which

enables the control to adapt to changes, until $k$ reaches the number of total sampling points in the prediction horizon $N_p$. This means that $u_{Np}(t)$ is realized which was predicted as $u_1(T_p)$ during the first iteration ($k = 1$). MPC is technically favorable since it naturally incorporates prediction models and constraints which ensure the MG's operation is steering along its desired path.

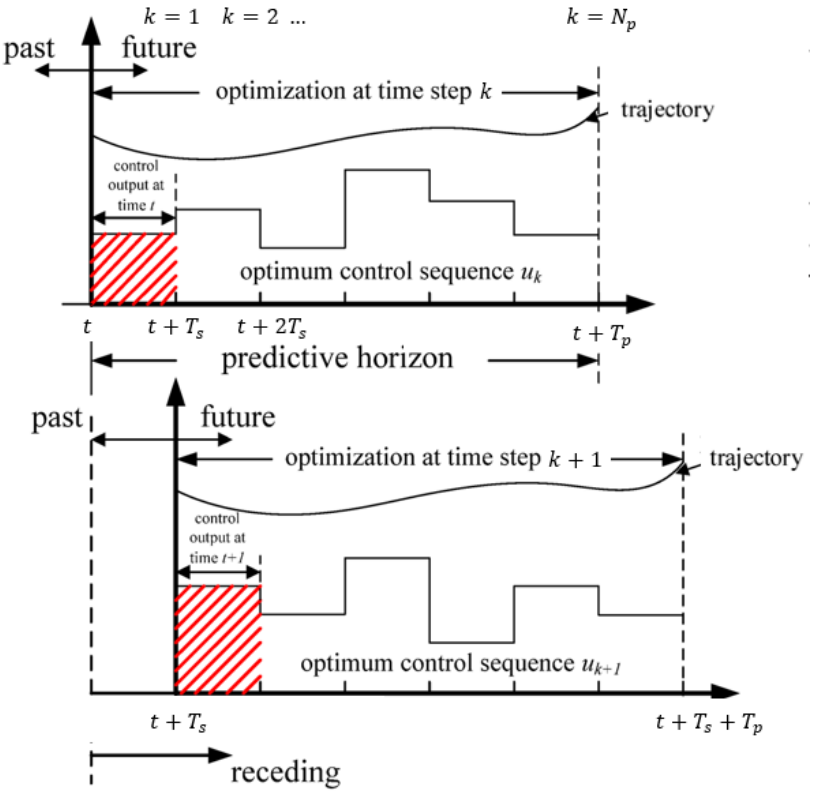


Figure 18. Schematic diagram of model predictive control. Adapted from [85]

Figure 19 shows the general scheme of the proposed MG-EMS, its input data, outputs and restrictions. As seen load, energy production and price forecast data and mathematical models of the BESS are fed into the MPC. For this thesis the feedback loop which in reality relies on various sensor data, is simulated by an error between predictions and actual values. The problem is formulated as a time discrete non-linear deterministic optimization model. The numerical solver fmincon in the Optimization Toolbox of MATLAB is used for the computation. The detailed objective function, constraints and battery models are elaborated in the following sections.

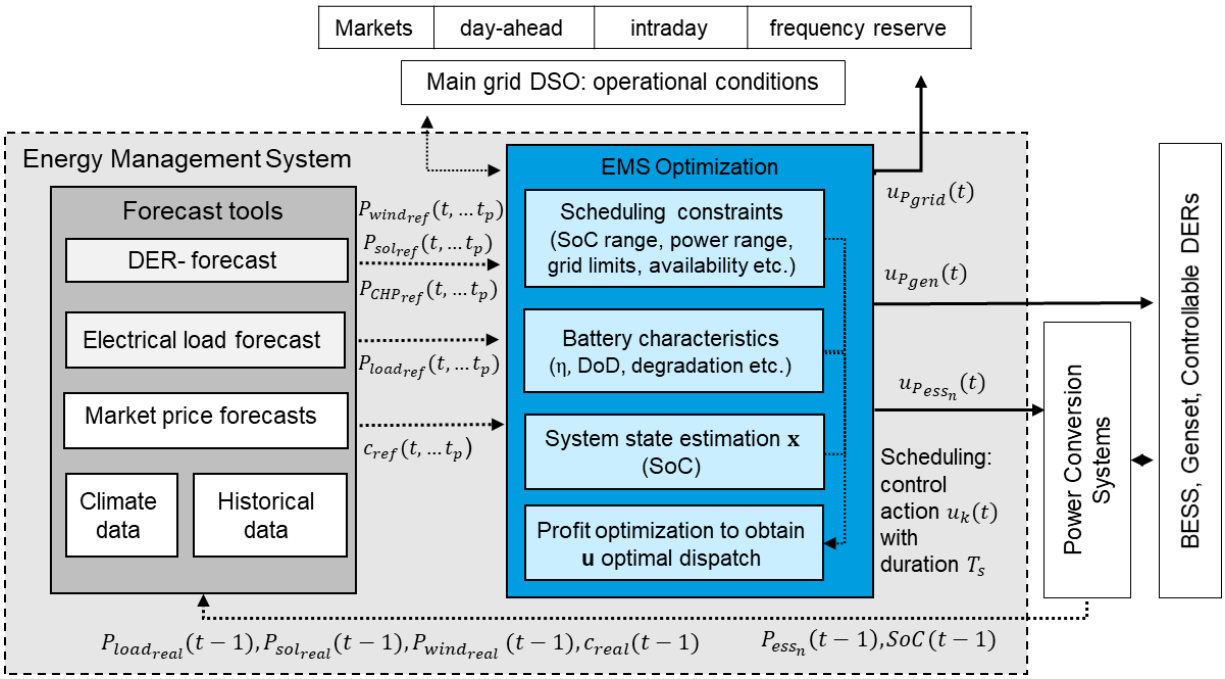


Figure 19. General scheme of MG-EMS. Own elaboration

## 4.2 MPC based problem formulation

### 4.2.1 Objective function

In this thesis, the energy scheduling of the MG is solved as an optimization problem, with the main aim of the EMS to maximize the profits from microgrid operation. In order to solve the problem with existing solvers it is translated into a minimization problem with the aim to minimize operational electricity costs. All planning, installation and capital expenditures are sunk costs and could not be altered by the energy management strategy. Hence, these costs are not included in the optimization.

Unless the microgrid is an intermediate solution, the operation time is unknown, which is why the costs are a summation over an infinite time.

$$min\ (cost) = \sum_{t=0}^{\infty} \mathrm{C(t)} \tag{24}$$

Applying MPC as an approximation this results in the following objective function in Eq. (25), which is subject to equality and inequality constraints.

$$\min_{u_k} \sum_{\mathrm{t=k}}^{k+Tp-1} \mathrm{C}(\mathrm{x_k}(t), u_k(t)) \tag{25}$$

Subject to

$$A(u_k) \leq B$$
$$Aeq(u_k) == Beq \tag{26}$$
$$u_k \triangleq [u_k(t), u_k(t+1) \dots u_k(t+T_p-1)]$$

The optimization can be run over an optimization horizon $T_n$ of 24 hours to analyze one day, yet

depending on the length of prediction horizon $T_p$ the last hours of the day will be optimized taking into account further hours of the next day.

The operational costs of a MG can be broken down into different components: The first component $C_{grid}(t)$ are the costs from power $P_{grid}(t)$ purchased minus the revenues from delivered power to the main grid e.g. via the day-ahead market at a time-varying market price $c_{DA}(t)$. The second term $C_{gen}(t)$ refers to generator fuel costs for operating a diesel or gas genset. The cost for RES generation (i.e. wind power, PV) from local assets is assumed to be zero. The third cost term $C_{ess}(t)$ incorporates degradation effects, since the lifetime of lithium-ion batteries is estimated based on cycle lifetime, rather than just calendar time. The fourth component assigns a penalty cost in case any constraints are not met (i.e. SoC boundary deviations). It only plays a role for solver algorithms that allow soft constraint violations. Finally, the last two optional components denote revenues from grid supportive operation such as avoided curtailment costs $R_{curt}(t)$ and frequency reserve markets $R_{FR}(t)$.

The objective function is subject to the following decision variables **u**: the charging/discharging power battery $P_{ess}$ of each battery, the conventional generator output power $P_{gen}$ and the quantity of power exchange with the main grid $P_{grid}$. All power variables represent the average power during a time step $k$.

Objective function

$$Min\ cost(k) = \min \sum_{\mathrm{t=k}}^{k+Tp-1} \mathrm{C(t)}$$
$$= \sum_{t=k}^{k+Tp-1} (C_{grid}(\mathrm{t}) + C_{gen}(\mathrm{t}) + C_{ess}(\mathrm{t}) + C_{penalty}(\mathrm{t}) - R_{Curt}(\mathrm{t}) - \mathrm{R}_{FR}(\mathrm{t})) \quad (27)$$

$$C_{grid}(t) = P_{grid}(t) * \mathrm{T_s} * c_{DA}(t) \quad (28)$$

$$C_{gen}(t) = P_{gen}(t) * \mathrm{T_s} * c_{fuel} \quad (29)$$

$$C_{ess}(t) = \sum_{\mathrm{n=1}}^{m} c_{\mathrm{deg}_n}(t) \quad (30)$$

### 4.2.2 Power balance and grid constraints

The constraints to be fulfilled while performing the economic minimization are provided by the prediction data and the mathematical model of the system. A vital constraint is formulated in Eq. (31) as an equality constraint. It assures the power balance within the microgrid so that supply matches the demand at any time.

Equality constraint

$$P_{PV}(t) + P_{WT}(t) + P_{grid}(t) + \sum_{n=1}^{m} P_{ess_n}(t) \quad = \mathrm{P_{load}}(t) \quad (31)$$

In addition, the power exchange with the main grid can be restricted i.e. for a grid supportive application. By limiting the amount of power sold to the grid $P_{grid}^{min}$ and purchased from the grid $P_{grid}^{max}$ it is assured that

the connection and transformer limits are satisfied and that the connected distribution grid remains within stable operations. If the MG switches to islanded mode, the grid power exchange limits will be set to zero.

Boundaries
$$P_{grid}^{min}(\mathrm{t}) \leq P_{grid}(\mathrm{t}) \leq \mathrm{P}_{grid}^{\max}(\mathrm{t}) \quad (32)$$

### 4.2.3 Battery modeling

Batteries can be modeled in several ways, i.e. electrochemical models, electric equivalent circuit models, mathematical energy flow or black box models. Depending on the model intention, the methods differ considerably with regards to complexity and time scales. Since this thesis aims to design an energy management strategy on the basis of load, generation and price input data in a resolution of 15 min to an hour, only the most important parameters are chosen for describing the batteries in operation. More complex dynamics are typically necessary at local device control level.

The batteries are directly controllable through power flow as in the rates of charge and discharge. Another key parameter is the SoC, representing the residual energy capacity, which is a significant key to regulate or control the operating states of a BESS. In the proposed model, the SoC is estimated based on the predicted control decisions for $P_{ess}$ . Separate models are defined for a VRFB and a LiB, which vary depending on technology specific characteristics.

#### *4.2.3.1 Vanadium redox flow battery model*

The battery models include the calculation of the operating state **x**, representing the $SoC_n$ or remaining energy level $E_{ess}$, variable charging/discharging system efficiencies $\eta_c(t)$ and $\eta_d(t)$ and operational constraints such as maximum charging $P_{ess}^{min}$ and discharging powers $P_{ess}^{max}$.

**State of charge**

$\mathrm{SoC}^{\min}$ and $\mathrm{SoC}^{max}$ in Eq. (33) denote the minimal and maximal admissible charging levels to prevent overcharge and overdischarge and differ between battery technologies. The remaining energy is implemented by applying the energy balance (cf. Eq. (34)). Since all values are time-discrete the output power $P_{ess.}$ is multiplied with sampling duration $T_s$.

$$\mathrm{SoC}_{\mathrm{n}}^{min}(\mathrm{t}) \leq SoC_n(\mathrm{t}) \leq \mathrm{SoC}_{\mathrm{n}}^{max}(\mathrm{t}) \quad (33)$$

State estimation **x**
$$E_{ess,n}(t) = \begin{cases} E_{ess,n}(t-1) - \eta_{sys,n}^{c}(t) * P_{ess,n}(t) * T_s \; for \; charge, P_{ess,n} < 0 \\ E_{ess_n}(t-1) - \frac{1}{\eta_{sys,n}^{\mathrm{d}}(t)} * P_{ess,n}(t) * T_s \; for \; discharge, P_{ess,n} > 0 \end{cases} \quad (34)$$

$$SoC_n(t) = \begin{cases} SoC_n(t-1) - \eta_{sys,n}^{c}(t) * \frac{P_{ess,n}(t)}{E_{nom,\mathrm{n}}} \\ SoC_n(t-1) - \frac{1}{\eta_{sys,n}^{\mathrm{d}}(t)} * \frac{P_{ess,n}(t)}{E_{nom,\mathrm{n}}} \end{cases} \quad (35)$$

**Efficiency**

For the formulation of the battery efficiency there are two main approaches. In the first approach, which is adopted in many papers, the efficiency is only determined by the battery state, whether it is in charge or discharge mode. In fact, the energy efficiencies are two constants in this method. However, this might lead to inaccurate BESS operation and economic evaluations. Contrary to this, the second approach considers that charging and discharging efficiencies in the energy balance depend on the charging/discharging power $P_{ess}$ or current $I_{ess}$ and the $SoC$. Applying the second concept, to retrieve the battery energy efficiency at different set points $\eta_{bat} = f(P_{ess}, SoC)$, data from repeated charge/discharge cycles with the previous generation CellCube (R3) at constant target power between 100 -150 kW is evaluated to create an efficiency map. In contrast to constant current mode, in constant power cases the current must frequently be adapted to compensate the change in the battery voltage and to keep the power constant. In addition, the charge and discharge duration are not equal anymore, since the current is increased to compensate the voltage drop during discharge, the minimum OCV is reached faster.

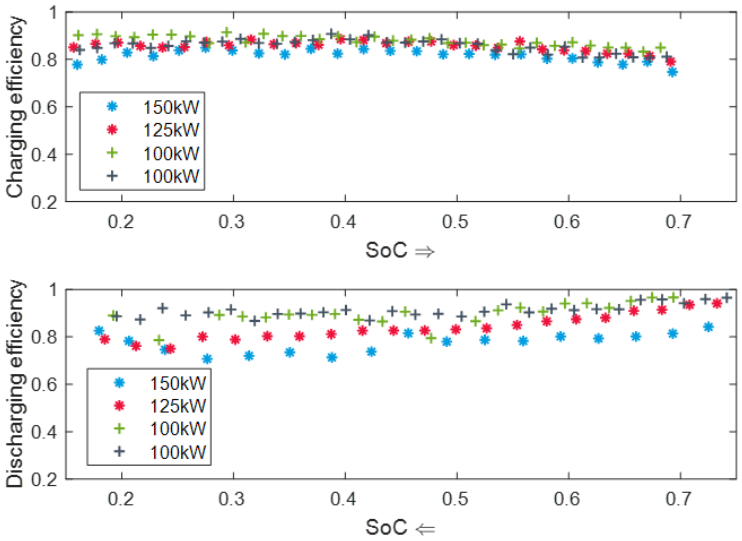


Figure 20. Effect of $SoC$ and $P_{ess}$ on VRFB discharging efficiency. Own elaboration.

The measured energy efficiency curves show the dependency of the $SoC$ and battery power $P_{ess}$ (cf. Figure 20). With increasing discharging power $P_{ess}$ the efficiency decreases. This trend is partly caused by ohmic losses due to internal resistances, which increase with the power. Accordingly, longer dis/charging durations due to lower dis/charging power or current are beneficial for the battery efficiency. An approximate linear relationship as in Eq. (36) is identified from the experimental data. The total DC-DC roundtrip efficiency $\eta_{\mathrm{bat}}$ can be retrieved by multiplication of the charge and discharge efficiencies.

$$\eta_{\mathrm{bat,d}}(P_{ess}) = \mathrm{a} * \mathrm{P_{ess}} + \mathrm{b} \tag{36}$$

Moreover, to analyze the impact of the SoC, independently from the battery power, the efficiency is curve is evaluated for the part where the power is kept constant. As seen in Figure 20 the efficiencies remain more or less constant within that SoC range. For discharge a slight decrease is noticeable.

Since, most microgrids are based on an AC grid, the total system efficiency is of more relevance which also includes the inverter and auxiliary losses. Hence, to obtain the efficiency of the inverter measurement data of an inverter fitted for a 200 kW CellCube VRFB has been examined. The results shown in Figure 21 reveal that apart from very small load $P_{ess} < 70\ kW$ the inverter achieves a high efficiency $\eta_{inv}$ of over 95 %. The obtained relationship between inverter efficiency and input power is non-linear and typical of most inverter types (cf. Appendix B-2). In this thesis the efficiency of the inverter is modeled using the efficiency curve obtained from the measurements.

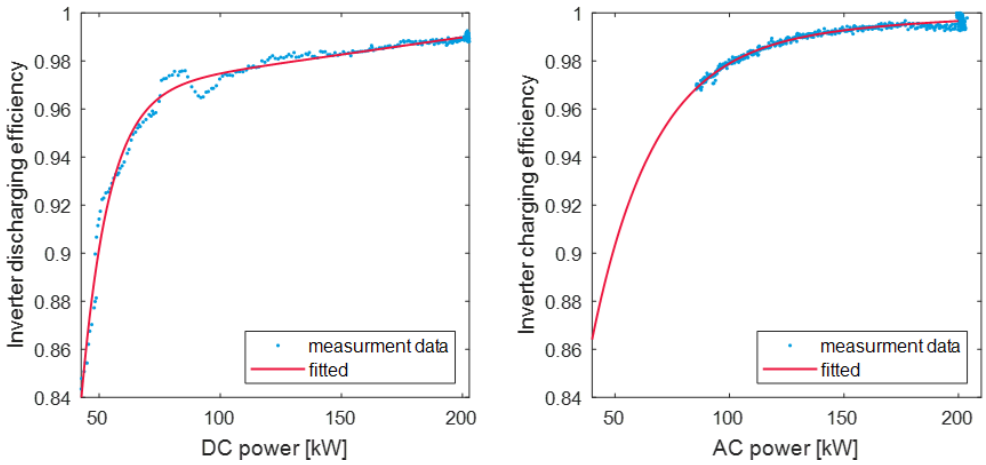


Figure 21. Inverter efficiency depending on input power. Own elaboration.

Furthermore, it must be noted that the auxiliary power including pumping power $P_{mech}$ for the electrolyte is often measured separately, since it is drawn from the grid rather than the battery. Therefore, it is important to estimate the consumption of auxiliary power in parallel. At low power output the coefficient of $P_{bat}/P_{mech}$ is low, since the pumps' power consumption do not decrease by the same factor as the battery power. Nevertheless, modular structures with several pumping cycles can provide better performance also at low power, by switching on or off complete cycles depending on the required battery power. The pump power also depends on the SoC, since the minimal required flow rate increases at the end of charge and discharge cycles due to the depletion of active vanadium species [86].

The final system efficiency map normalized to the efficiency at rated power and SoC of 50 % is illustrated in Figure 22. The combination of the real measurement data from the CellCube and the trend identified in [51] is used to create the efficiency distribution. For the final system efficiency an exponential curve is applied as an approximated model for the relationship between system efficiency and target AC battery power. Mainly due to auxiliary losses the efficiency changes with SoC and decreases at the end of charging and discharging.

$$\eta_{\mathrm{system}}\left(\mathrm{P_{ess}}\right) = \mathrm{a} * \mathrm{e}^{\mathrm{b}*\mathrm{P_{ess}}} + c * e^{d*Pess} \tag{37}$$

To integrate the efficiency in the equation for the charge level (35) the charging and discharging efficiency $\eta_{\mathrm{sys,charge}} = \sqrt{\eta_{\mathrm{system}}}$ are retrieved.

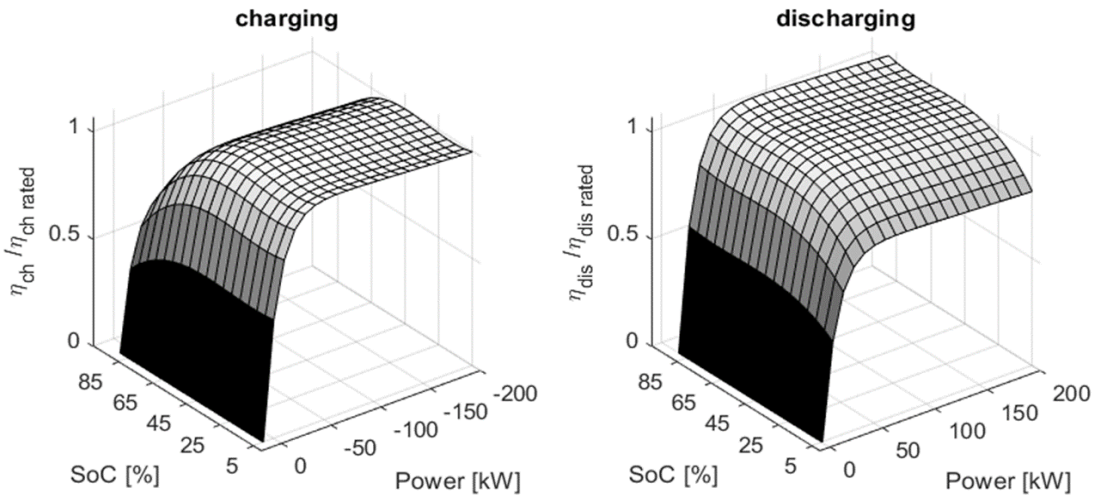


Figure 22. Normalized system efficiency depending on SoC and battery power. Own elaboration.

Lowest efficiencies are noted at very low power levels. This is due to the auxiliary losses from pump and inverter which become less significant as the battery power increases. The highest efficiencies are recorded around 100-150 kW rather than at rated power.

**Maximum charge and discharge power curve**

In addition to variable efficiencies, another distinctive battery property is that during the charging process the active battery charging power is reduced when the SoC is approaching the maximum SoC limits (cf. Figure 23).

This implies that only during a certain SoC window between the minimum charge level $SoC^{min}$ and $SoC^{rc}$ the battery can be charged at maximum power. Instead of continuing to charge with a constant current or constant power, the current/ power is reduced continuously (tapering/ saturation charge) and finally terminated when the maximum battery voltage is reached. Similar behavior exists during the discharge when the battery voltage is approaching its minimum. The power is limited after reaching the boundary $SoC^{rd}$. This effect is typical of various battery technologies, but characteristic thresholds vary depending on power rating and technology, which is why they should be integrated in the optimization model. Here this factor is included by adding linear charging and discharging power constraints (40) and (41).

Boundaries

$$P_{ess_n}^{min}(\mathrm{t}) \leq P_{ess_n}(\mathrm{t}) \leq P_{ess_n}^{max}(\mathrm{t}) \tag{38}$$

$$P_{ess,n}(t) = P_{discharge,n}(t) - P_{charge,n}(t) \tag{39}$$

Charging

$$P_{ess}(t) \leq \frac{P_{ess}^{min}}{1 - SoC_n^{rc}}(1 - SoC_n(t)) \tag{40}$$

Discharging

$$P_{ess}(t) \leq \frac{P_{ess}^{max}}{SoC_n^{rd}} SoC_n(t) \tag{41}$$

Figure 23 shows experimental measurements from a CellCube R3 charge and discharge cycle at 125 kW and the modeled SoC applying a linear relationship between SoC and reduction in charging/discharging power. The modeled SoC deviates only slightly from the measurements.

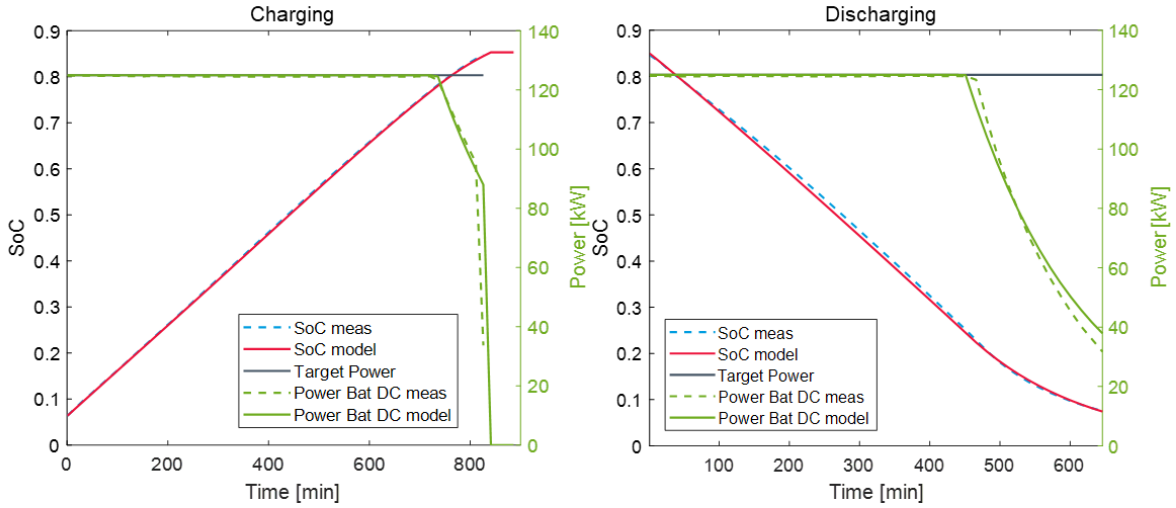


Figure 23. Charging and discharging power constraints VRFB model vs. measurement for SoC limits 5% and 85%. Own elaboration.

**Performance degradation**

VRFB are known for their long durability in comparison to other battery types, since they do not suffer from processes leading to mechanical degradation of the active materials or formation of dendrites. Although capacity decay can occur due to ionic diffusion of active species through the cell membrane or hydrogen evolution, the processes are reversible e.g. by electrochemically rebalancing the cells. In addition, by adhering to certain operation limits for instance by restricting the maximum SoC, they can be reduced significantly. Thus, for this work the SoC range is limited to avoid undesirable side reactions. The critical factor restricting the lifetime is reported to be the stability of the cell membrane [87]. Since the share of performance degradation which can be altered by the operation regime is not critical, it is omitted for this VRFB model.

**Additional parameters**

Self-discharge is not considered for VRFB or LIB, since both technologies have a very low self-discharge rate. Also, the influence of fluctuating outdoor temperatures on the battery performance is ignored.

### *4.2.3.2 Lithium-ion battery model*

For the lithium-ion battery model, most formulated equations from the VRFB can be replicated. Nonetheless, there are a few important distinctions:

**Efficiency**

Similar to the approach of [87] the charging and discharging efficiencies for the LiB battery are assumed independent from SoC but linearly decreasing with regard to the power $P_{ess}$ (cf. Appendix B-3). In accordance with the VRFB the LiB system efficiency $\eta_{sys}$ includes apart from the battery efficiency $\eta_{bat}$ also the inverter efficiency $\eta_{inv}$, which is highly nonlinear at low input power. In order to avoid the low efficiency area of the PCS at low power levels, the nonlinear efficiency characteristics are integrated into the LiB system model.

**Maximum charge and discharge power**

In accordance with the VRFB model, the active charging and discharging power curve are implemented. Maximum charge and discharge limits for LiB are not necessarily equal, manufacturers often state two different power limits. During charge the active power is regulated via voltage and current and reduced to allow full charging. For discharge the switch from constant current/ constant power is typically around an $SoC_n^{rdc}$ of 10 % but often even earlier [87].

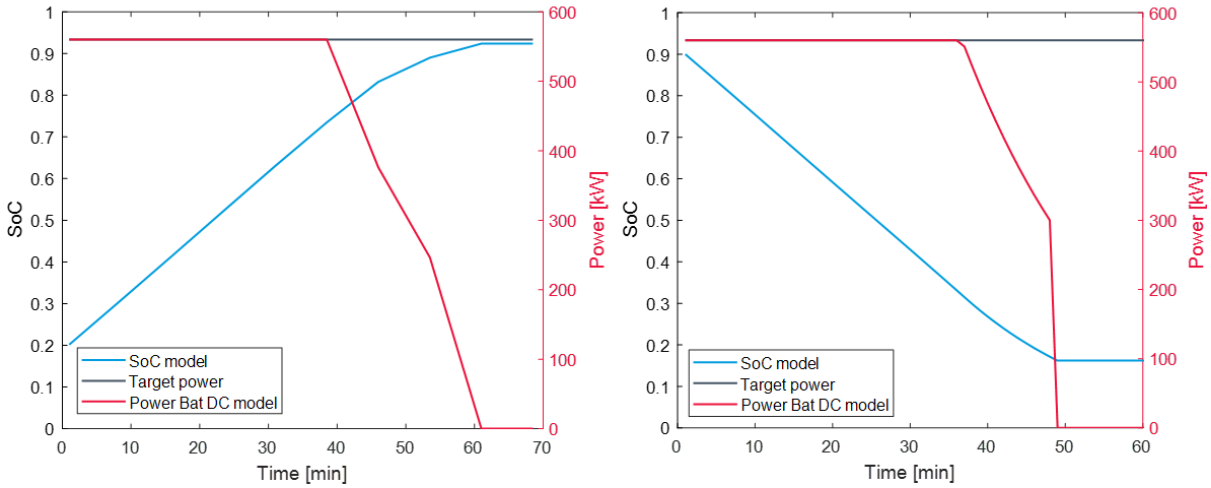


Figure 24. Charging (left) and discharging (right) power constraints for LiB with SoC limits 20% and 90%. Own elaboration.

**Degradation**

For lithium or lead-acid batteries, aging in the form of capacity fade is significant. The key manifestation of aging for lithium batteries is the formation of the Solid Electrolyte Interphase layer on the graphite anode, resulting in an increasing resistance and capacity loss. Therefore, battery degradation costs should be included in the objective function. Aging processes can be divided into two groups: aging related to cycle life and aging related to calendar life. As calendar aging cannot be altered by the operation mode of the BESS, it is not comprised in the optimization.

Research has proposed a variety of degradation modeling methods i.e. [88], [89]. The simplest way, realized by [90], is to assume the degradation of the LiB to be proportional to the total energy throughput, which cycles through the battery. Throughput is defined as the change in energy level, measured after charging losses and before discharging losses [91]. Nonetheless, this method does not account for the cycle depths ($\Delta DoD/\Delta SoC$), which has been found the primary aging stressor. Apart from $\Delta DoD$, advanced models also include the average SoC and temperature stress factors. For this thesis temperature effects are not considered, assuming that the LiB HVAC systems are able to assure that temperatures stay within limits which preserve battery life.

To integrate the degradation into the objective function the marginal cost of battery operation is required. Some battery manufacturers state the cycle lifetime vs. DoD curve, where $DoD = 1 - SoC$. To determine the cycle life an End of Life (EoL) capacity of 60-80 % is applied, depending on the testing standard. For EVs the EoL is 70-80 %, whereas the EoL for industrial applications is 60-70 % [92].

Typically, the curve is acquired by repeatedly discharging the battery to a specified DoD and recharging it to the full capacity. Accordingly, the problem related to these data is, that it is obtained under operating conditions which are fare from a stationary battery installed in a microgrid, where the batteries are cycling around different SoC-level due to the volatility of PV and wind resources and are not fully recharged after every cycle. This operation is often referred to as “irregular cycling”.

SAFT, the LiB manufacturer for Pellworm, provides a general range (cf. Appendix B-1) and states that the cycle life is 3500 - 4400 at DoD of 80 % depending on the C-rate for the NMC LiB. Since the data from SAFT is not sufficient, the measurements and battery degradation model from [93] is used supplementary, which also analyzes a NMC LiB for stationary applications. The measurement data can be fitted with a quadratic curve (cf. Figure 25 left).

$$cycle\ life = p_1 * DoD^2 + p_2 * DoD + p_3$$
$$p_1 = 6.54 * 10^4, p_2 = -1.15 * 10^5, p_3 = 5.361 * 10^4 \quad (42)$$

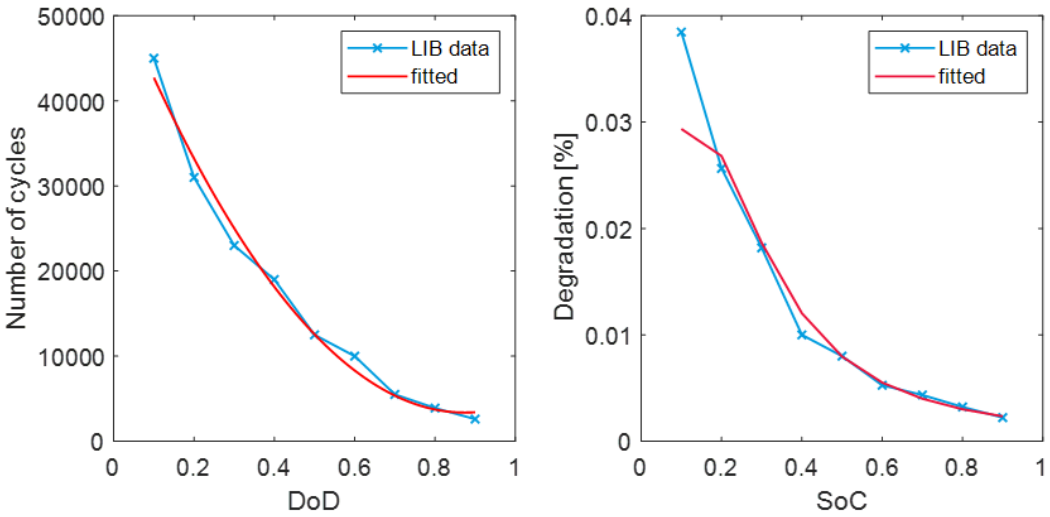


Figure 25. Cycle life versus DoD curve for NMC LiB (left) Degradation versus SoC curve (right).

Moreover, the paper [93] assumes that cycle degradation cost can be calculated by the units-of-production depreciation method. This method is used to compute depreciation in terms of the total number of units (number of cycles) expected to be produced. If the total number of the battery cycles is 4000 with 80 % DoD, it means every regular cycle from 100 % to 20 % consumes 1/4000 = 0.025 % of its total life. The degradation is determined for each time step $k$ by measuring the degradation $\Phi_k$ dependent on the ΔSoC. The degradation Φ is the inverse function of the number of cycles (cf. Figure 25). As a simplification the degradation is determined by assuming regular cycles. The factor 0.5 in Eq. (43) indicates that a charging/discharging process only stands for half a regular cycle. If the battery is cycled from 80 % SoC to 40 % SoC during one step, the degradation is $0.5 * |0.0031\ \% - 0.012\ \%| = 0.0044\ \%$. The degradation is translated into costs with the help of the LIB replacement cost $C_{rp}$. Yet, instead of multiplication with the total replacement cost, only the part is considered which can be altered by the operation regime. Since the shelf life cannot be influenced for neither of the batteries, only the difference between replacing the battery at its shelf life $T_{shelf}$ or earlier due to intense cycling at $T_{min}$ is

regarded. The replacement costs anticipate a further cost reduction of LiB and are discounted to a net present value. $N$ is the number of years left till $T_{min}$ and $T_{shelf}$ are reached.

$$\Phi_k = 0.5 * \left|\Phi_{reg}\left(SoC(t)\right) - \Phi_{reg}(SoC(t-1))\right| \quad (43)$$

$$c_{\deg k} = \Phi_k * \Delta C_{rp} \quad (44)$$

$$\Delta C_{rp} = \frac{C_{rp}(T_{min})}{(1+i)^{N_{min}}} - \frac{C_{rp}(T_{shelf})}{(1+i)^{N_{shelf}}} \quad (45)$$

### 4.2.4 Flexible generators

Flexible generators are common in microgrids, since they can follow the load. Diesel generators are most common, but also generators based on natural gas exist. For the optimization they are modeled as controllable sources which can output any power between the boundaries $\mathrm{P}_{\mathrm{gen}}^{\min/\max}$ and the operation causes fuel costs $C_{gen}$ as formulated in Eq. (29). In practice, generators additionally have specific ramp rates and variable efficiencies depending on their load. However, since the chosen time resolution is 15min/1h these effects can be ignored.

Boundaries $$\mathrm{P}_{\mathrm{gen,}}^{\min} \leq \mathrm{P}_{\mathrm{gen}}(\mathrm{t}) \leq \mathrm{P}_{\mathrm{gen}}^{max} \quad (46)$$

### 4.2.5 Prediction tools

In order to run the optimization, the following prediction data for the MG needs to be gathered.

- 15 min/hourly load demand forecast
- 15min/hourly Wind, PV, CHP generation power forecast

There are different approaches to obtain the necessary forecasts and they vary largely in accuracy, computational burden and robustness. Prediction methods are not within the scope of this thesis, yet they significantly influence the performance of the EMS. In order to test and optimize the MG operation under realistic conditions, the historical input data is altered with state-of-the-art prediction errors.

The accuracy of forecasts is typically measured as Root Mean Square Error (RMSE) or Mean Absolute Error (MAE)/ Mean Absolute Percentage Error (MAPE) (cf. Annex B.2). As illustrated in Appendix B-5 the error is a function of the forecast horizon. Additionally, single site RES power forecasts exhibit higher errors than aggregated predictions. Based on these facts, the RES output and load in this thesis is modeled with a gradient uncertainty level, in which the forecast error increases when the receding horizon becomes larger.

To create the artificial forecast a normally distributed random function is employed, which generates the forecast $p^{forecast}$ from the smoothed original data considering the relationship between prediction horizon and the average forecast error (MAPE). The forecast error $e(t)$ is assumed to follow a random normal distribution with mean μ and a standard deviation of σ. The original data is first smoothed as most forecast methods do not predict local extrema.

$$p^{forecast}(t) = p^{true} + e(t) * p^{true} \quad (47)$$

### 4.2.6 MPC design decisions and algorithm

The performance of an MPC problem largely depends on the chosen time parameters. An MPC with longer prediction horizon $T_p$ and shorter sampling times $T_s$ is assumed to provide better results if the computation time is fast enough to allow real time control. Since the day-ahead market offers products with a minimum block size of 1 h blocks $T_s$ is set to one hour. As the intraday market allows blocks of 15 min, alternatively $T_s$ can be reduced to 0.25 h. However, this will increase solving speed significantly.

The proposed MPC algorithm is composed of the following steps:

1. At $k = 0$ forecasts of RES generation, load demand and day-ahead market prices are obtained for the next $N_p$ periods.
2. After updating the constraints with the new prediction data, the new control sequence $u_1$ for $t$ till $t + T_p$ is calculated by running the cost optimization taking into account the predicted system states $x_1$ for the battery SoC.
3. At time step $k = 1$ the first control action $u_1(t)$ of the control sequence $u_1$ is implemented for sampling duration $T_s$.
4. Via measurements the actual RES generation, load and power output are obtained. The simulation applies an error as described above. Necessary deviations from $u_1(t)$ due to forecast errors are adjusted via power from the grid bought at an additional charge as for example on the intraday market. The authors in [94] model mismatches with an increased cost between 3-10 % of the base electricity price. Yet, other studies state higher deviation penalties [95]. Commonly, a second hierarchy level is implemented which adjusts the control signals for flexible MG generation for the timeframe, which is below the time resolution of the supervisory level.
5. The time moves one step forward k=k+1 and starts again with step 1 until k reaches the end of the simulation horizon $T_n$.

### 4.2.7 Assumptions and simplifications

The EMS optimization model in this study makes a few key assumptions and necessary simplifications:

- It is restricted to a supervisory control, which only controls the active power. Power quality, frequency and voltage stability are supposed to be controlled at the local control level.
- Microgrid black start or synchronization with the main grid are not considered.
- The MG is a considered a price taker, any trade with the main grid does not affect the spot price or the prices on the frequency regulation market.
- All RES energy from the MG is market directly at spot market prices, feed-in tariffs or premium payment are not included.

# 5 Case study - Pellworm Island

This section applies the developed optimization model to the Pellworm microgrid with a VRFB and a LiB hybrid BESS, to determine the optimal schedule under different scenarios. All input data for this case study are summarized in the following section, before the obtained results will be presented. In general, to adapt the proposed EMS to a specific case with a specific BESS, it first should be parametrized. This allows modification of the developed operation model formulation with the specific battery parameters. Three main use cases for the battery storage will be discussed: Arbitrage, improved utilization of existing assets by peak shaving and promotion of local energy and power quality services via secondary frequency provision.

## 5.1 Case introduction

The case of study is a grid-connected microgrid on the island of Pellworm in the North-Sea in Germany with coordinates 54.53 °N and 8.66 °E. It belongs to the administrative district of North Frisia. Pellworm has around 1100 inhabitants and its economy is dominated by tourism and agriculture requiring 8.5 GWh of electricity annually. The island has a high annual RES generation of around 32 GWh/a, primarily from wind but also solar PV and a biogas CHP. The smaller Hallig Hooge also belongs to Pellworm and also receives its electrical energy from Pellworm. Firstly, the rationale for this case is that although an island and thus due to its location the most common reason for a microgrid set up, it is grid-connected via two 20 kV cables, allowing the BESS to make use of multiple of the applications described in Chapter 3.1. Secondly, the data availability was given due to a former research project “Smart Region Pellworm”, where a hybrid power plant was tested with a Hybrid Energy Storage System (HESS) of a VRFB and a LiB battery. Thirdly, the case has high potential of deducing implications for similar constellations, as the high overproduction of RES is representative of many other North-Sea islands and regions.

## 5.2 Case specific input

### 5.2.1 Decision variables

The following parameters in Table 6 and describe the flexible resources within the microgrid system on Pellworm island. The decision variables are the dispatched battery power, the diesel or fossil fuel back-up generation and the power exchanged with the grid.

Table 6. Decision variables and their lower and upper boundaries.

| Variable | Definition | Lower boundary | Upper boundary |
|---|---|---|---|
| $P_{ess_1}$ | Dispatched VRFB power | -200 kW (charge) | 200 kW (discharge) |
| $P_{ess_2}$ | Dispatched LiB power | -560 kW | 1000 kW |
| $P_{gen}$ | Dispatched power from conventional generator | 0 | 150 |
| $P_{grid}$ | Power purchased from/ sold to the main grid | | Depends on Scenario |

### 5.2.2 Battery data

For the duration of the demonstration project, the island had been equipped with two large scale battery energy systems, a CellCube FB200-1600, with a rated power of 200 kW and with an energy capacity of 1600 kWh and a Saft Intensium Max20M LiB with 560 kW charge and 1000 kW rated discharge power and an energy capacity of 560 kWh. Both batteries were connected to the AC grid via an individual battery inverter. Table 7 summarizes the specific battery characteristics which have been chosen as inputs for the optimization.

Table 7. Battery specific characteristics.

| Variable | Definition | Lower boundary | Upper boundary |
|---|---|---|---|
| $SoC_1$ | State of charge limits VRFB | 5 % | 85 % |
| $SoC_2$ | State of charge limits LiB | 20 % | 90 % |
| $SoC^{rd/rc}$ | Dis/charging limit after which dis/charging power is reduced for VRFB | 25 % | 75 % |
| $SoC^{rd/rc}$ | Dis/charging limit after which dis/charging power is reduced for LiB | 25 % | 85 % |
| $\eta_{sys_1}^{d/c}$ | Rated VRFB system efficiency during dis/charging | 80 % | 80 % |
| $\eta_{sys_2}^{d/c}$ | Rated LiB system efficiency during dis/charging | 91 % | 93 % |
| $T_{shelf}$ | Shelf life of LiB | 13 years | |
| $C_{rp}(T_{shelf})$ | Replacement cost of the LIB at end of shelf life, discounted | $c_{rp} = 250\ EUR/kWh$ | 98,000 EUR |
| $C_{rp}(T_{min})$ | Replacement cost if replaced within 7 years, discounted | $c_{rp} = 310\ EUR/kWh$ | 154,000 EUR |

Sources: [35], [94], [95]

The data has been obtained from manufacturer specifications and data provided by Enerox and Saft as well as from literature: The efficiencies are rated efficiencies, when charged or discharged at rated power/current. The final system efficiency for VRFB is derived is a function of SoC and power. The LiB battery efficiency is multiplied with the inverter efficiency and only a function of power. The replacement costs signify the costs for replacing the LiB at the end of its life and they commonly differ from the initial

capital cost, because of further cost reductions over time. The values for different years are discounted to 2018. The shelf life is the average calendar life of a LiB, which is stated to be 13 years [35], [96].

### 5.2.3 Conventional generator data

Apart from costs or revenues from power purchased or sold to the grid, the objective function also considers fuel costs for back-up generators. The most common emergency energy supply are diesel gensets. Also, on Pellworm several gensets exist, providing back-up for essential loads like lighthouses and the local medical care center.

Depending on power rating, load factor and efficiency a diesel genset consumes between 0.3 to 0.5 l/kWh [97]. Assuming the German diesel price, an average fuel price $c_{fuel}$ per unit generated electricity of 0.5 EUR/kWh is considered.

$$c_{fuel} = 0.4\ l/kWh * 1.25\ EUR/l = 0.5\ EUR/kWh \quad (48)$$

### 5.2.4 Load data

As described in 4.2.5 reference load profiles are the basis of many forecast tools for electricity consumption prediction, which is why the BDEW profiles are used also for the Pellworm case. With the known yearly total consumption of approximately 8450 GWh and the shares of different consumption types, it is possible to generate a reference prediction for Pellworm with a 15-minute resolution for the whole year. The distribution among different load types represented in Table 8 is estimated based on an innovation survey conducted in 2011, with small adjustments to reflect the updated situation [98].

Table 8. Consumption distribution for Pellworm island.

| Load type | Consumption share | Standard Profile |
|---|---|---|
| **Residential** | 46 % | H0 |
| **Commercial** | 17 % | G0 |
| **Storage heating** | 12 % | SH* |
| **Heat-pumps** | 3 % | P0* |
| **Agriculture** | 2 % | L0 |
| **Special** | 21 % | - |
| **Total consumption** | 100 % | **8450 MWh/a** |

Source: [98], [99]. *Semi-standardized

Apart from the standard load profiles for residential households (H0), commercial (G0) and agriculture (L0), 15 % of total electricity consumption is allocated to temperature-dependent load such as electric storage heating and heat-pumps. For this kind of loads many grid companies and utilities use semi-standardized tables $f(t, TMZ)$ which contain time and temperature-dependent data to construct the reference profiles [100]. To calculate the TMZ, a temperature index, the daily mean temperatures $T_m$ are required, which for this case are obtained from by DWD weather station in the nearby town of Sankt

Peter Ording (54.31°N, 8.63°E). Finally, the load profiles which are commonly normalized to an annual consumption of 1000 kWh, are scaled with Pellworm's yearly consumption of 8450 MWh.

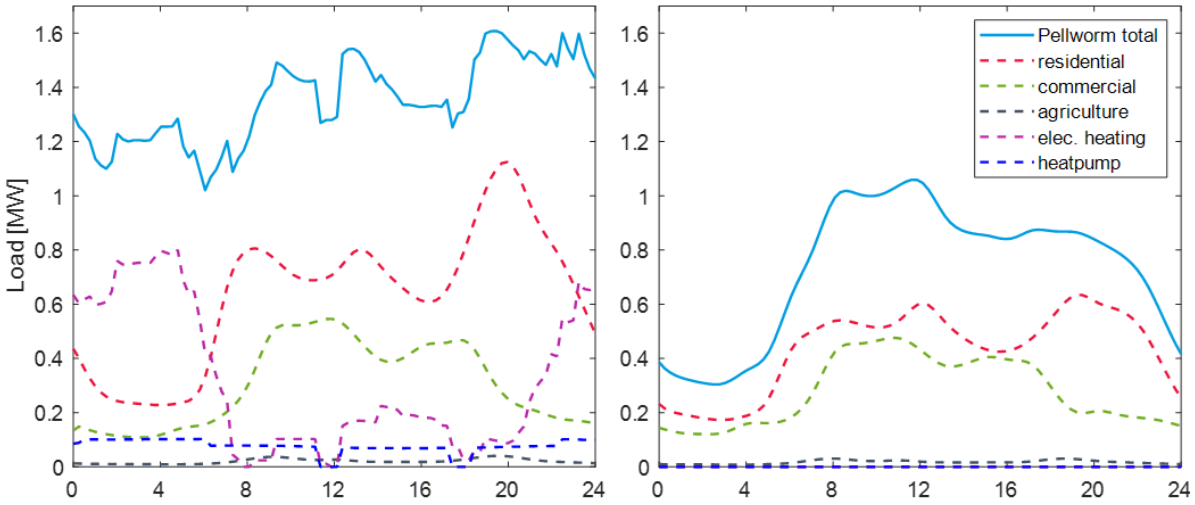


Figure 26. Load profile Pellworm winterday (left) & summerday (right). Own elaboration.

### 5.2.5 Generation data

Table 9 offers an overview over the power generation on Pellworm. The data for installed capacity for different technologies is from 2018, and the annual generation is estimated based on previous data from 2015 provided by Schleswig-Holstein Netz AG (SH Netz). The yearly production naturally varies due to different weather conditions. In addition, since 2015 many of the old small or medium scale wind turbines have been decommissioned and instead new Enercon E-70-E4 have been installed with a higher power rating as part of the repowering actions. According to SH Netz the latest addition has been three new E-70-E4. Thus, a significant increase in annual generation is estimated.

Table 9: Overview power generation on Pellworm.

| Technology | Installed capacity [MW] | Annual generation [GWh/a] | Details |
|---|---|---|---|
| Wind | 12 | 23.5 | Include 3x new Enercon E70-E4 2.3 MW |
| PV | 4.75 | 4.4 | 161 installations since 2004 |
| Biogas CHP | 0.55 | 4.5 | 0.576 $MW_{th}$ |
| Fossil generators | > 0.15 | - | Backup diesel generators, Mini CHP |
| **Total** | **17.45** | **32.4** | |

Source: [99], [101]

Figure 27 depicts the total generation profile which is adopted as input for the simulation. It has a resolution of one hour. Since the generation is composed of 100 % renewables it is highly fluctuating: from no RES production to an hourly average of more than 12 MW. The following section elaborates the technology specific generation profiles for Pellworm and elaborates how they have been obtained.

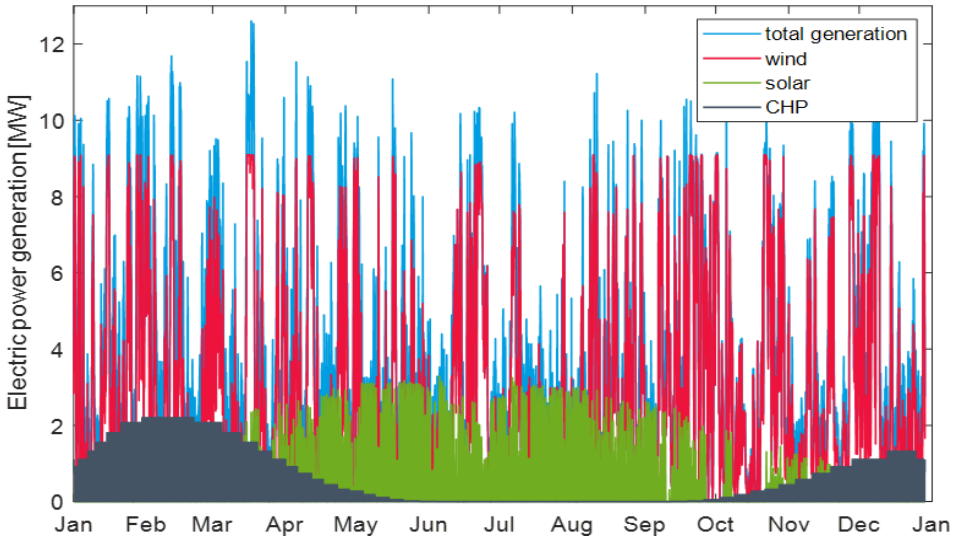


Figure 27. Electricity production on Pellworm - estimated profile 2018. Own elaboration.

**Wind generation**

Wind is the main energy resource on Pellworm and the total wind capacity has been expanded steadily. The wind conditions are excellent. At Hallig Hooge DWD weather station in 2018 the total mean wind speed $v_{10}$ at 10 m below ground was 7.35 m/s and applying a logarithmic relationship and a roughness class of 0.5, this equals a mean wind speed at 50 m $v_{50}$ of 8.77 m/s. The value coincides with the Global Wind Atlas, which states a general mean wind speed $v_{50}$ of 8 m/s for Pellworm [102]. In Europe on land, only the British and Irish coastal regions achieve better wind conditions.

Today, Pellworm has four turbines of this same type, which is why the total wind generation is simulated based on the same generation profile (cf. Figure 28). All the Enercon turbines can be controlled to limit the power output if necessary. This is implemented by active pitch (blade angle adjustment) and yaw control (rotation of the whole turbine).

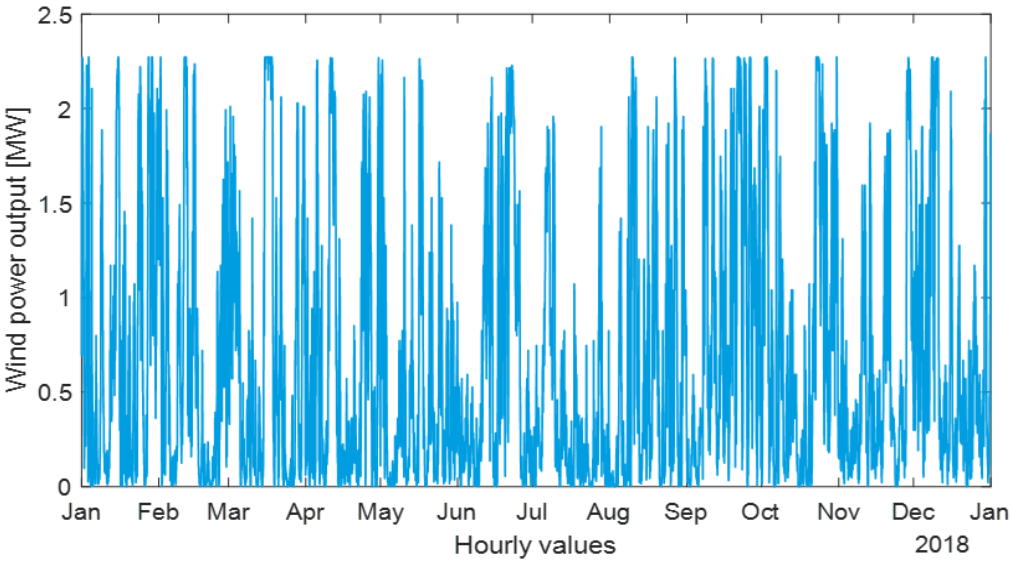


Figure 28. Wind production with single Enercon E70-E4 in 2018. Own elaboration.

**Solar generation**

Pellworm has a total solar photovoltaic capacity of 4.75 $MW_{peak}$. Since it is not known which type, which orientation and declination all the modules have, the production data from the ground-mounted 772 $kW_p$ photovoltaic installation which is part of the hybrid power plant is used as a reference and scaled up. As PV generators have a high PV to PV correlation coefficient, this is a feasible approach. [103] measured a correlation over 0.9 for 10 ground-mounted PV installations on different sites on the same substation. The reference installation on Pellworm has grown historically and therefore is composed of different module types and was partially refurbished in the end of 2015. Scaling is done with respect to total installed capacity and the total annual PV energy output. It is taken into account that roof-mounted installations often do not have the ideal tilt and orientation as the ground-mounted reference which is facing south.

The solar generation curve (Figure 29) has a typical shape with its highest generation in May and lower output during the winter months. The maximum generation peak exceeds 3 MW. The gap in October is caused by missing data recordings in the original dataset.

**Biogas CHP generation**

CHP plants are typically controlled based on the heat demand. Therefore, the co-generated electricity output depends on the total thermal load and is maximal during winter months and there is no electricity output during summer. The CHP power profile is modeled using a temperature dependent reference profile, applying the hourly mean temperature of 2018. The proceedings are equivalent to the formation of the load profile for heat pumps as described in 5.2.2. The CHP production is normalized with the known annual generation of 4.5 $GWh_{el.}$

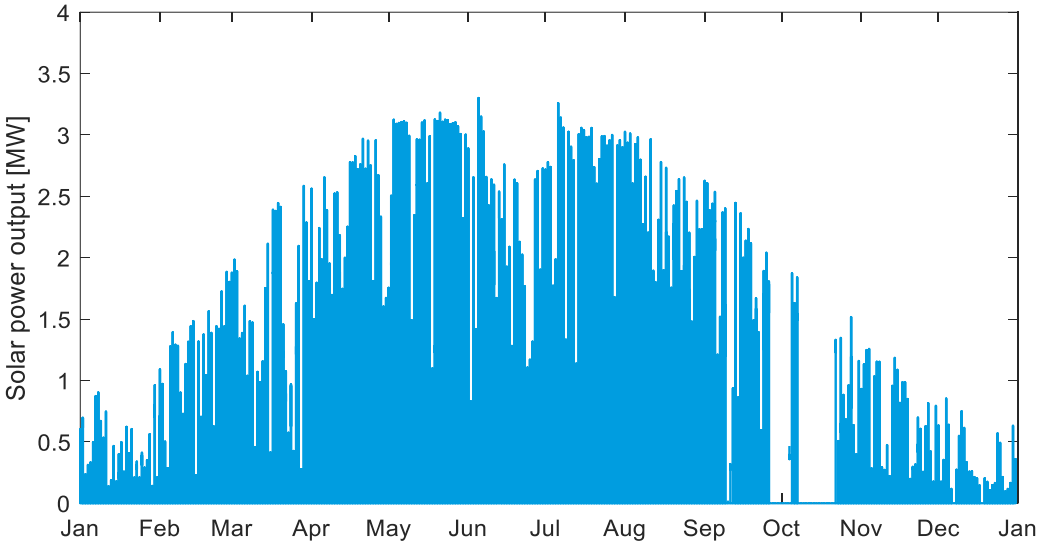


Figure 29. Solar power production on Pellworm in 2018. Own elaboration.

### 5.2.6 Forecast errors

To exemplify a deviation of the RES power production from its prediction, it would be ideal to have actual power forecast data available. However, this is not the case and an artificial forecast needs to be created. The real data is modified as described in (47) to reveal an error in respect to the original data.

Typical error distributions are gathered from literature. In [104] the dependence between the error and forecasting horizon was considered for wind prediction of a microgrid. 1-hour-ahead forecasts disclose 5 % MAPE increasing linearly until 35 % for forecasting horizons of 24 hours. Recent studies on wind predictions present better results ranging from 5-15 % MAPE [105], [106].

Table 10. Average forecast MAPE depending on the prediction horizon.

| **Forecast** | **Wind** | **PV** | **Load & CHP** |
|---|---|---|---|
| **MAPE [%]** | 24 h: 14 % | 24 h: 22 % | 24 h: 11 % |
| | 12 h: 12 % | 12 h: 16 % | 12 h: 8 % |
| | 1 h: 6 % | 1 h: 7 % | 1 h: 6 % |

For solar production forecast the prediction accuracy is very good for clear days (<9 % day-ahead) but rather bad for cloudy days (>20 % day-ahead). Forecasts based on auto-regressive integrated moving average models, a statistical method, achieved 6-12 % MAPE for a prediction horizon from 1 to 6 hours [107]. Day-ahead prognosis revealed errors of 20-26 % [108].

Load forecasting highly depends on the number of different consumers but is more accurate than RES prediction. For a grid with a total consumption ranging from 7-39 MW the day-ahead error is 2.4 % [109]. The load prediction for a smaller Norwegian microgrid with 6000 household achieved 6 -11 % MAPE for a prediction horizon of 1-24 hours [110].

The main characteristic for a correct prediction of the CHP production is the heat demand, which mainly

depends on the temperature, solar radiation and behavioral influences. For the best case scenario [111] accomplished a MAPE of 5.6 % for a day-ahead forecast applying a machine learning approach. Here, the same error distribution as for load-prediction is assumed.

As in reality a specific forecast might reveal different errors, only over a large sample the distribution as described in Table 10 will occur. Figure 30 exemplifies the method for a solar generation forecast.

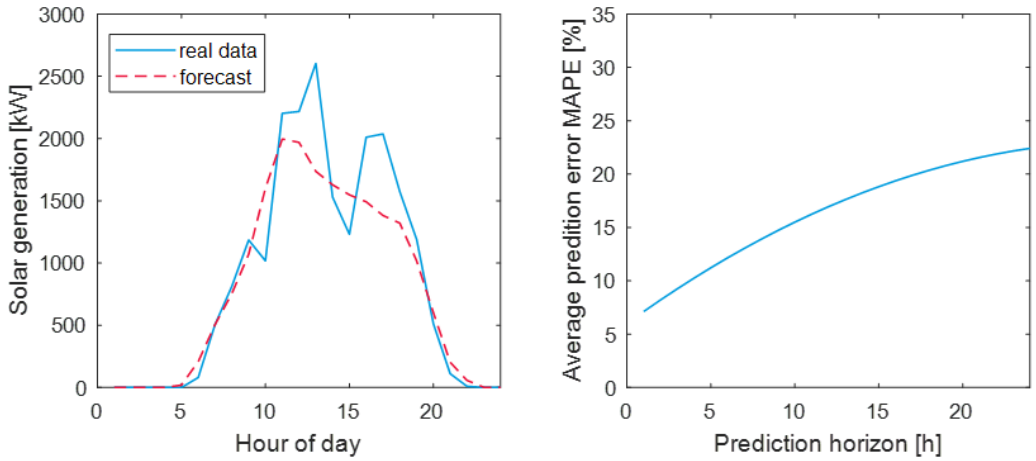


Figure 30. Artificial forecast for solar production on a partially cloudy summer day (left) and MAPE error for solar as a function of prediction horizon (right). Own elaboration.

### 5.2.7 Price data for power exchange and control reserve markets

Since EEG 2012 Germany moved away from guaranteed feed-in tariffs and more and more RES energy is marketed directly via the exchange. By direct marketing RES owners can theoretically earn more by strategically increasing and decreasing their output based on price signals. With the optimal operation of the hybrid storage on Pellworm additional revenues from generation arbitrage can be expected.

The buying and selling price for electricity is set equivalent to the hourly EPEX day-ahead electricity market price (EPEX Spot Phelix Day Ahead). Hence for Scenario 1 it is assumed that there are no additional transaction fees, taxes etc. which in practice lead to higher prices for buying from the grid than prices for selling surplus energy to the grid. Also, the technology-dependent market premium which RES owners receive when market directly, is not taken into account, since it is an inflexible price component and will not influence the BESS operation. Evidently, the electricity prices fluctuate immensely during the course of the year, occasionally reaching negative values. In the considered data set with German hourly prices of 2018 an average price for the day ahead product of 44.9 EUR/MWh with a standard deviation of 17.60 can be found. Nevertheless, the typical daily price curves with peaks in the morning and late afternoon are manifest during summer and winter. It turns out that daily price spreads are higher in winter than during summer (cf. Figure 31).

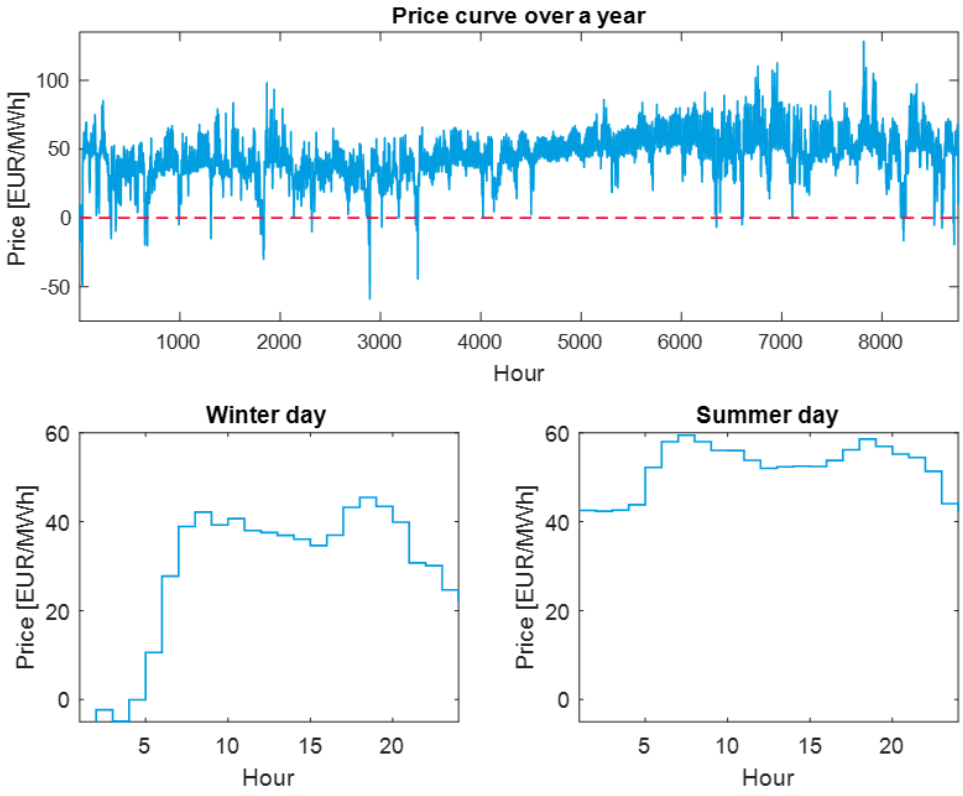


Figure 31. German day-ahead spot market price curves. Own elaboration.

For ancillary services, different prices and remuneration mechanisms exit. FCR or primary frequency reserve is traded in a weekly auction for all four German TSOs together. Each provider who meets prequalification standards is allowed to submit a bid offering a certain amount of reserve at a proposed offering price in EUR/MW. For FCR the reserve power can only be offered as a symmetric product, meaning that the installation needs to be able to provide power or reduce infeed or absorb power from the grid. All incoming bids will be ordered based on their price, then depending on the total demand estimation they are accepted for the following week. For this case study the average FCR price of 2018 is applied which was 2170 EUR/MW per week or 310 EUR/MW per day [112]. FCR prices show a decreasing trend.

Table 11. Average prices for balancing services in 2018.

| | Reserve price [EUR/MW/day] | Activated energy price [EUR/MWh] |
|---|---|---|
| **FCR** | 310 | - |
| **aFRR positive** | 57.1 | 65 |
| **aFRR negative** | 18.9 | 0-5 |
| **mFRR positive** | 7.5 | 65 |
| **mFRR negative** | 2.9 | 0-5[1] |

FRR or secondary frequency reserve is traded for each TSO separately. Pellworm is located in the TSO region of TenneT. Auctions take place daily in blocks of 4 hours (from 0-4 h, 4-8 h etc.). Unlike FCR, FRR is not a symmetric product, which means that there are separate auctions for positive and negative reserve power. FRR has two types of remuneration, a capacity reserve price (EUR/MW) and a working price for actual delivered energy (EUR/MWh) which are both submitted in a pay-as-you bid auction. The market is cleared via a merit-order-curve where the marginal capacity price denotes the last unit which receives bid acceptance.

Figure 32 illustrates the volatility of the marginal capacity and energy prices, which reveal large fluctuations within one month and an even bigger spread within one year. The marginal price in EUR/MW is per block of 4 hours. One reason for the differences between August and December might be that the regulations and the clearing mechanism have been reformed in July 2018.

The marginal price is significantly higher than the average price. The latter is simply calculated by dividing the expenses for FRR through the demand. The average capacity price in 2018 was 400 EUR/$MW_{pos}$ per week and 132 EUR/$MW_{neg}$ per week. The actual price for activated aFFR energy was 65 EUR/$MWh_{pos}$ and around 0-5 EUR/$MWh_{neg}$ for small participants offering less than 100 MW.

mFRR prices are commonly lower than aFRR (cf. Table 11). As opposed to the longtime trend of primary control (FCR), the analysis detected a high price increase for FRR in 2019 compared to previous years. Prices doubled for positive aFFR and increased with more than factor 5 for negative aFFR and both types of mFFR. In fact, after the introduction of the new bidding process a trend towards higher capacity prices and lower energy prices can be noticed.

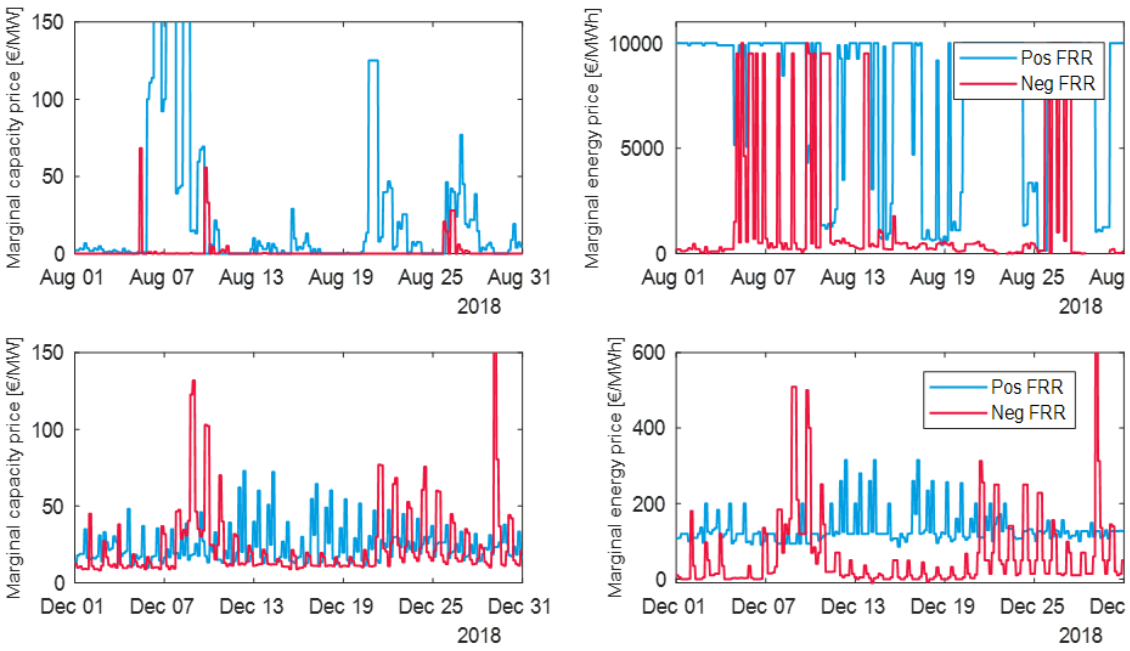


Figure 32: German aFRR marginal prices for August and December. Own elaboration.

## 5.3 Case study results

This section presents and discusses the dispatch results for the case study and conducted scenarios. The cases were all investigated in grid-connected mode. Islanded operation would require a more dynamic analysis with higher resolution than one hour, since major challenges are maintaining frequency, voltage levels and enabling fast resynchronization processes. As a base case, there is a scenario without any energy storage technology (Scenario 0). Further scenarios distinguish different applications for the microgrid with BESS which are energy arbitrage in the day-ahead market (Scenario 1), increased utilization of existing assets via grid services and promotion of local energy use (Scenario 2) and provision of power quality by participation in frequency regulation markets (Scenario 3).

### 5.3.1 Scenario 0: Operation without storage

This base scenario is employed as a benchmark, allowing comparisons for the following scenarios. It discloses the power exchanged with the grid in the case that there is no battery storage in operation. As visible in Figure 33 Pellworm is a net electricity producer and most of the time exports power to the main grid. It already accomplishes a self-sufficiency rate (SSR) of approximately 96.3 % and only had a net deficit for 1120 hours. Due to the RES overcapacity the self-consumption rate (SCR) was only 25 %. The maximum hourly grid export is 12720 kWh and the maximum import is 1570 kWh. The highest occurrence of a net deficit is found at 7 pm, which correlates with the daily duck curve and higher demand in the evening. The diesel back-up is not dispatched, since the fuel costs of 0.5 EUR/kWh are still higher than the maximum EPEX price of 0.13 EUR/kWh. The total profit for the simulated year is 911,280 EUR, without consideration of any surplus charges due to prediction errors.

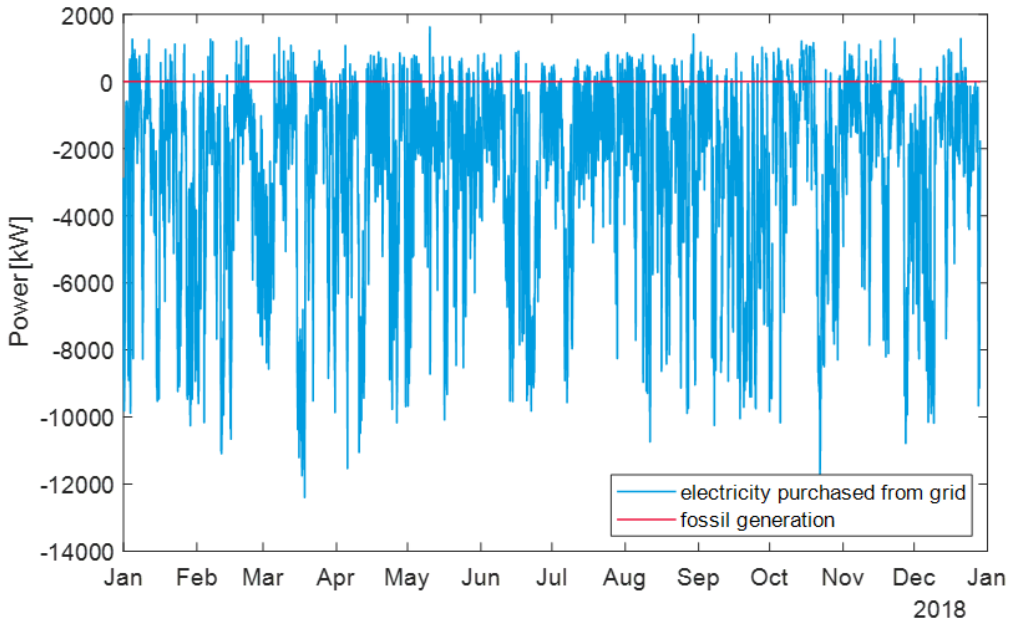


Figure 33. Scenario 0 - power dispatch without battery storage. Own elaboration.

### 5.3.2 Scenario 1: Energy arbitrage

Scenario 1 runs the optimization with the single purpose of maximizing the MG's profit, respectively minimizing the cost by exploiting price spreads.

Figure 34 illustrates the dispatch results of a typical day with high wind production fluctuations. The maximum BESS discharge correlates with the peak electricity price, whereas the maximal charge occurs simultaneously to the lowest price at night. At the end of the day the batteries are not necessarily completely discharged, because as in reality the problem is not finite and dispatch routine already considers the following 12 hours from the next day for its decisions. This enables energy shifting over one day.

It can be noted that due to the large RES generation within the microgrid, the BESS are primarily used to store the overproduction and sell it at times with higher prices, maximizing the revenues from sold electricity. Peak prices occur frequently during the morning (8-10 am) or afternoon (4-8 pm) (cf. Figure 34 ). It can be called generation arbitrage, whereas the typical load shifting occurs as well but only when there is an energy deficit on the island and electricity must be procured.

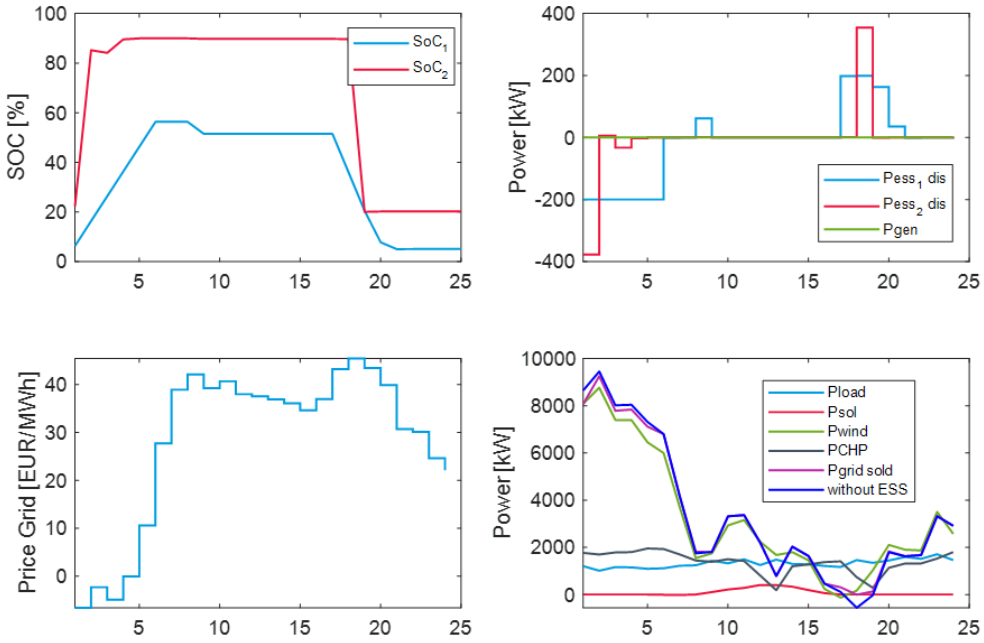


Figure 34. Scenario 1 - dispatch results for winter day ($n = 16$, $T_p = 12$). Own elaboration.

An example of load shifting occurs during hour 17-19 (4-7 pm) of the winter day in January in Figure 34 , where the need to purchase power can be completely avoided in the Scenario 1 with storage, reaching a self-sufficiency of 100 % during that specific day. The same pattern can be extracted form Figure 35, where a day in December and July respectively is compared with and without arbitrage operation.

For the summer day it is visible that the battery is charged from 11-12 pm at night, even if there is a net deficit in the microgrid which is further increased due to storage operation. As aforementioned in this scenario there is no price difference between sold and purchased power, therefore the optimization does not distinguish between local and grid power and will charge the battery when the price is the lowest,

which is usually during night.

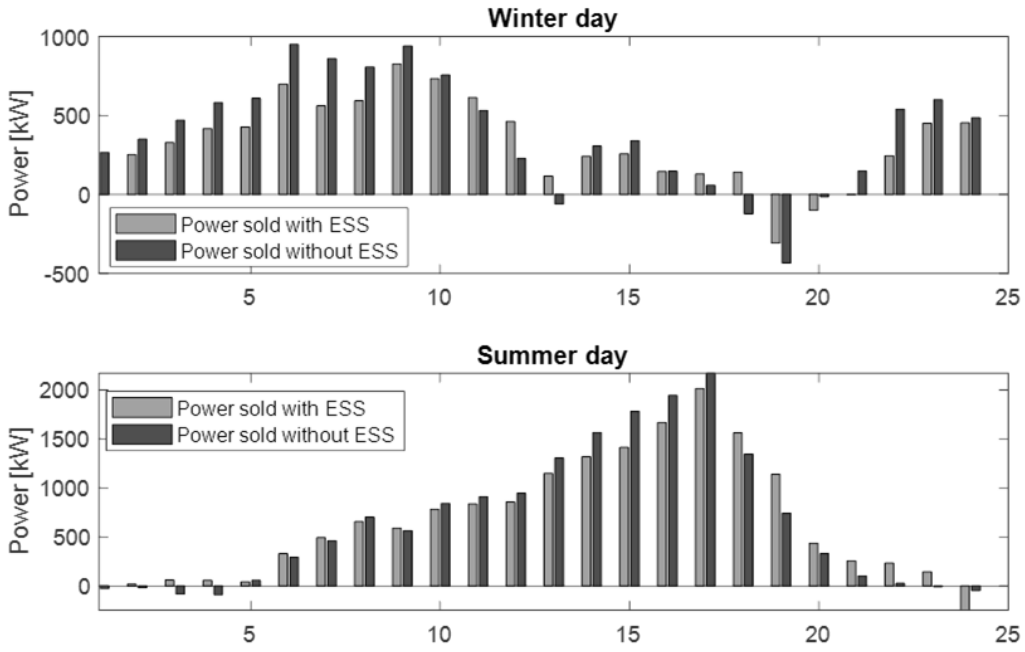


Figure 35. Comparison between grid exchange with and without storage. Own elaboration.

As seen in Table 12, which displays the scheduling results of one week in January and one week in July, additional economic benefits can be realized with the installed hybrid BESS system in comparison to the base case without storage. The profit only includes the net profit from grid exchange. However, it also occurs that the batteries remain at the same energy level for several days, which signifies that the price spread is not large enough to compensate for the efficiency losses. For the VRFB, which is subject to higher losses the price peak needs to be at least 1.55 times higher than the minimum depending on the initial SoC level. This means if the price is 35 EUR/MWh a price of 54.3 EUR/MWh is required. In particular during summer, where the daily price spread in average is lower, the VRFB is not charged.

Table 12. Scenario 1 – dispatch result analysis for two different weeks.

| | **Week January 2018** | | **Week July 2018** | |
|---|---|---|---|---|
| | Scenario 0 | Scenario 1 ($T_p = 12$) | Scenario 0 | Scenario 1 ($T_p = 12$) |
| Economic profit [EUR] | 12290 | 12510 (+220) | 10073 | 10096 (+28.4) |
| Degradation LiB [Cycles/ %] | - | 9.06/ 0.23 % | | 8.24/ 0.20 % |
| Self-sufficiency [%] | 98.4 | 99.0 | 83.8 | 83.4 |
| Self-consumption [%] | 29.0 | 30.0 | 32.3 | 32.4 |
| Throughput VRFB [MWh] | - | 3.84 | | 0.41 |
| Throughput LiB [MWh] | - | 2.93 | | 3.17 |

In the weekly analysis the energy throughput is between 0.41-3.84 MWh for VRFB and 2.93-3.17 MWh for LiB, which discloses that VRFB achieves between 0-0.34 Equivalent Full Cycles (EFC) per day and LiB approximately 0.75 EFC per day. The cycling behavior shows that the LiB usually performs full cycles, whereas the VRFB might only be charged to an SoC of 60 % before being discharged. This is due to the different energy to power ratios (E/P). The VRFB has an E/P of eight and thus requires a low price over five hours to be charged constantly and reach the upper SoC limit. The LiB has an E/P ratio of one, which means that it can be recharged within one hour.

The simulation of the arbitrage operation strategy for one year, excluding LiB degradation cost, results in additional profits of around 5544 EUR with the hybrid storage. Due to missing data points for approximately 20 days the economic profit result has been extrapolated. Self-consumption and self-sufficiency can be increased slightly. Since, the calculation of SCR and SSR with storage are not clear within existing literature, the applied formulas are described in Annex C.2. Contrary to expectations, the throughput of VRFB is lower than for LiB, although the energy capacity of the VRFB is higher. This result can be traced back to the lower system efficiency of VRFB and the requirement for higher price gaps within a day. With the given data input, the VRFB is responsible for 48.1 % of the revenues.

The LiB degradation of cycle life for one year is 13.5 % or 540 regular cycles. In fact, with this cycling behavior the LiB will not reach the 13 years of average shelf life but only 7-7.5 years. Therefore, for arbitrage only operation within this market environment, it makes sense to include additional degradation factors to avoid intense cycling as discussed in Chapter 4.2.3.2.

Table 13. Scenario 1 – dispatch results for annual simulation.

| **Annual results** | **Scenario 0** | **Scenario 1** |
|---|---|---|
| Economic profit [EUR] | 911,280 | 916,824 (+5544) |
| Self-consumption [%] | 24.97 | 24.98 |
| Self-sufficiency [%] | 96.29 | 96.33 |
| Max export [MWh/h] | 12.72 | 12.79 |
| Max import [MWh/h] | 1.57 | 1.57 |
| Throughput VRFB [MWh] | - | 179.4 |
| Throughput LiB [MWh] | - | 194.8 |
| Degradation LiB [Cycles] | | 541 (13.5%) |

Before the evaluation of other business models, a sensitivity analysis has been performed to assess how different parameters affect the dispatch results and thus change operation and revenues of the system. The following parameters were assessed for the primary model of arbitrage:

- Algorithm type
- Prediction horizon
- Round-trip efficiency
- Replacement costs

**Impact of algorithm**

To test the outcomes of the MPC approach, it is compared with a day-ahead optimization, which optimizes the schedule for the coming 24 hours at once without any feedback during the day. For the comparison the prediction horizon has been set to 24 hours, which means that for the first hours the error should be within the same range. As expected, the MPC can reduce the error in the following hours and thus the mismatch cost. For the simulated day (cf. Figure 36) the MAPE of the day-ahead optimization is 12.6 % and 6.2 % for the proposed MPC. Hence the implementation of a receding horizon it is one way, to deal with uncertainty due to intermittent RES and consumption behaviors. In the simulation real price data is taken instead of predictions. Consequently, since the main influence for the arbitrage only model is the spot price, in reality the advantages from applying an MPC approach recedingly improving the price predictions will be greater.

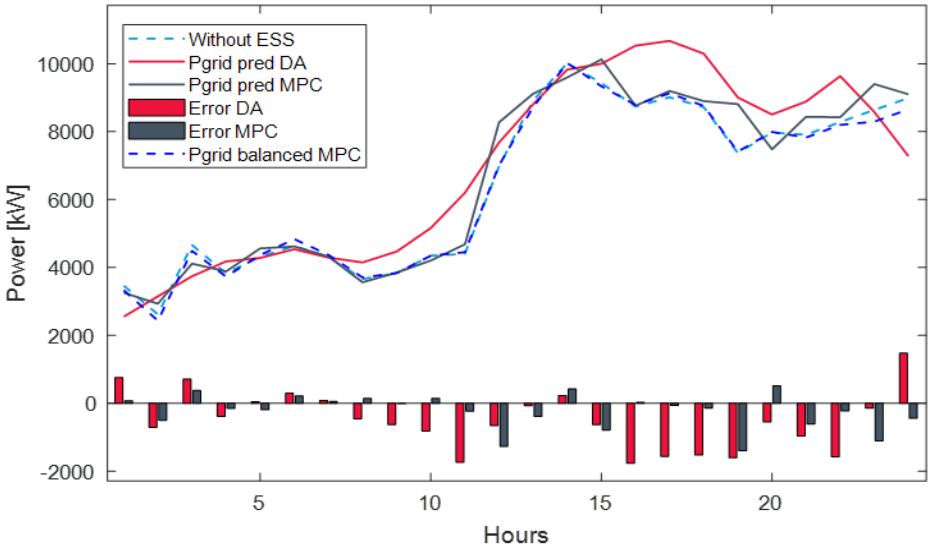


Figure 36. Comparison of MPC and day-ahead optimization on power mismatch. Own elaboration.

**Impact of prediction horizon**

The analysis performed for different prediction horizon length for the arbitrage model discloses that prediction horizon between 8-12 hours achieve slightly better results in terms of revenues (cf. Table 14). Prediction horizons of less than six hours lead to only a minimal benefit, since the predicted price spread within four hours is not enough to compensate efficiency losses from cycling or degradation costs and thus the BESS are only rarely charged. A longer prediction horizon helps to steer the operation onto a desired path. It avoids the problem that the BESS is empty when demand and prices are high or full when it would be cheap to recharge. However, a very long prediction horizon over 12 hours does not provide an improvement because the forecasts degrade as time increases and the decisions made are based on data with larger errors. Hence in this setting, there is a trade-off between prediction horizon and prediction accuracy. This finding complies with [85], who implemented a RHC for a microgrid with a wind turbine and an unspecific battery and concluded that that a longer prediction length does not necessary imply that the result is getting better.

Table 14. Sensitivity analysis for Scenario 1 with various prediction horizons.

| | | Scenario 1 | | | | | |
|---|---|---|---|---|---|---|---|
| | Prediction horizon [h] | **4** | **6** | **8** | **10** | **12** | **18** |
| **Week in January** | Additional profit from power exchange [EUR] | +142 | +185 | +219 | +219 | +221 | +217 |
| **Week in July** | Add. profit from power exchange [EUR] | +4.0 | +6.6 | +22.3 | +18.2 | +28.4 | +8.9 |
| | Computation time per day [sec] | 2-4 | 8-15 | 20-25 | 24-32 | 45-55 | >65 |

In addition, long prediction horizons larger than 12 hours increase the computation. The iteration for one day with $T_p$ of 12 hours takes approximately 45 seconds, whereas it is about 12 seconds for a prediction horizon of 6 hours. The main adjustment by choosing a longer prediction horizon is noticed for the VRFB, which is charged to a higher energy level before being discharged again and thus has a larger energy throughput. This result is expectable and applies not only to this optimization. If the planning horizon is shorter, the revenues from the next hour values more for the total profit within the planned time. In contrast, if the planning horizon is long, one is willing to have less profit for the next hour if at the end the total profit will be larger. This implicates that more energy will be shifted over time.

**Impact of battery system efficiency**

The efficiency is assumed to have a significant impact, since it defines the losses which need to be compensated by higher price spreads. A better system roundtrip efficiency will increase the feasibility also for markets with smaller differences between peak and off-peak prices. The LiB already has a roundtrip efficiency of over 85 %, therefore the investigation focuses on the impact of different rated efficiencies of the VRFB, which still has potential in boosting the efficiency.

Table 15. Sensitivity analysis with various VRFB efficiencies.

| **System round-trip efficiency VRFB** | **Additional revenue arbitrage** | | **Total share VRFB** |
|---|---|---|---|
| **64 %** | +5544 | - | 48.1 % |
| **70 %** | +6710 | +21.0 % | 56.0 % |
| **76 %** | +8090 | +45.9 % | 62.9 % |
| **82 %** | +9503 | +71.4 % | 68.1 % |

Already during recent years progress has been made to improve VRFB efficiency and compared to the system installed on Pellworm in 2013, new systems achieve higher roundtrip efficiency of 70-75 %. The simulation demonstrated that with an improved system efficiency of 82 % the revenues can be

significantly enhanced by 71.4 %. Subsequently, also the energy throughput of VRFB rises with the efficiency to more than 423 MWh/a and so does the amount of additional revenue which can be traced to the VRFB.

**Impact of degradation cost**

The previous simulations have been performed without considering a degradation cost factor in the objective function. Nevertheless, without it, the LiB life would only last around 7-9 years before the remaining capacity would be less than 70 %. Given that the degradation is non-linear its integration increases computation time, therefore the evaluation period is limited to one month. Figure 37 exemplifies the cycle differences for one day and Table 16 summarizes the obtained results for the one-month simulation. It is evident that the no degradation case A makes use of the LiB battery more aggressively, generating more energy throughput, in comparison to the other cases (B-D) which consider degradation costs. If degradation cost is set too high, the LiB is not charged since arbitrage cannot compensate degradation losses. which is the case for C and D for the respective day shown in Figure 37.

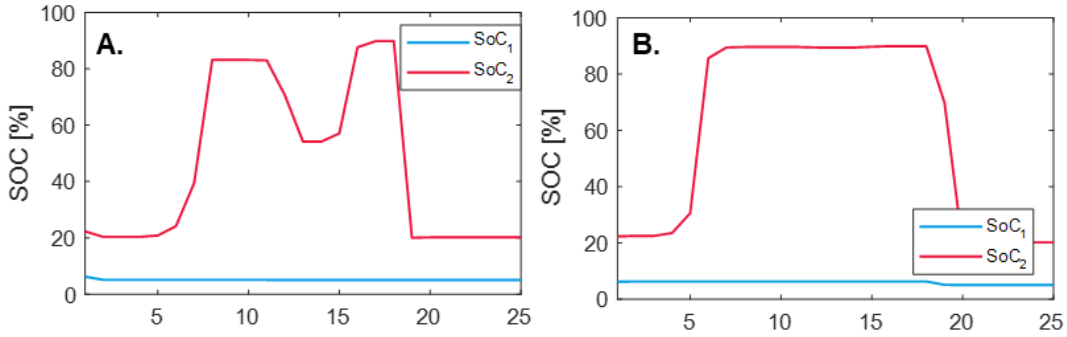


Figure 37. SoC curves for one day with different costs for LiB degradation. Own elaboration.

The highest monthly benefit is acquired for the case A where no degradation was incorporated in the objective function. Despite this, the case also experiences the highest degradation (1.07 %), concluding in the shortest battery lifetime. In general, rising degradation costs limit the flexibility of the LiB operation and thus restrict the optimization, resulting in lower profits but increase battery lifetime. When the spread of the battery replacement increases to 100 EUR/kWh (Case C), the LiB rarely reaches a DoD of more than 40 % and the total profit from power exchange decreases.

Table 16: Dispatch results under various LiB replacement costs for one month.

| Δ LiB replacement cost EUR | Δ Replacement cost EUR/kWh | Δ Monthly benefit [EUR] | Degradation [%, cycles] | Lifetime [years] |
|---|---|---|---|---|
| **A. None** | - | +791 | 1.07 %, 42.9 | 7.8 |
| **B. 11200** | 20 | +674 | 0.79 %, 31.6 | 10.5 |
| **C. 56000** | 100 | +575 | 0.37 %, 14.7 | >13 |
| **D. 98000** | 175 | +571 | 0.21 %, 8.4 | >>13 |

Even higher degradation costs (Case D) only lead to minimal changes in dispatch results. Since in the

applied degradation model cost rise quadratically with DoD of the battery, only deep cycles generate significant additional costs.

Figure 38 illustrates the consequences of degradation costs over one week during winter. Whereas the blue line (without a degradation cost factor) presents small spikes and utilizes the whole SoC range, with increasing replacement costs the SoC range decreases and the valleys get flatter. It is difficult to determine an accurate degradation cost value for the objective function. While in winter the revenue losses are acceptable, in summer it often makes the difference whether the LiB operates or is in idle mode.

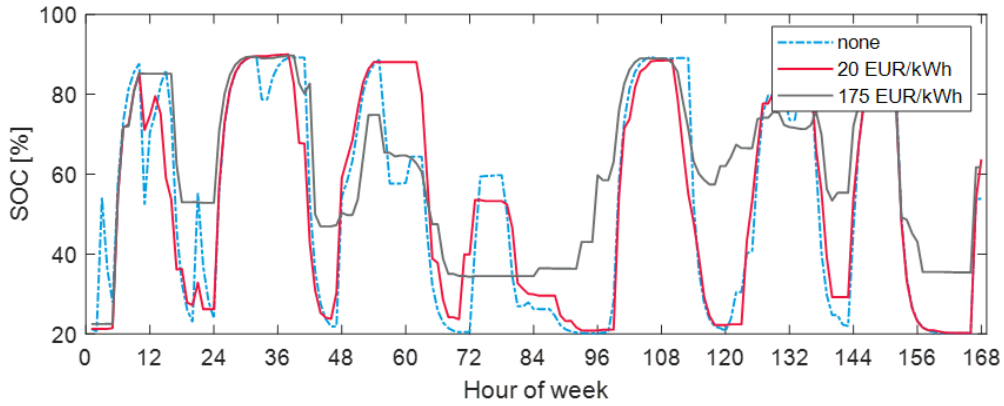


Figure 38. LiB cycling with different degradation cost factors. Own elaboration.

### 5.3.3 Scenario 2: Increased utilization of existing assets

#### A. Grid supportive peak shaving

Energy arbitrage only allows a limited revenue, which is why other applications should be explored in parallel. Scenario 2 runs the optimization as a combined application of energy arbitrage as in Scenario 1 and provision of services to the grid by reducing the peak value of the power flow to the main grid.

This type of peak-shaving prevents congestion and improves the optimal usage of the existing grid assets deferring the necessity for large investments in new infrastructure. The combined storage application is simulated by using the economic optimization of Scenario 1 under the additional constraint equation (32), meaning that the power exchange to the main grid may not exceed a predefined level. Nevertheless, when choosing an unreachable low grid limit the optimization becomes infeasible. Therefore, if the value is not exactly known in advance adaptable soft limits, which penalize any surpassing by a comparatively high cost in the objective function, can be implemented instead.

Looking at a week with very high wind production in March, the differences are summarized in Table 17. Two soft limits of 12 MW and 11 MW have been tested. For the 12 MW case, the maximum power exchange can be successfully be reduced by 2.4 % for the day with the highest peak and with 12.08 MW only surpasses the limit slightly. For another day it can be kept at 12 MW.

Table 17. Comparative results for one week with a limited grid level in Scenario 2A.

| | **Scenario 0** | **Scenario 1** | **Scenario 2A** High limit | **Scenario 2A** Low limit |
|---|---|---|---|---|
| Economic profit [EUR] | 14755 | 14831 | 14820 | 14812 |
| Max export [MWh/h] | 12.40 | 12.19 | 12.08 | 11.81 |
| Soft limit [MW] | - | - | 12.0 | 11.0 |
| Throughput [MWh] | - | 4.82<br>3.15 | 4.38<br>2.51 | 4.23<br>2.38 |

For the 11 MW limit, a drop of the peak by 4.75 % is realized (cf. Figure 39). It is apparent that during several hours the feed-in is reduced with the energy storage. If a lower limit than 11 MW is chosen, the arbitrage model will not function accurately, since the main goal will be to utilize the battery so that the power exported will remain close to the limit and consequently no profits can be obtained from price spreads anymore. Therefore, it will be a tradeoff, between minimizing the peak grid exchange and maximizing arbitrage revenues. Hence, if the benefits of the DSO, which are avoidance or deferral of grid investments, lower grid losses and lower curtailment compensation, are to be monetarized by service agreements, the payment needs to exceed these losses. Yet, as seen in the simulated week, arbitrage only already reduces the peak grid exchange without implementing any additional grid limits. This behavior is likely due to the correlation between the peak load and the peak market prices. It facilitates the operation of a BESS for peak shaving as a grid service and energy arbitrage simultaneously.

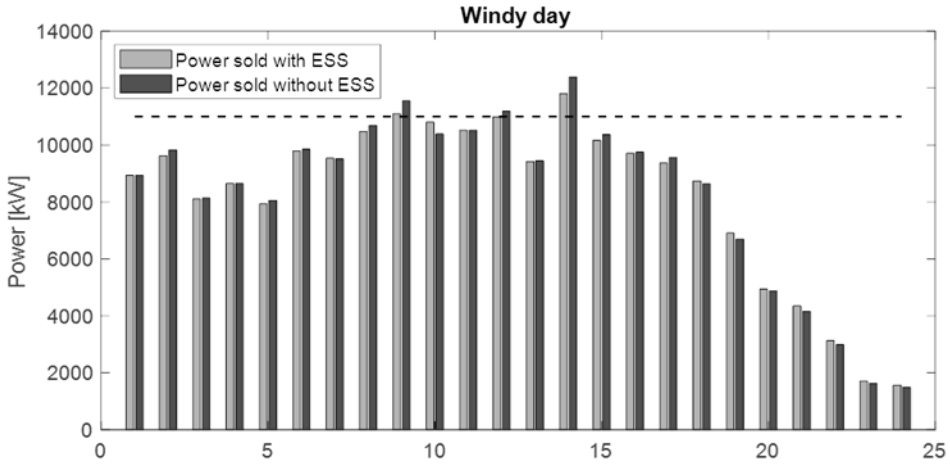


Figure 39. Scenario 2A - grid exchange with soft grid limit of 11 MW. Own elaboration.

According to SH Netz curtailment had to be performed for RES generation on Pellworm during 648 hours in 2018, this equals 7.4 % of all hours. Within the DSO region, where Pellworm is connected to the main grid for 77.5 % of the time RES curtailment had been necessary. The owner of the generation asset is to be compensated by its DSO. In 2018 the total curtailment in Germany was 5403 GWh with an average compensation cost of 117.6 EUR/MWh [113]. With the Pellworm HESS the maximum peak

reduction which can be achieved is approximately 600 kWh/h as demonstrated in Figure 39.

If we assume that the full reduction is not always manageable, in particular due to the limit that a continuous reduction for more than two hours is not possible and thus figure in an average reduction of 70 %, this would generate an additional profit of around 20000 EUR. The estimation as conducted in Table 18 already considers the lost revenues from arbitrage induced by the additional constraint for load-leveling and only reimburses the energy left after cycle losses. This kind of service can be based on bilateral contracts but in the past encountered regulatory issues, since DSOs are highly regulated and limited in their activities how to deal with congestion.

Table 18. Scenario 2A - additional profit via peak shaving for grid.

| | **Estimation for 2018** |
|---|---|
| **Avoided curtailment** | 648 hours |
| **Average reduction with ESS** | 0.7*600 =430 kWh |
| **Average compensation** | 117.6 EUR/MWh |
| **Cycle losses** | 20-25 % |
| **Additional revenues** | 25313 EUR |
| **Average profit loss arbitrage** | 5110 EUR/a |
| **Additional profit** | 20203 EUR |

### B. Increased self-consumption

In addition to peak-shaving which is supportive to the grid, it can also be performed to increase self-consumption and sufficiency, optimizing the utilization of the existing generation assets in the MG. Whereas the arbitrage model utilizes price spreads, and thus a rise in the average day-ahead price does not result in any profit growth for the BESS owner, there is incentive for increasing self-consumption due to the normal spread between the price for buying and selling electricity. The electricity price for end-consumers is significantly higher. In Germany, households pay 30 ct/kWh and industrial customers pay 15 ct/kWh, which is up to 10 times the day-ahead prices from which half of the surcharge is dedicated to taxes and subsidies [114]. The model in Scenario 1 simplified this issue by assuming that the price is the same, since no standardized tariff structure exits yet for the surplus generation or consumption for microgrids. Nowadays, it depends on the size of the microgrid and its ownership and is likely to be a mix of electricity and power-based tariff, which also gives an economic incentive to reduce peak exchange with the grid. A high self-consumption and self-sufficiency is a big motive for microgrids. Hence, a case is simulated, promoting local use of energy, where the spread between power sold and power purchased is set to 5 ct/kWh. To do this the objective function is modified separating $P_{grid}$ and implementing different prices $c_{DA}^{buy}$ and $c_{DA}^{sell}$. Degradation costs are not included in the objective function. With the altered problem formulation, self-consumption is increased to 25.3 % and the self-sufficiency to 97.6 %. The energy throughput is increased significantly in comparison to arbitrage only and both batteries are cycled more aggressively as evident in Appendix C-2. The VRFB achieves 0.72 and the LiB reaches

1.03 EFC per day. Accordingly, also the degradation for LiB with 603 regular cycles is greater than in Scenario 1. The annual degradation reveals that the LiB battery is cycled down to DoD of 80 % more than 1.5 times a day, which would result in a lifetime of 6-7 years, which is half the shelf lifetime. The additional storage revenues amount to approximately 30,590 EUR. When including degradation cost the throughput of LiB decreases by 23 % and the degradation is reduced to 8.8 % and thus lifetime can be extended to 11.5 years. Revenue falls by 6.5 % to 28,590 EUR.

Table 19. Scenario 2B - dispatch results for annual simulation.

| **Annual results** | **Scenario 0** | **Scenario 2B** | **Only VRFB** |
|---|---|---|---|
| Additional profit [EUR] | - | +30590 | +19800 |
| Self-consumption [%] | 24.97 | 25.31 | 25.19 |
| Self-sufficiency [%] | 96.29 | 97.60 | 97.13 |
| Max export [MWh/h] | 12.72 | 12.55 | 12.59 |
| Max import [MWh/h] | 1.57 | 1.53 | 1.54 |
| Throughput VRFB [MWh] | - | 421.6 | 427.0 |
| Throughput LiB [MWh] | - | 211.1 | - |
| Degradation LiB [Cycles] | | 603 (15.07%) | - |

### 5.3.4 Scenario 3: Power quality - frequency regulation

As aforementioned batteries are in general suitable to provide balancing services to improve the power quality and maintain a stable grid frequency. As pointed out in 3.1.1 there are three main frequency reserve products, FCR, aFRR and mFRR which provide different revenue opportunities for a VRFB. To participate in the respective markets certain requirements need to be fulfilled. First, this section evaluates the stacked application of secondary frequency response (aFRR) and arbitrage, building on the developed operation optimization model of Scenario 1. Afterwards a brief overview and techno-economic analysis is given regarding the possibility of providing FCR.

**A. Frequency regulation reserve and arbitrage**

With the previously studied services, a strategy is created where more than one service is offered in parallel, as a stacked model, in order to investigate if this could be a feasible solution.

BESS must comply with specific requirements to be prequalified for FRR, which allows to take part in the auctions. Since July 2018 there is a daily auction where the asset owner can choose between offering positive, negative or both types of aFRR, where positive FRR means power upregulation in the form of discharging active power to the grid and negative FRR signifies downregulation by charging the battery. aFRR is traded in 4-hour blocks on a pay-as-you-bid principle. For each block a bid in the form of a capacity price (EUR/MW) and an energy price (EUR/MWh) is submitted. Any BESS has to prove that it can supply the FRR power for 60 min without recharging measures. In addition, for the whole four hours it must prove that the power can be supplied with measures such as spot market intraday

transactions.

Table 20. aFRR requirements and parameters for Pellworm case.

| FRR secondary reserve | Requirement 2019 | Value | |
|---|---|---|---|
| **Offered FRR power** | $P_{FRR} \geq 1\ MW$ (single) | $500\ kW$ (Pool) | |
| **Limit for upper charge level $C_{ub}$** for $P_{FRR_{neg}}$ | $C_{ub} = \frac{E_{max} - 1h * P_{FCR} * \eta_{sys}^{c}}{E_{nom}}$ | $= \frac{(1340 + 504)kWh - 500\ kWh * 0.9}{(1600 + 560)kWh} = 0.644$ | (49) |
| | For LiB | $C_{ub\_2} = \frac{504kWh - 187.5\ kWh * 0.9}{560\ \text{kWh}} = 0.598$ | (50) |
| **Limit for lower charge level $C_{lb}$** for $P_{FRR_{pos}}$ | $C_{lb} = \frac{E_{min} + 1h * P_{FCR}/\eta_{sys}^{d}}{E_{nom}}$ | $= \frac{192\ kWh + 500\ kWh/0.8}{(1600 + 560)kWh} = 0.378$ | (51) |
| | For LiB | $C_{lb\_2} = \frac{112kWh + 300\ kWh/0.9}{560\ \text{kWh}} = 0.795$ | (52) |

The HESS system on Pellworm is not able to provide the minimum of 1 MW FRR power, since the maximum charge and discharge power of the VRFB are too low and the LiB does meet the requirement, that it can provide constant power for 60 min. Still, the system can become part of a pool. The VRFB can supply 200 kW for several hours, yet for the LiB recharging measures will be necessary. If we assume an FRR power of 0.5 MW as part of an aFRR pool, the following charge limits have to be considered as shown in Table 20 to maintain the prequalification criteria. In the case the full aFRR power is requested the VRFB can only provide around 200 kW, therefore the LiB has to provide the rest, which is why additional constraints (50) apply for LiB. In reality, the duration of one activation is far less than an hour, on average below 15 min, and can be reduced by choosing a bidding strategy with a high energy price.

By adding the following revenue component (53) to the arbitrage objective function and altering the SoC limits as described in Eq. (49) and (51), the benefits can be simulated. The new additional reserve is implemented as a combined constraint of both batteries, as if the HESS had one SoC.

$$R_{FRR}(t) = P_{FRR} * c_{FCR_{res}}(t) + E_{FRR-N}(t) * c_{FRR-N_{act}} + E_{FRR-P}(t) * c_{FRR-P_{act}} \quad (53)$$

$$E_{FRR-N}(t) = P_{FRR} * \Delta t_{FCR,N} \quad (54)$$

As seen in Figure 32 the prices for aFRR obtained from [112] are highly volatile and are fraught with risk. For the simulation two combinations of capacity and energy prices are tested, based on the analysis of historic bid data (cf. Figure 40).

In a strategy without arbitrage the maximum revenue from the reserve price only can be achieved with bids of approximately 10 EUR/MW for negative and 15 EUR/MW for positive. For Pellworm this would result in revenues of 8000-9900 EUR/a. In a stacked scenario with arbitrage the participation in FRR the SoC range is more restricted and the capacity price needs to compensate the losses from arbitrage. Hence, a minimum bid price of 15-20 EUR/MW is selected for hours where the battery typically operates

for arbitrage (9 am-8 pm).

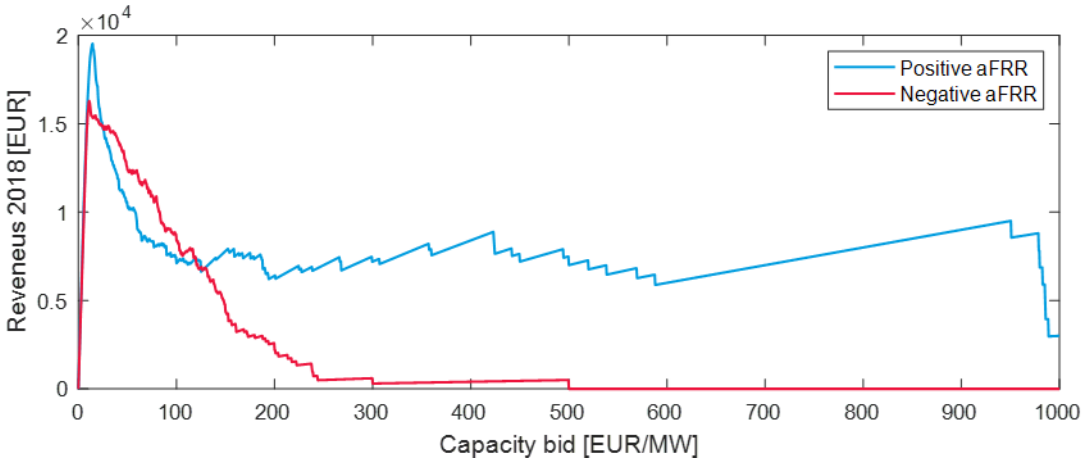


Figure 40. Positive and negative capacity bid aFRR versus capacity revenues in 2018. Own elaboration.

The first option is to offer negative aFRR allowing the battery to be recharged for free. Another option is to offer positive aFRR with a relative high energy price to reduce the chance of activation to avoid the risk of interfering with the arbitrage model (cf. Table 21).

Table 21. Scenario 3A aFRR simulated bidding strategies.

| Bidding strategy | Capacity price [EUR/MW] | Energy price [EUR/MWh] |
|---|---|---|
| **Negative 0-24** | 30 & 20 &15 | 200 |
| **Positive 0-24** | 15 &40 | 1000 |

In the negative aFRR scenario, around 7450 EUR come from the reserve and 4500 EUR from the activation. The arbitrage revenues remain in a similar range as in Scenario 1. Although the SoC is more restricted for 3066 hours, it can compensate the losses due to the free electricity for recharging the battery when activated, which happens 180 times if a bidding strategy of 200 EUR/MWh is chosen. Figure 41 shows a typical day, where the bid is below the marginal capacity price (grey line) only during the morning and the night and where two activations take place (red bars), which means that the marginal energy price exceeds 200 EUR/MWh. After activation the SoC urges back to the predefined limits in the following hour in case of another activation. As soon as the capacity price is not met, the additional SoC limits are lifted and normal arbitrage can take place (from 8 am till 8 pm).

For positive aFRR a higher activation bid has been chosen to avoid that the battery is discharged when spot prices peak, and revenue is generated from arbitrage. Still, with a 1000 EUR/MWh bid the activation happened 82 times. Assuming on average the maximum energy is required for 15-20 minutes more than 10000 EUR can be obtained from the provision. In contrast to negative aFRR this leads to a reduction of revenues from arbitrage. The energy throughput also changes in this case to 197 MWh (VRFB) and 130 MWh (LiB).

The degradation is low with 6.9 % (276 cycles), so that even without including degradation cost, a lifetime

of 13 years can be attained. On the one hand the LiB is more restricted than the VRFB in the reserve mode, which reduces the throughput but increases battery life and on the other hand the VRFB is cycled more often, because the high energy price compensates efficiency losses.

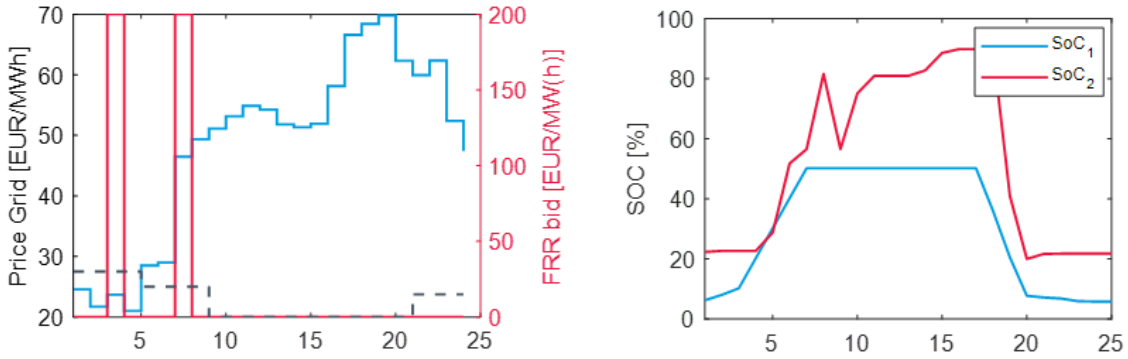


Figure 41. Scenario 3A - SoC curve for negative aFRR and arbitrage application. Own elaboration.

It should be noted that revenues are likely to be larger if the bidding strategy is adapted more frequently and with more market knowhow which factors influence the prices, than executed for this simulation. To utilize arbitrage in parallel, the aFRR reserve can also be limited to certain periods and positive and negative aFRR can be provided alternatingly. However, the results (cf. Table 22) provide a good overview as to how much can be earned with a very simple conservative strategy.

The SmartRegion Pellworm project also made a rough estimate for all three frequency markets as stand-alone application based on only the average reserve capacity price of 2017 and the assumption of 100 % bidding success and calculates a revenue of 9928 EUR for aFRR positive and 2900 EUR for aFRR negative [115]. However, as seen from the simulation, additional revenues from activation can be obtained.

Table 22. Scenario 3A - results of a combination of aFRR and arbitrage.

| **Bidding strategy** | **Revenue aFRR** | | **Arbitrage** | **Total** |
|---|---|---|---|---|
| | Capacity | Energy | | |
| **Negative** | 7452 (35 %) | 4500 (180x) | +4302 | 16254 |
| **Positive** | 7987 (41 %) | 10375 (83x) | +2813 | 21175 |

### B. Frequency containment reserve (FCR) – primary reserve

FCR is a power-based application, requiring high power for maximum 15 minutes, and thus not the primary choice for VRFB. Notwithstanding this, FCR is an attractive option for batteries and today several large-scale batteries already take part in the German FCR market. For BESS it has been the dominant option from the three frequency reserve markets, which is why a short comparison is included in this thesis.

Unlike FRR, a stacked service with FCR is difficult, since FCR is activated several times an hour and any arbitrage transaction would hardly comply with the absolute power and direction required for FCR**.**

The auction for FCR take place weekly and it is a symmetric product, so the asset must be able to provide positive and negative frequency response. FCR requires 0.5 MW as minimal prequalified power $P_{FCR}$. The prequalified power $P_{FCR}$ depends on the maximal charge $P_{ess}^{min}$ and discharge power $P_{ess}^{min}$ as well as the nominal energy capacity $E_{nom}$ since the requirements also define upper and lower boundaries for the charge level. According to the current regulations (cf. Appendix C-6) around 500 kW could be prequalified for Pellworm, without the necessity of becoming part of pool in the form of a virtual power plant.

The requested charge limits for prequalification can be satisfied without a significant adjustment of the existing $SoC$ limits. Still, to avoid overshooting, the existing limits should be further adjusted similar to equation (49), with the difference that the maximum time duration for FCR is 15 minutes instead of 60 minutes for FRR. Additionally, to the requested limits, a fast response within 30 seconds has to be assured. To take part in FCR the activation must work automatically, which means that the battery or its PCC needs to constantly measure the grid frequency and voltage and respond autonomously if it exceeds a certain limit (49.99 Hz or 50.01 HZ) by reducing and increasing active power P(f) or reactive power Q(U). For FCR, the resolution of the grid frequency measurement has to be one second. Besides, an availability of 100 % must be assured during the reserve period.

The revenues are obtained from the capacity reserve price only as there is no additional energy remuneration. The activated FCR power depends on the deviation from the normal grid frequency of 50 Hz and ranges from 5-100 % of the prequalified power (cf. Appendix C-7). Negative and positive activation have the same statistical probability, which keeps the SoC around 50 %. Only, due to system losses, occasionally energy must be procured via the spot market to keep a steady charge level. It is assumed that the bidding offers are accepted for all weeks and that the surplus energy cost can be kept below 100 EUR/a by using the possibility for overfulfillment or provision of FCR within the deadband to adjust the SoC (e.g. recharge) for free

$$C_{FCR}(t) = P_{FCR} * c_{FCR_{res}}(t) \tag{55}$$

Prices for FCR have been experiencing high fluctuations, not only due to reformulation of requirements and market procedures but also because they are influenced by the specific bidding strategy and structure of other market participants. As a simplification the average price of 2018 of 2170 EUR/MW/week is applied.

Table 23. Scenario 3B - revenues from FCR.

| | **FCR primary reserve** |
|---|---|
| **Prequalified power $P_{FCR}$** | 500 kW |
| **Average price $c_{FCR_{res}}$** | 2170 EUR/MW/week |
| **Additional revenue $C_{FCR}$** | 56320 EUR/year |

The findings show that FCR market has a high attractivity for batteries. With regard to VRFB which has a high CAPEX per power the FCR market is more suitable in the form of a hybrid storage system, with another type of storage which can provide a high power, like a LiB as in the case study or a capacitor as discussed in [116] .The VRFB is able to back up the power unit to allow prequalification of storage types with low energy capacity.

### 5.3.5 Economic feasibility

In the previous sections it has been demonstrated that all operation strategies will provide additional revenues for Pellworm and thus are beneficial within the operational planning horizon. Figure 42 summarizes the obtained revenues of the case study analysis. For the best-case improved conditions are applied, including an enhanced roundtrip efficiency of 76 % (VRFB) for arbitrage, a price spread of 7.5 ct/kWh instead of 5 ct/kWh for the local consumption strategy and improved revenues by 25 % from aFRR, due to better bidding strategies. It becomes evident that an operation offering primary frequency regulation, FCR, provides the largest revenues, followed by local consumption and a combined model of positive aFRR and arbitrage. All combined applications with arbitrage increase the revenue of the standalone arbitrage case by 2 to 4 times.

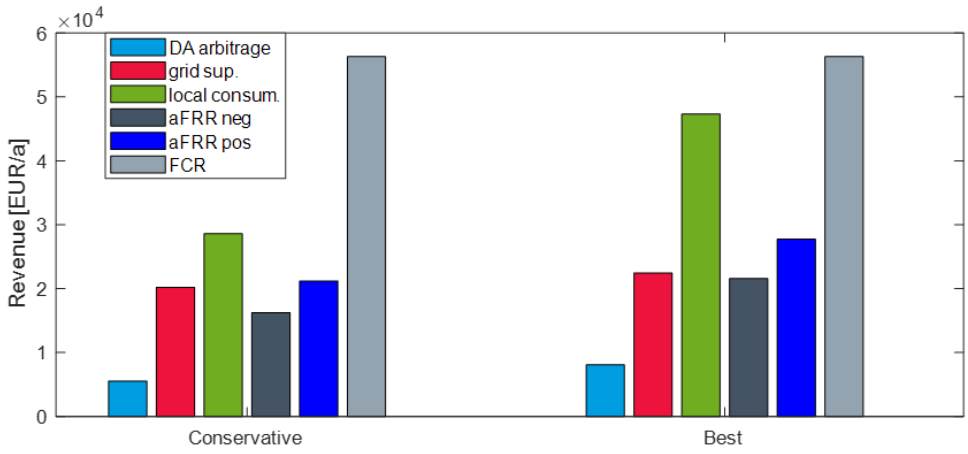


Figure 42. Summary of case results - annual revenues for different applications. Own elaboration.

The focus of the thesis is the operational planning-horizon, as in optimizing the operation of existing assets. Nevertheless, to get an idea whether the integration of VRFB is also a feasible investment an economic evaluation is carried out and the revenues generated from operation are compared with the necessary expenditures. Capital costs for VRFB vary widely according to existing offers and literature. This thesis considers a current case with 530 EUR/kWh and 590 EUR/kWh and a prediction if the

investment was done in 2025 with 238 EUR/kWh and 282 EUR/kWh. The values are obtained from manufacturer prices for large scale systems in the MWh range and additional references from literature [35], [117]. The economic assessments include payback time and Net Present Value (NPV).

The analysis is conducted over 20 years. For ongoing maintenance costs 1 % of the investment costs are adopted. The calculation interest rate is 4 % and the assumed lifetime is 20 years for VRFB and 13 years for LiB if the degradation model is employed to ensure a long cycle life [35], [62].

Table 24. Overview economic results for different applications. Conservative Case.

| ***Conservative*** | **Arbitrage** | **+ grid supportive** | **+ local consum.** | **+ aFRR (neg, pos)** | | **FCR only** |
|---|---|---|---|---|---|---|
| Revenue [EUR] | 5,500 | 20,200 | 28,600 | 16,300 | 21,200 | 56,300 |
| NPV [EUR] | -1.266,000 | -1,091,900 | -923,870 | -1,211,200 | -1,064,000 | -603,200 |
| Payback [years] | - | 140.0 | 70.1 | 263.7 | 125.5 | 26.5 |

The outcomes demonstrate that with the given setting none of the studied applications provide revenues high enough to recover investment cost and an appropriate internal rate of return. The one closest to being financially feasible under current conditions is the provision of FCR as a stand-alone application, followed by local consumption if the price difference between power bought and sold exceeds the simulated 5 ct/kWh spread. Nonetheless, with a reduced CAPEX (by 50-55 %) as it is predicted for 2025 [35], FCR and local-consumption will generate a positive NPV and the other combined applications will all be close to breakeven reaching payback times between 20-35 years. Even though an optimized arbitrage dispatch strategy has been selected, the operation with single purpose spot market arbitrage cannot be considered economically feasible with regard to long-term investments.

Table 25. Overview economic results for different applications. Best Case.

| ***Best*** | **Arbitrage** | **+ grid supportive** | **+ local consum.** | **+ aFRR (neg, pos)** | | **FCR only** |
|---|---|---|---|---|---|---|
| **Revenue [EUR]** | 8,090 | 22,400 | 47,300 | 21,500 | 26,700 | 56,300 |
| **NPV [EUR]** | -505,600 | -232,200 | 264,797 | -330,000 | -262,400 | 124,100 |
| **Payback** | 199 | 31.6 | 12.9 | 33.4 | 25.3 | 10.6 |

However, to deduce any investment implications for new projects, it should be noted that size as for example the E/P ratio of the system under study is not optimized. The high E/P ratio of the VRFB would require longer price valleys and peaks to utilize the whole capacity. For most of the assessed applications a smaller ratio would be more beneficial. According to the authors in [118] profitability from energy trade can be increased by reducing the energy-to-power ratio. For FCR a ratio of 1:1 is assumed to be ideal [119] and 4:1 for aFRR [118]. In addition, larger battery projects in the multi-megawatt scale will reduce specific CAPEX. However, the determination of the ideal size and E/P is an investment decision outside of the daily operational-planning horizon.

# 6 Discussion and implications

This thesis was focused on two major research questions. As an answer to the first formulated problem how to determine the optimal dispatch of a VRFB within a microgrid under uncertain conditions, an optimization algorithm has been developed with the primary application for energy arbitrage which can be extended by secondary use cases as peak shaving and frequency reserve services.

The developed MG-EMS tool can be used as an operational-planning framework for grid-connected microgrids with BESS. It provides an analytical tool for the operator to facilitate and scheduling the VRFB battery operation, either as a single technology or paired with LiB. In addition, the use of model predictive control strategy for optimizing the microgrid power dispatch and VRFB charge and discharge was explored. The proposed formulation includes the equipment power constraints, variable bounds in power rates, state of charge constraints, efficiency criteria, and degradation to prevent early BESS failure while economically allocating the system demand and maximizing revenues from power exchange with the main grid. It was demonstrated that the MPC approach is able to counteract undesired impacts due to uncertain factors, like large power mismatches, which would occur in offline optimizations.

To test the proposed operation strategies and to quantify the economic benefits from the VRFB, the second research question, a case study has been conducted with data from the Island Pellworm. Based on the case study analysis this thesis proposes a few recommendations:

The analysis concluded that for single value streams such as arbitrage the VRFB does not have sufficient economic merit yet. Energy arbitrage has low technical requirements, but the revenues are limited by the daily price spread, which in the German spot market is not enough. This outcome complies with a study by the Fuel Cells and Hydrogen Joint Undertaking (FCH JU) [118] which evaluated time-shifting with various electrochemical storage technologies in the German market and found that neither of them will achieve a positive NPV, unless the price spread doubles in the future. A finding of this thesis is that in a hybrid setting of VRFB and LiB, the VRFB performs deep cycles utilizing longer trends in the price profile, whereas the LiB makes shallow cycles exploiting short-time price volatility. This corresponds to expectations, since the VRFB is characterized by a lower efficiency and a higher E/P ratio. The Pellworm case revealed that for the VRFB the price gap is often not enough to cover the storage losses, leading to long times of no usage. A smaller E/P ratio of the VRFB and additional intraday arbitrage might improve the economic outcomes.

A future focus should be improving the system efficiency from VRFB, which as observed from the sensitivity analysis, has a high impact on the economic viability. In comparison with other papers [115], the obtained revenues from energy trade are lower. Yet, most other techno-economic studies use simulations with perfect foresight resulting in an overestimation of the benefits of BESS since it allows to choose the ideal operation strategy.

The findings suggest that by combining revenue streams from different applications the integration of VRFB has a potential to result in total gains. Adding additional revenues by peakshaving as a congestion

management service for the DSO to avoid curtailment and high grid losses, demonstrated to be a very suitable use case for VRFB paired with LiB. Despite this, any cooperation with DSO/TSO is very limited due to strict regulations and the unbundling requirement.

It has been shown that local consumption should always be considered if the price for selling electricity is lower than the one for consumption. In particular, for industrial or campus microgrids, where the owner structure and regulatory issues are clearer and many levies and charges on the electricity price can be avoided by self-consumption, this is the main business case.

The available frequency reserve markets are characterized by higher technological entry barriers but also higher revenues. The primary reserve, FCR, is the ancillary services product which requires the shortest reaction time and has the highest revenue. The frequency regulation market highly depends on price evolvement, which will be influenced by the number of competitors and the demand for balancing power. If the bids are adjusted the revenues increase or decrease linearly with the reserve and energy price. Whereas many researchers predicted falling prices [120], for 2019 this is only the case for FCR. In particular, the FRR market demonstrates an increasing demand and a rise in prices for 2019. A stacked model with negative aFRR and arbitrage can be beneficial since the free energy from activation can be sold via the day-ahead market. In addition, by combined business models the risk of bidding is reduced, since the battery can be operated fully for arbitrage in case the bid is not accepted.

The results of this study correspond to research on single and combined business models for batteries which demonstrated additional profits by stacking applications: Terlouw et al. [121] showed a promising combination of arbitrage and peak shaving and Klausen et al. [122] concluded that a combination of day-ahead arbitrage and secondary reserve (FRR) will work well together.

Moreover, the case results strongly point out that VRFB and LiB can and should be used complementarily as a hybrid storage system. Many applications require high power but also the certainty that it can be provided for a time duration of up to 4 hours without a long notice in advance to adjust SoC beforehand. Here, a LiB with increased energy capacity would become very expensive. Especially, since 1 kWh of rated energy capacity for VRFB and LiB are not equivalently utilizable. For LiB the useful SoC range is smaller since the DoD should be restricted to avoid fast degradation. The optimization with LiB degradation revealed that in order to reach shelf-life a DoD of 60 % would rarely be exceeded.

To sum up, the thesis provides a data driven operation optimization tool, which allows to simulate different applications with battery-technology specific characteristics and is able to determine a beneficial schedule for the MG. The case study showed that vanadium redox batteries are a versatile solution for MGs, able to generate additional revenues. Their economic feasibility for future investments in MGs highly depends on the MG ownership and tariff structure, battery size and scale and realization of future cost reductions.

# 7 Limitations and future research

With the developed scheduling tool and the tecno-economic case analysis this thesis contributes to the research on battery storage in microgrids, addressing the operational planning perspective and the application of vanadium redox flow technology.

Despite this, the thesis has several limitations, due to the selected simulation and case study research approach and the chosen scope and thus will leave opportunities for future research:

First, a major drawback which all research based on simulations experiences, is that the underlying models only reconstruct part of the reality. Although, this thesis tried to validate and justify its assumptions by using real measurement input or rely on existing studies, uncertainties still remain. Hence, it would be insightful to further follow up and implement the proposed MG-EMS algorithm in a test bed in order to verify its feasibility and determine software and hardware requirements. For realization, when computation speed is highly relevant piecewise linearization of the non-linear properties is suggested.

A second limitation is that the minimum timescale of the proposed energy management strategies is 15 min/1 hour. However, to optimize the power quality within the microgrid or to offer services such as voltage or reactive power regulation to the connected distribution grid, models allowing higher time resolution in seconds are necessary. Closely linked to this and a rich field of further exploration is the evaluation of the effects of the VRFB integration over the grid, considering the problem from the point of view of the DSO.

A high uncertainty exists due to the regulatory unclarity of MGs and BESS. Not only does it remain a question, who apart from the utility will be able to own a microgrid or how the revenues or savings from MG operation will be distributed, but it is also uncertain if a community microgrid can be regarded as “behind the meter” and thus receive tax levitations. If so, how would operators be paid when they are supplying backup power to the microgrid? These questions will have an impact on the feasibility and operation of any kind of battery storage.

Work also remains in the study of hybrid energy storage systems. As seen in the case study a combination of VRFB with LiB has the potential to overcome the limitations of a single technology. Other hybridizations should be studied in the microgrid context.

Microgrids also allow the integration of decentralized batteries and demand response, which has been excluded in this work. Therefore, future research should incorporate additional flexible assets like smart electric vehicle charging and heat pumps. A comparison between different flexibility options in terms of costs and benefits, would deliver valuable insights for future microgrid design and operation.

The levelized costs of wind and photovoltaic have been decreasing steadily, therefore an obvious alternative to VRFB is the oversizing of RES capacity and operating DERs as dispatchable controllable generation instead off constant maximum power. Although challenges result from the unpredictability of RES, it is an interesting option and would avoid ESS cost and conversion losses.

# Appendices

# A Differentiation of ESS applications

Load Leveling and Peak Shaving are often used to describe very similar but not identical applications, as illustrated in the following graphic.

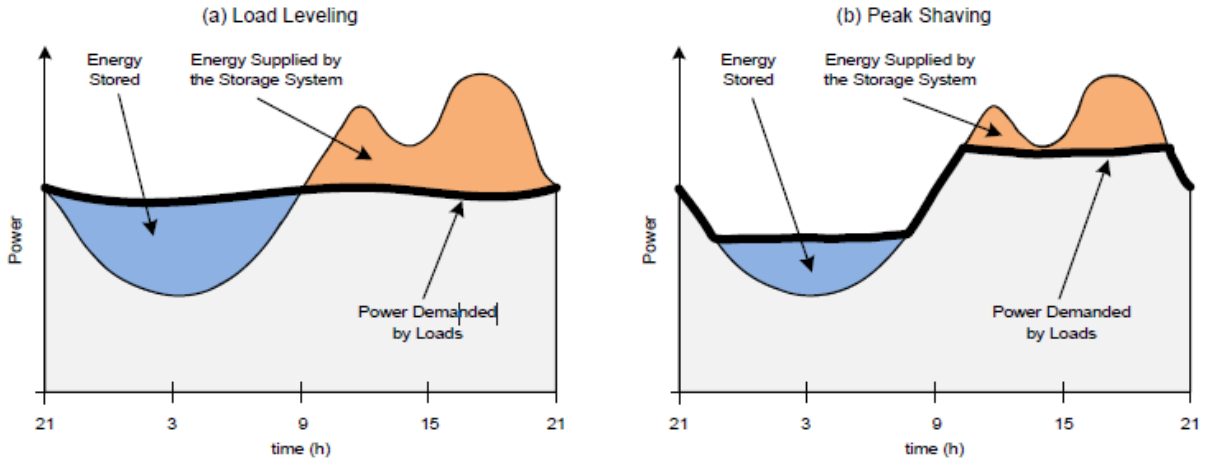


Appendix A-1. Comparison between load leveling (left) and peak shaving (right). [123]

# B Additional case study specifications

## B.1 Technical data battery and inverter

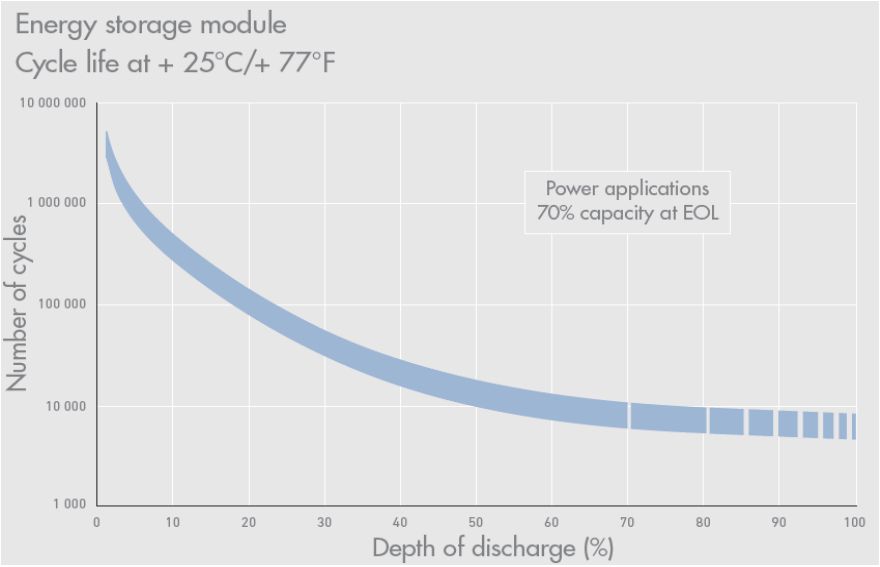


Appendix B-1. Saft Intensium manufacturer data cycle life vs. DoD. [96]

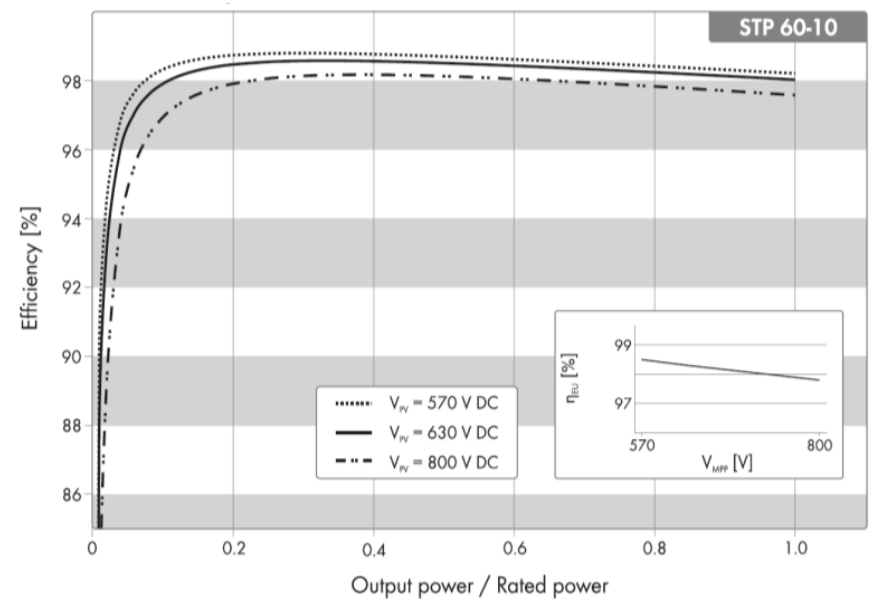


Appendix B-2.Typical battery inverter efficiency curve from SMA. [124]

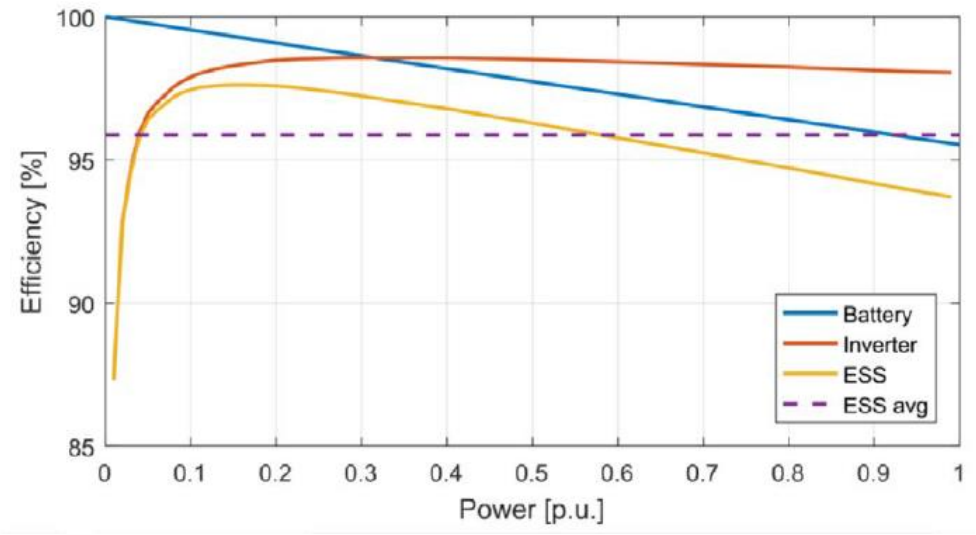


Appendix B-3. LiB ESS, battery and inverter (SMA STP60) efficiency curve. [87]

## B.2 Generation forecast errors

$$RMSE = \sqrt{\frac{1}{T}\sum_{i=1}^{T}\left(p_i^{true} - p_i^{forecast}\right)^2} \tag{56}$$

$$MAE = \frac{1}{T}\sum_{i=1}^{T}\left|p_i^{true} - p_i^{forecast}\right| \tag{57}$$

$$MAPE = \frac{1}{T}\sum_{i=1}^{T}\frac{\left|p_i^{true} - p_i^{forecast}\right|}{p_i^{true}} \tag{58}$$

Appendix B-4. Calculation of prediction errors.

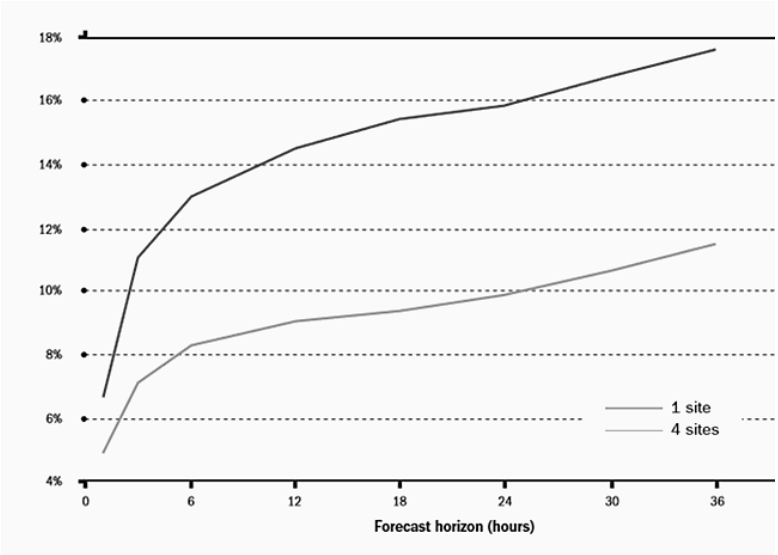


Appendix B-5. MAPE wind prediction error as function of forecast horizon. [125]

## B.3 Generation profiles Pellworm

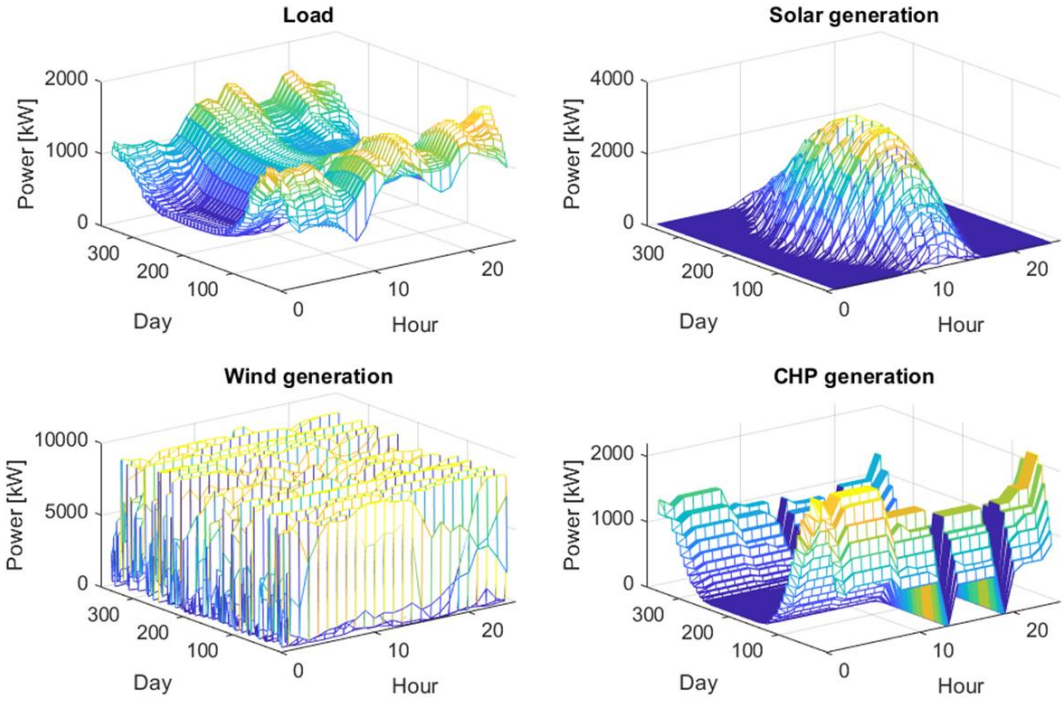


Appendix B-6. Pellworm RES generation input data.

# C Additional case study results

## C.1 Scenario 1 – energy arbitrage

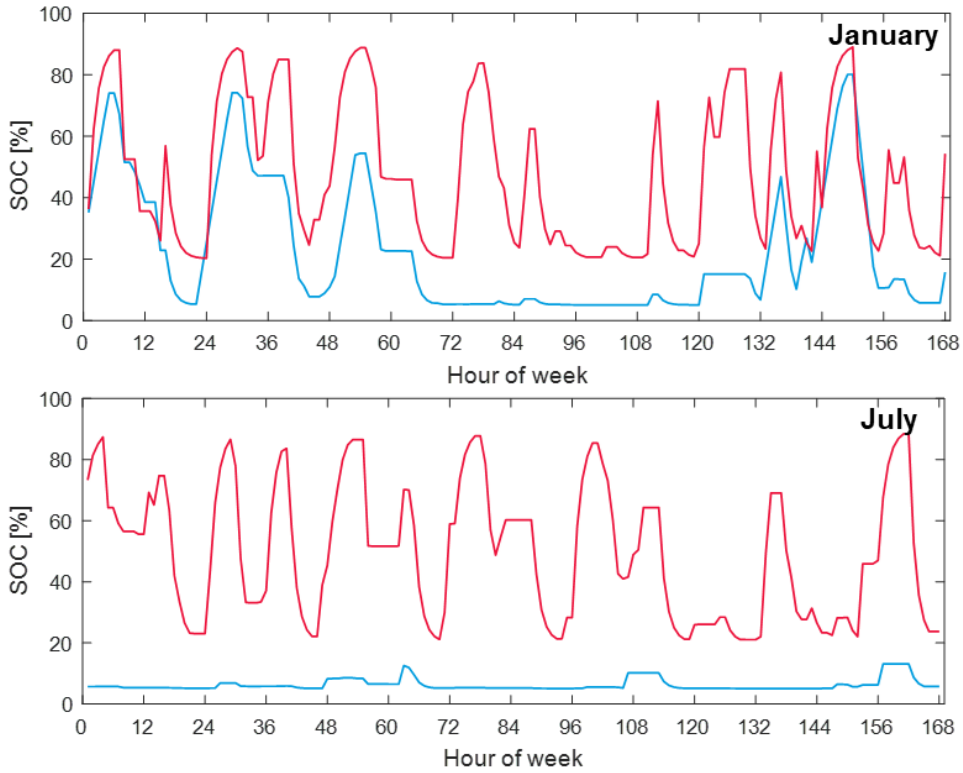


Appendix C-1. Scenario 1 - SoC curves during winter and summer week. Own elaboration.

(n=8-14, n=211-217, $T_p$=12)

## C.2 Self-consumption and self-sufficiency with BESS

Without any storage sinks the definition of self-consumption and self-sufficiency rate is clear:

SCR denotes the ratio between the energy simultaneously self-consumed and the total energy generation from own assets. SSR is defined as the ratio between the self-consumed energy and the total yearly energy demand [120].

However, with battery storage integration, the definitions of SCR and SSR are not that straightforward. Many definitions either add the total energy charged or discharged from the battery to the numerator [71], [126]. Yet, in this case study this would lead to an overestimation of the self-consumption since the discharged battery power might be sold to the grid due to the generation surplus. For this work, the $SCR_{ess}$ it is defined as the ratio of direct self-consumption plus the energy discharged from the battery for own consumption which has been produced locally to the total energy produced. $SSR_{ess}$ is calculated similarly (cf. Eq. (62)) and equals the direct self-consumption plus battery energy divided by the total MG consumption.

$$SCR_{ess} = \frac{E_{direct} + \min\left(E_{charge}^{surplus}, E_{discharge}^{deficit}\right)}{E_{res}} \tag{59}$$

$$E_{direct} = E_{res} - \left| \iint P_{grid}^{0}(P_{grid}^{0} < 0)dt \right| \tag{60}$$

$$\min\left(E_{charge}^{surplus}, E_{discharge}^{deficit}\right) = \min\left( \left| \iint P_{ess}(P_{grid}^{0} < 0)dt \right|, \left| \iint P_{ess}(P_{grid}^{0} > 0))dt \right| \right. \tag{61}$$

$$SSR_{ess} = \frac{E_{direct} + \min\left(E_{charge}^{surplus}, E_{discharge}^{deficit}\right)}{E_{load}} \tag{62}$$

## C.3 Scenario 2 - arbitrage + local consumption

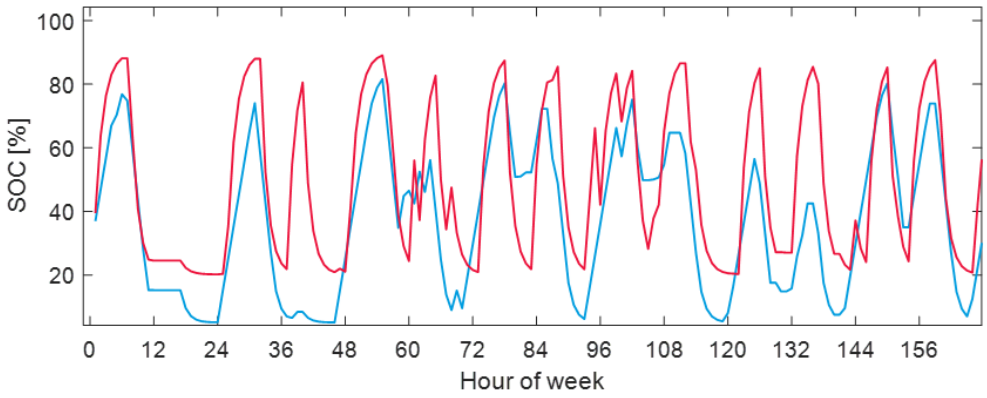


Appendix C-2.Scenario 2B - SoC curve over one week. Own elaboration

Increased self-consumption with a price spread of 5ct/kWh.

## C.4 Scenario 3 – energy arbitrage + aFRR

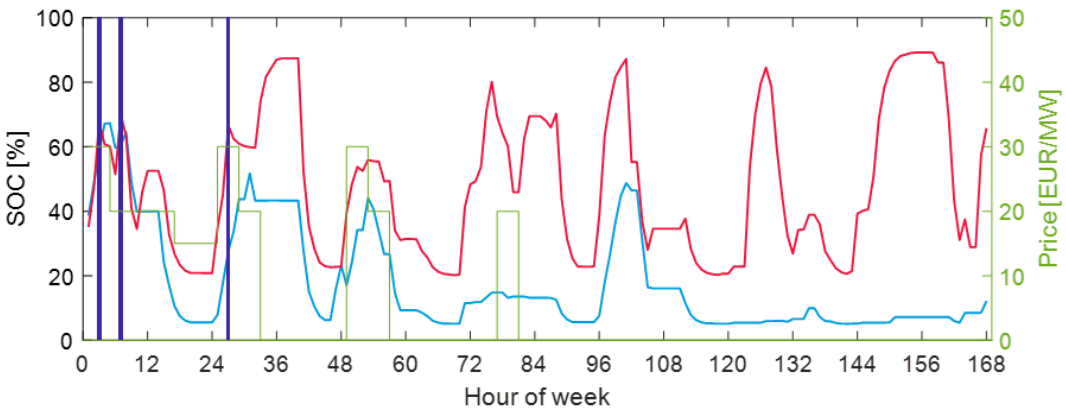


Appendix C-3. Scenario 3 - SoC curve negative aFRR (n=344-350, Tp=12.)

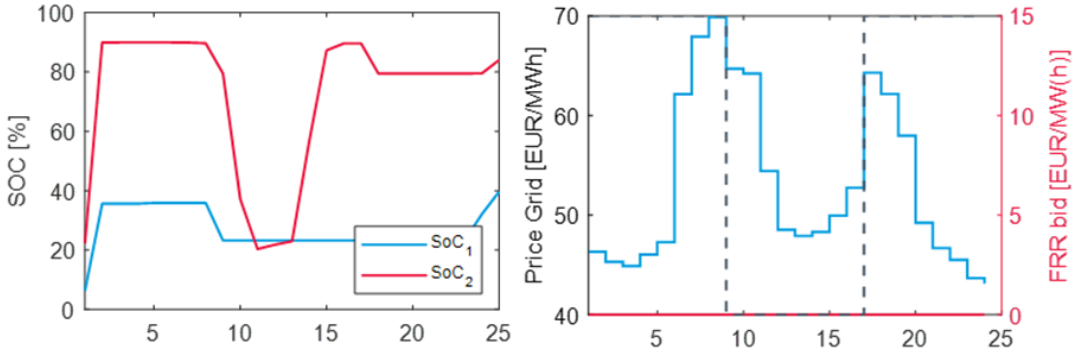


Appendix C-4. Scenario 3 - daily dispatch arbitrage and positive aFRR.

(Grey line shows that bid got accepted from 0-8 am and from 4-12 pm)

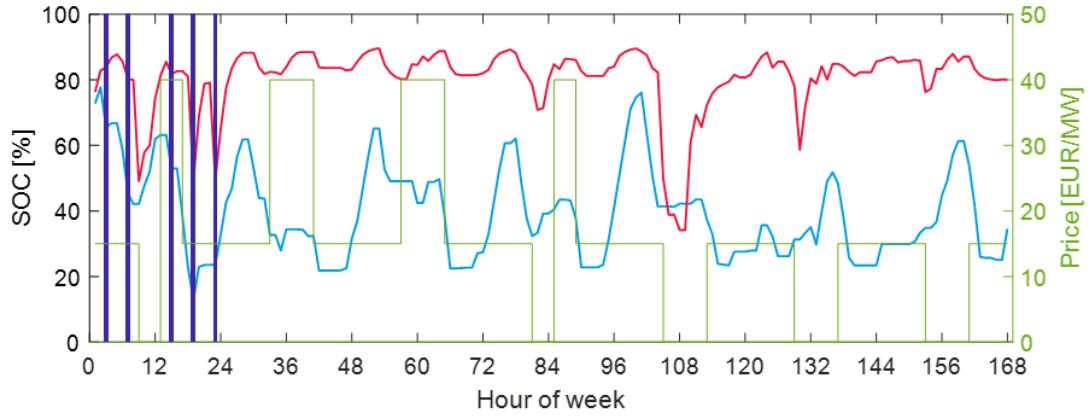


Appendix C-5: Scenario 3 aFRR positive - weekly dispatch in September (n=288-294, Tp=12).

Blue bars denote that an activation of aFRR is taking place and the green line the bid capacity price. If it is larger than zero it was accepted and the specific SoC limits must be considered.

## C.5 Scenario 3 – power quality – FCR

| FCR primary reserve | Formula version 2019 | Value |
|---|---|---|
| **Prequalified power $P_{FCR}$** | $P_{FCR_{pos}} \leq 0.75 * P_{d\,max}$<br>$P_{FCR_{neg}} \leq 0.75 * P_{c,max}$ | $= 0.75\,(1000 + 200) = 900\ kW$<br>$= 0.75 * (200 + 560) = 570\ kW$<br>500 kW |
| **Limit for upper charge level $C_{ub}$** | $C_{ub} = \frac{E_{nom} - 0.25h * P_{FCR}}{E_{nom}}$ | $= \frac{(1600 + 560)kWh - 0.25 * 500\ kW}{(1600 + 560)kWh}$<br>$= 0.94$ |
| **Limit for lower charge level $C_{lb}$** | $C_{lb} = \frac{0.25h * P_{FCR}}{E_{nom}}$ | $= \frac{0.25 * 500kW}{(1600 + 560)kWh} = 0.058$ |

Appendix C-6. Prequalification parameters for FCR in Germany for the Pellworm case.

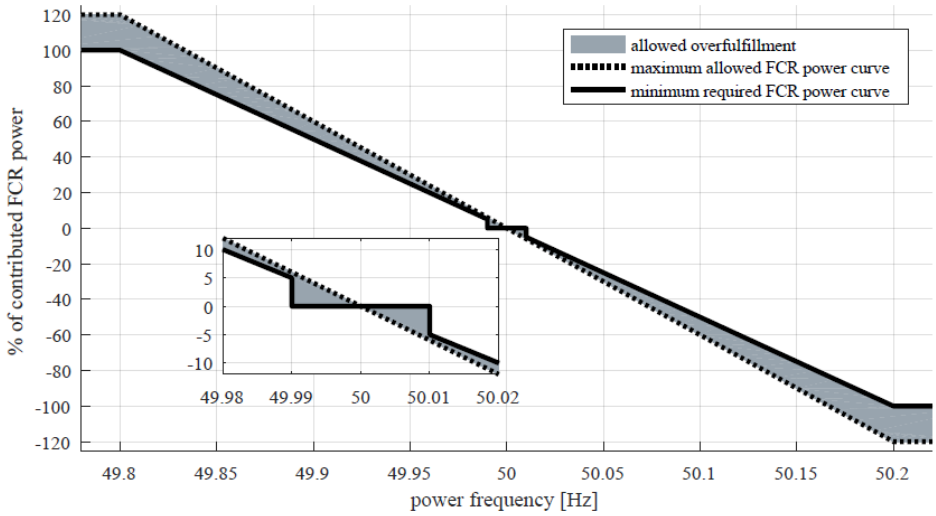


Appendix C-7. Required FCR power depending on frequency deviation. [120]

# Bibliography


[1] C. Marnay *et al.*, “Microgrid Evolution Roadmap,” in *2015 International Symposium on Smart Electric Distribution Systems and Technologies (EDST)*, 2015, pp. 139–144.

[2] E. Sortomme and M. A. El-Sharkawi, “Optimal power flow for a system of microgrids with controllable loads and battery storage,” in *2009 IEEE/PES Power Systems Conference and Exposition*, 2009, pp. 1–5.

[3] X. Tan, Q. Li, and H. Wang, “Advances and trends of energy storage technology in Microgrid,” *Int. J. Electr. Power Energy Syst.*, vol. 44, no. 1, pp. 179–191, Jan. 2013.

[4] J. Leadbetter and L. G. Swan, “Selection of battery technology to support grid-integrated renewable electricity,” *J. Power Sources*, vol. 216, pp. 376–386, Oct. 2012.

[5] M. R. Aghamohammadi and H. Abdolahinia, “A new approach for optimal sizing of battery energy storage system for primary frequency control of islanded microgrid,” *Int. J. Electr. Power Energy Syst.*, vol. 54, pp. 325–333, 2014.

[6] S. X. Chen, H. B. Gooi, and M. Wang, “Sizing of energy storage for microgrids,” *IEEE Trans. Smart Grid*, vol. 3, no. 1, pp. 142–151, 2011.

[7] J. P. Fossati, A. Galarza, A. Martín-Villate, and L. Fontan, “A method for optimal sizing energy storage systems for microgrids,” *Renew. Energy*, vol. 77, pp. 539–549, 2015.

[8] Q. Sun, B. Huang, D. Li, D. Ma, and Y. Zhang, “Optimal placement of energy storage devices in microgrids via structure preserving energy function,” *IEEE Trans. Ind. Inform.*, vol. 12, no. 3, pp. 1166–1179, 2016.

[9] C. Chen, S. Duan, T. Cai, B. Liu, and G. Hu, “Smart energy management system for optimal microgrid economic operation,” *IET Renew. Power Gener.*, vol. 5, no. 3, pp. 258–267, 2011.

[10] A. C. Hernandez, L. Meng, N. L. Diaz, M. Graells, J. C. Vasquez, and J. M. Guerrero, “Online energy management systems for microgrids: experimental validation and assessment framework,” *IEEE Trans. Power Electron.*, vol. 33, no. 3, pp. 2201–2215, 2017.

[11] D. T. Ton and M. A. Smith, “The U.S. Department of Energy’s Microgrid Initiative,” *Electr. J.*, vol. 25, no. 8, pp. 84–94, Oct. 2012.

[12] P. Asmus, “Microgrids: A global view,” presented at the International Symposium on Microgrids, Newcastle, Australia, 2017.

[13] E. Wood, “Microgrid Market Forecast to Reach $30.9B by 2027: Navigant,” *Microgrid Knowledge*, Aug-2018. .

[14] L. Meng, E. R. Sanseverino, A. Luna, T. Dragicevic, J. C. Vasquez, and J. M. Guerrero, “Microgrid supervisory controllers and energy management systems: A literature review,” *Renew. Sustain. Energy Rev.*, vol. 60, pp. 1263–1273, Jul. 2016.

[15] M. Musio, A. Serpi, C. Musio, and A. Damiano, “Optimal management strategy of energy storage systems for RES-based microgrids,” in *IECON 2015-41st Annual Conference of the IEEE Industrial Electronics Society*, 2015.

[16] Y. Yoldaş, A. Önen, S. M. Muyeen, A. V. Vasilakos, and İ. Alan, “Enhancing smart grid with microgrids: Challenges and opportunities,” *Renew. Sustain. Energy Rev.*, vol. 72, pp. 205–214, 2017.

[17] S. Parhizi, H. Lotfi, A. Khodaei, and S. Bahramirad, “State of the art in research on microgrids: A review,” *Ieee Access*, vol. 3, pp. 890–925, 2015.

[18] IEEE Power and Energy Society, “IEEE Standard for the Specification of Microgrid Controllers,” New York, IEEE 2030.7, 2018.

[19] K. Antoniadou-Plytaria and G. Pinares, “Specifications of functional requirements,” ERA-Net Smart Grids Plus, Gothenborg, m2m-grid project report Deliverable 2.2, 2018.

[20] A. C. L. Hernández, “Energy Management Systems for Microgrids Equipped with Renewable Energy Sources and Battery Units,” PhD Thesis, Aalborg Universitetsforlag, 2017.

[21] S. Phrakonkham, J.-Y. Le Chenadec, D. Diallo, G. Remy, and C. Marchand, “Reviews on micro-grid configuration and dedicated hybrid system optimization software tools: application to Laos,” *Eng. J.*, vol. 14, no. 3, pp. 15–34, 2010.

[22] X. Liu, P. Wang, and P. C. Loh, “A hybrid AC/DC microgrid and its coordination control,” *IEEE Trans. Smart Grid*, vol. 2, no. 2, pp. 278–286, 2011.

[23] J. M. Guerrero, M. Chandorkar, T. Lee, and P. C. Loh, “Advanced Control Architectures for Intelligent Microgrids—Part I: Decentralized and Hierarchical Control,” *IEEE Trans. Ind. Electron.*, vol. 60, no. 4, pp. 1254–1262, Apr. 2013.

[24] M. F. Zia, E. Elbouchikhi, and M. Benbouzid, “Microgrids energy management systems: A critical review on methods, solutions, and prospects,” *Appl. Energy*, 2018.

[25] A. K. Basu, S. P. Chowdhury, S. Chowdhury, and S. Paul, “Microgrids: Energy management by strategic deployment of DERs—A comprehensive survey,” *Renew. Sustain. Energy Rev.*, vol. 15, no. 9, pp. 4348–4356, 2011.

[26] L. Munuera, “Energy storage. Tracking Clean Energy Progress,” *International Energy Agency (IEA)*, Jun-2019. [Online]. Available: https://www.iea.org/tcep/energyintegration/energystorage/. [Accessed: 18-Aug-2019].

[27] Navigant Research, “Market Data: Energy Storage for Microgrids,” *Market Data: Energy Storage for Microgrids*, 2017. [Online]. Available: https://www.navigantresearch.com/reports/market-data-energy-storage-for-microgrids. [Accessed: 18-Aug-2019].

[28] F.-B. Wu, B. Yang, and J.-L. Ye, Eds., “Chapter 2 - Technologies of energy storage systems,” in *Grid-scale Energy Storage Systems and Applications*, Academic Press, 2019, pp. 17–56.

[29] H. Ibrahim, A. Ilinca, and J. Perron, “Energy storage systems—Characteristics and comparisons,” *Renew. Sustain. Energy Rev.*, vol. 12, no. 5, pp. 1221–1250, 2008.

[30] P. Breeze, *Power System Energy Storage Technologies*. Academic Press, 2018.

[31] I. E. Commission, “Grid Integration of Large Capacity Renewable Energy Sources and Use of Large-capacity Electrical Energy Storage,” Geneva, 2012.

[32] H. Chen, T. N. Cong, W. Yang, C. Tan, Y. Li, and Y. Ding, “Progress in electrical energy storage system: A critical review,” *Prog. Nat. Sci.*, vol. 19, no. 3, pp. 291–312, Mar. 2009.

[33] R. Schmalensee, *The future of solar energy: an interdisciplinary MIT study*. Energy Initiative, Massachusetts Institute of Technology, 2015.

[34] X. Luo, J. Wang, M. Dooner, and J. Clarke, “Overview of current development in electrical energy storage technologies and the application potential in power system operation,” *Appl. Energy*, vol. 137, pp. 511–536, Jan. 2015.

[35] O. Schmidt, S. Melchior, A. Hawkes, and I. Staffell, “Projecting the future levelized cost of electricity storage technologies,” *Joule*, vol. 3, no. 1, pp. 81–100, 2019.

[36] M. Sterner and I. Stadler, *Energiespeicher-Bedarf, Technologien, Integration*. Springer-Verlag, 2014.

[37] B. Zakeri and S. Syri, “Electrical energy storage systems: A comparative life cycle cost analysis,” *Renew. Sustain. Energy Rev.*, vol. 42, pp. 569–596, Feb. 2015.

[38] V. Jülch, “Comparison of electricity storage options using levelized cost of storage (LCOS) method,” *Appl. Energy*, vol. 183, pp. 1594–1606, Dec. 2016.

[39] Lazard, “Lazard’s levelized cost of storage analysis,” Version 3.0, 2017.

[40] A. Smallbone, V. Jülch, R. Wardle, and A. P. Roskilly, “Levelised Cost of Storage for Pumped Heat Energy Storage in comparison with other energy storage technologies,” *Energy Convers. Manag.*, vol. 152, pp. 221–228, Nov. 2017.

[41] M. Ulaganathan, V. Aravindan, Q. Yan, S. Madhavi, M. Skyllas-Kazacos, and T. M. Lim, “Recent Advancements in All-Vanadium Redox Flow Batteries,” *Adv. Mater. Interfaces*, vol. 3, no. 1, p. 1500309, Jan. 2016.

[42] M. Skyllas-Kazacos and J. F. McCann, “Vanadium redox flow batteries (VRBs) for medium-and

large-scale energy storage," in *Advances in batteries for medium and large-scale energy storage*, Elsevier, 2015, pp. 329–386.

[43] P. Leung, X. Li, C. P. De León, L. Berlouis, C. J. Low, and F. C. Walsh, "Progress in redox flow batteries, remaining challenges and their applications in energy storage," *Rsc Adv.*, vol. 2, no. 27, pp. 10125–10156, 2012.

[44] M. Marinelli, S. Massucco, and F. Silvestro, "Wind Turbine and Electrochemical Based Storage Modeling and Integrated Control Strategies to Improve Renewable Energy Integration in the Grid," 2011.

[45] V. Fernão Pires, E. Romero-Cadaval, D. Vinnikov, I. Roasto, and J. F. Martins, "Power converter interfaces for electrochemical energy storage systems – A review," *Energy Convers. Manag.*, vol. 86, pp. 453–475, Oct. 2014.

[46] D. Everett, "Redox chemistry," *Education in Chemistry*, 03-Jul-2015. [Online]. Available: https://eic.rsc.org/cpd/redox-chemistry/2000011.article. [Accessed: 12-Aug-2019].

[47] W. Li, R. Zaffou, C. C. Sholvin, M. L. Perry, and Y. She, "Vanadium redox-flow-battery electrolyte preparation with reducing agents," *ECS Trans.*, vol. 53, no. 7, pp. 93–99, 2013.

[48] C. Ponce de León, A. Frías-Ferrer, J. González-García, D. A. Szánto, and F. C. Walsh, "Redox flow cells for energy conversion," *J. Power Sources*, vol. 160, no. 1, pp. 716–732, Sep. 2006.

[49] S. König, "Model-based design and optimization of vanadium redox flow batteries," Karlsruhe Institute of Technology (KIT), Karlsruhe, 2017.

[50] K. W. Knehr and E. C. Kumbur, "Open circuit voltage of vanadium redox flow batteries: Discrepancy between models and experiments," *Electrochem. Commun.*, vol. 13, no. 4, pp. 342–345, Apr. 2011.

[51] B. Türker, S. Klein, E. Hammer, B. Lenz, and L. Komsiyska, "Modeling a vanadium redox flow battery system for large scale applications," *Energy Convers. Manag.*, vol. 66, pp. 26–32, Feb. 2013.

[52] C. Blanc and A. Rufer, "Understanding the Vanadium Redox Flow Batteries," Shanghai, 2010.

[53] S. Eckroad, "Vanadium redox flow batteries: an in-depth analysis," *Electr. Power Res. Inst. Palo Alto CA*, vol. 1014836, 2007.

[54] VisBlue, "VisBlue product datasheet–Vanadium Redox Flow Battery." 2019.

[55] W. Byrne, C. Pineda, B. Smith, R. Wartena, and K. Moy, "Integrated Solar PV, Vanadium Redox Flow Battery, and Microgrid Demonstration Report," California Energy Commission Foresight Renewable Solutions and Growing Energy Labs, 2017.

[56] B. R. Chalamala, T. Soundappan, G. R. Fisher, M. R. Anstey, V. V. Viswanathan, and M. L. Perry, "Redox flow batteries: an engineering perspective," *Proc. IEEE*, vol. 102, no. 6, pp. 976–999, 2014.

[57] Enerox GmbH, "Technical data CellCube FB250-1000." 2019.

[58] Beatriz Ruiz Castello and Huamin Zhang, *IEC 62932 Flow Battery Systems for Stationary applications Part 1 & 2*, vol. TC 21. 2019.

[59] R. Dell, D. A. J. Rand, and R. Bailey Jr, *Understanding batteries*. Royal Society of Chemistry, 2001.

[60] T. Shigematsu, "Redox flow battery for energy storage," *SEI Tech. Rev.*, vol. 73, no. 7, p. 13, 2011.

[61] C. Doetsch and J. Burfeind, "Vanadium Redox Flow Batteries," in *Storing Energy*, Elsevier, 2016, pp. 227–246.

[62] S. Weber, J. F. Peters, M. Baumann, and M. Weil, "Life cycle assessment of a vanadium redox flow battery," *Environ. Sci. Technol.*, vol. 52, no. 18, pp. 10864–10873, 2018.

[63] M. Skyllas-Kazacos, M. H. Chakrabarti, S. A. Hajimolana, F. S. Mjalli, and M. Saleem, "Progress in flow battery research and development," *J. Electrochem. Soc.*, vol. 158, no. 8, pp. R55–R79, 2011.

[64] M. Guarnieri, P. Mattavelli, G. Petrone, and G. Spagnuolo, “Vanadium Redox Flow Batteries,” *IEEE Ind Electron Mag*, vol. 10, pp. 20–31, 2016.

[65] C. Minke, U. Kunz, and T. Turek, “Techno-economic assessment of novel vanadium redox flow batteries with large-area cells,” *J. Power Sources*, vol. 361, pp. 105–114, Sep. 2017.

[66] A. Malhotra, B. Battke, M. Beuse, A. Stephan, and T. Schmidt, “Use cases for stationary battery technologies: A review of the literature and existing projects,” *Renew. Sustain. Energy Rev.*, vol. 56, pp. 705–721, Apr. 2016.

[67] B. Battke and T. S. Schmidt, “Cost-efficient demand-pull policies for multi-purpose technologies – The case of stationary electricity storage,” *Appl. Energy*, vol. 155, pp. 334–348, Oct. 2015.

[68] European Network of Transmission System Operators for Electricity, “An Overview of the European Balancing Market and Electricity Balancing Guideline,” entso-e, Nov. 2018.

[69] A. K. Arani, G. B. Gharehpetian, and M. Abedi, “Review on energy storage systems control methods in microgrids,” *Int. J. Electr. Power Energy Syst.*, vol. 107, pp. 745–757, 2019.

[70] D. Semënov, G. Mirzaeva, C. D. Townsend, and G. C. Goodwin, “A battery storage control scheme for AC microgrids,” in *2017 20th International Conference on Electrical Machines and Systems (ICEMS)*, 2017, pp. 1–6.

[71] A. Anvari-Moghaddam, J. Dulout, C. Alonso, B. Jammes, and J. M. Guerrero, “Optimal Design and Operation Management of Battery-Based Energy Storage Systems (BESS) in Microgrids,” *Adv. Energy Storage Technol.*, p. 145, 2018.

[72] O. Palizban and K. Kauhaniemi, “Hierarchical control structure in microgrids with distributed generation: Island and grid-connected mode,” *Renew. Sustain. Energy Rev.*, vol. 44, pp. 797–813, Apr. 2015.

[73] X. Feng, A. Shekhar, F. Yang, R. E. Hebner, and P. Bauer, “Comparison of hierarchical control and distributed control for microgrid,” *Electr. Power Compon. Syst.*, vol. 45, no. 10, pp. 1043–1056, 2017.

[74] M. Guarnieri, A. Bovo, A. Giovannelli, and P. Mattavelli, “A Real Multitechnology Microgrid in Venice: A Design Review,” *IEEE Ind. Electron. Mag.*, vol. 12, no. 3, pp. 19–31, 2018.

[75] J. Lee *et al.*, “Optimal Operation of an Energy Management System Using Model Predictive Control and Gaussian Process Time-Series Modeling,” *IEEE J. Emerg. Sel. Top. Power Electron.*, vol. 6, no. 4, pp. 1783–1795, 2018.

[76] E.-K. Lee, W. Shi, R. Gadh, and W. Kim, “Design and Implementation of a Microgrid Energy Management System,” *Sustainability*, vol. 8, p. 1143, Nov. 2016.

[77] J. Ma and X. Ma, “A review of forecasting algorithms and energy management strategies for microgrids,” *Syst. Sci. Control Eng.*, vol. 6, no. 1, pp. 237–248, Jan. 2018.

[78] D. Neves, M. C. Brito, and C. A. Silva, “Impact of solar and wind forecast uncertainties on demand response of isolated microgrids,” *Renew. Energy*, vol. 87, pp. 1003–1015, Mar. 2016.

[79] D. Tran and A. M. Khambadkone, “Energy Management for Lifetime Extension of Energy Storage System in Micro-Grid Applications,” *IEEE Trans. Smart Grid*, vol. 4, no. 3, pp. 1289–1296, Sep. 2013.

[80] S. M. Nosratabadi, R.-A. Hooshmand, and E. Gholipour, “A comprehensive review on microgrid and virtual power plant concepts employed for distributed energy resources scheduling in power systems,” *Renew. Sustain. Energy Rev.*, vol. 67, pp. 341–363, 2017.

[81] S. Mohammadi, S. Soleymani, and B. Mozafari, “Scenario-based stochastic operation management of MicroGrid including Wind, Photovoltaic, Micro-Turbine, Fuel Cell and Energy Storage Devices,” *Int. J. Electr. Power Energy Syst.*, vol. 54, pp. 525–535, Jan. 2014.

[82] A. Parisio and L. Glielmo, “A mixed integer linear formulation for microgrid economic scheduling,” in *2011 IEEE International Conference on Smart Grid Communications (SmartGridComm)*, 2011, pp. 505–510.

[83] M.-H. Lin, J.-F. Tsai, and C.-S. Yu, “A review of deterministic optimization methods in engineering and management,” *Math. Probl. Eng.*, vol. 2012, 2012.

[84] H. Li, A. T. Eseye, J. Zhang, and D. Zheng, “Optimal energy management for industrial microgrids with high-penetration renewables,” *Prot. Control Mod. Power Syst.*, vol. 2, no. 1, p. 12, Apr. 2017.

[85] C. Hu, S. Luo, Z. Li, X. Wang, and L. Sun, “Energy Coordinative Optimization of Wind-Storage-Load Microgrids Based on Short-Term Prediction,” *Energies*, vol. 8, no. 2, pp. 1505–1528, Feb. 2015.

[86] B. Turker, S. Arroyo Klein, E.-M. Hammer, B. Lenz, and L. Komsiyska, “Modeling a vanadium redox flow battery system for large scale applications,” *Energy Convers. Manag.*, vol. 66, pp. 26–32, Feb. 2013.

[87] A. Hentunen, J. Forsström, and V. Mukherjee-VTT, “Smart system of renewable energy storage based on INtegrated EVs and bAtteries to empower mobile, Distributed and centralised Energy storage in the distribution grid,” 2018.

[88] M. Koller, T. Borsche, A. Ulbig, and G. Andersson, “Defining a degradation cost function for optimal control of a battery energy storage system,” in *2013 IEEE Grenoble Conference*, 2013, pp. 1–6.

[89] B. Xu, A. Oudalov, A. Ulbig, G. Andersson, and D. S. Kirschen, “Modeling of Lithium-Ion Battery Degradation for Cell Life Assessment,” *IEEE Trans. Smart Grid*, vol. 9, no. 2, pp. 1131–1140, Mar. 2018.

[90] L. K. Gan, J. Reniers, and D. Howey, “A hybrid vanadium redox/lithium-ion energy storage system for off-grid renewable power,” in *2017 IEEE Energy Conversion Congress and Exposition (ECCE)*, 2017, pp. 1016–1023.

[91] HOMER Energy, “Battery Throughput,” *Battery throughput*. [Online]. Available: https://www.homerenergy.com/products/pro/docs/latest/battery_throughput.html. [Accessed: 06-Oct-2019].

[92] S. Saxena, C. Le Floch, J. MacDonald, and S. Moura, “Quantifying EV battery end-of-life through analysis of travel needs with vehicle powertrain models,” *J. Power Sources*, vol. 282, pp. 265–276, May 2015.

[93] W. Ying, Z. Zhi, A. Botterud, K. Zhang, and D. Qia, “Stochastic coordinated operation of wind and battery energy storage system considering battery degradation,” *J. Mod. Power Syst. Clean Energy*, vol. 4, no. 4, pp. 581–592, 2016.

[94] G. Gowrisankaran, S. S. Reynolds, and M. Samano, “Intermittency and the value of renewable energy,” *J. Polit. Econ.*, vol. 124, no. 4, pp. 1187–1234, 2016.

[95] H. Holttinen and G. Koreneff, “Imbalance Costs of Wind Power for a Hydro Power Producer in Finland,” *Wind Eng.*, vol. 36, no. 1, pp. 53–67, Feb. 2012.

[96] Saft Batteries, “Lithium battery life - Energy Storage Systems Technical data sheet,” May 2014.

[97] Power Calculation, “Genset (diesel engine, diesel generator) consumption, power and energy calculator - free on-line tool,” 2018. [Online]. Available: https://power-calculation.com/generator-diesel-energy-calculator-genset.php. [Accessed: 05-Sep-2019].

[98] Schütt, Reiner Johannes and Nicolai, Steffen, “Innovationsstudie Pellworm. Zukünftige elektrische Energieversorgung der Insel Pellworm. Technik.,” West Coast University of Applied Scienes. Fraunhofer AST. E.ON Hanse., Heide, Abschlussbericht, 2011.

[99] Schleswig-Holstein Netz AG, “Energie Überblick - Pellworm.” 2015.

[100] ED Netze GmbH, “Lastprofile, Temperaturtabellen,” *Lastprofile und Temperaturtabellen*, 2019. [Online]. Available: https://www.ednetze.de/geschaeftspartner/lieferanten/lastprofile-temperaturtabellen/. [Accessed: 13-Aug-2019].

[101] Bundesnetzagentur, “Marktstammdatenregister,” *Marktstammdatenregister*, 31-Dec-2018. [Online]. Available: https://www.marktstammdatenregister.de/MaStR/Einheit/Einheiten/OeffentlicheEinheitenuebersicht#_. [Accessed: 27-Aug-2019].

[102] Technical University of Denmark (DTU), “Global Wind Atlas 2.0,” *Global Wind Atlas 2.0, a free, web-based application developed, owned and operated by the Technical University of Denmark (DTU) in partnership with the World Bank Group, utilizing data provided by Vortex, with funding*

*provided by the Energy Sector Management Assistance Program (ESMAP)*, 2019. [Online]. Available: https://globalwindatlas.info. [Accessed: 28-Aug-2019].

[103] S. Nykamp, “Integrating renewables in distribution grids: Storage, regulation and the interaction of different stakeholders in future grids,” Oct. 2013.

[104] Z. Li, C. Zang, P. Zeng, and H. Yu, “Combined Two-Stage Stochastic Programming and Receding Horizon Control Strategy for Microgrid Energy Management Considering Uncertainty,” *Energies*, vol. 9, no. 7, p. 499, Jul. 2016.

[105] A. M. Foley, P. G. Leahy, A. Marvuglia, and E. J. McKeogh, “Current methods and advances in forecasting of wind power generation,” *Renew. Energy*, vol. 37, no. 1, pp. 1–8, 2012.

[106] E. Xydas, M. Qadrdan, C. Marmaras, L. Cipcigan, N. Jenkins, and H. Ameli, “Probabilistic wind power forecasting and its application in the scheduling of gas-fired generators,” *Appl. Energy*, vol. 192, pp. 382–394, Apr. 2017.

[107] R. Huang, T. Huang, R. Gadh, and N. Li, “Solar generation prediction using the ARMA model in a laboratory-level micro-grid,” in *2012 IEEE Third International Conference on Smart Grid Communications (SmartGridComm)*, 2012, pp. 528–533.

[108] D. P. Larson, L. Nonnenmacher, and C. F. Coimbra, “Day-ahead forecasting of solar power output from photovoltaic plants in the American Southwest,” *Renew. Energy*, vol. 91, pp. 11–20, 2016.

[109] L. Hernández, C. Baladrón, J. M. Aguiar, B. Carro, A. Sánchez-Esguevillas, and J. Lloret, “Artificial neural networks for short-term load forecasting in microgrids environment,” *Energy*, vol. 75, pp. 252–264, Oct. 2014.

[110] Y.-J. Ma and M.-Y. Zhai, “Day-Ahead Prediction of Microgrid Electricity Demand Using a Hybrid Artificial Intelligence Model,” *Processes*, vol. 7, no. 6, p. 320, Jun. 2019.

[111] S. Idowu, S. Saguna, C. \AAhlund, and O. Schelén, “Forecasting heat load for smart district heating systems: A machine learning approach,” in *2014 IEEE International Conference on Smart Grid Communications (SmartGridComm)*, 2014, pp. 554–559.

[112] 50Hertz, Amprion, TenneT TSO, and TransnetBW, “Datacenter FCR/aFRR/mFRR.” [Online]. Available: https://www.regelleistung.net/apps/datacenter/tenders/?productTypes=SRL&from=2019-09-09&to=2018-09-09&tid=SRL_20180909_D1. [Accessed: 26-Aug-2019].

[113] Bundesnetzagentur, “4. Quartalsbericht 2018 zu Netz-und Systemsicherheitsmaßnahmen [4th quarterly report on network and system security-measures],” 2019.

[114] Eurostat, “Electricity prices for non-household consumers, second half 2018 (EUR per kWh),” 2018. [Online]. Available: https://ec.europa.eu/eurostat/statistics-explained/index.php?title=File:Electricity_prices_for_non-household_consumers,_second_half_2018_(EUR_per_kWh).png. [Accessed: 18-Sep-2019].

[115] HanseWerk AG, “Smart Region Pellworm 2.0 Energiewende und Batteriespeicher - Wirtschaftlichkeit im Test,” Quickborn, Ergebnisse der 2.Phase des Forschungsprojektes, May 2018.

[116] S. M. Vaca, C. Patsios, and P. Taylor, “Enhancing frequency response of wind farms using hybrid energy storage systems,” in *2016 IEEE International Conference on Renewable Energy Research and Applications (ICRERA)*, 2016, pp. 325–329.

[117] A. IRENA, *Electricity storage and renewables: Costs and markets to 2030*. Author Abu Dhabi, 2017.

[118] J. FCH, “Commercialisation of energy storage in Europe,” *Fuel Cells Hydrog. Jt. Undert. FCH JU*, vol. 19, Mar. 2015.

[119] J. Engels, B. Claessens, and G. Deconinck, “Techno-economic analysis and optimal control of battery storage for frequency control services, applied to the German market,” *Appl. Energy*, vol. 242, pp. 1036–1049, 2019.

[120] D.-B. Steber, “Integration of Decentralized Battery Energy Storage Systems into the German Electrical Power System,” 2018.

[121] T. Terlouw, T. AlSkaif, C. Bauer, and W. van Sark, “Multi-objective optimization of energy arbitrage in community energy storage systems using different battery technologies,” *Appl. Energy*, vol. 239, pp. 356–372, Apr. 2019.

[122] M. Klausen, M. Resch, and J. Bühler, “Analyis of a Potential Single and Combined Business Model for Stationary Battery Storage Systems,” *Energy Procedia*, vol. 99, pp. 321–331, 2016.

[123] Á. Cunha *et al.*, “Assessment of the use of vanadium redox flow batteries for energy storage and fast charging of electric vehicles in gas stations,” *Energy*, vol. 115, pp. 1478–1494, Nov. 2016.

[124] SMA Solar Technology, “Technical Information -Efficiency and Derating. Sunny Boy/ Sunny Bol Storage/ Sunny Tripower Central,” 2017.

[125] I. Okumus and A. Dinler, “Current status of wind energy forecasting and a hybrid method for hourly predictions,” *Energy Convers. Manag.*, vol. 123, pp. 362–371, Sep. 2016.

[126] J. Dulout, “Optimal sizing and energy management of storage systems for renewable sources deployment, design of a LVDC microgrid,” PhD Thesis, 2017.